HADLEY CENTRE TECHNICAL NOTE NO. 13

THE IMPACT OF INCREASING HORIZONTAL RESOLUTION ON THE HADAM3 CLIMATE SIMULATION

By

R A Stratton

December 1999

Hadley Centre for Climate Prediction and Research
Meteorological Office
London Road
Bracknell
Berkshire RG12 2SY

The impact of increasing horizontal resolution on the HadAM3 climate simulation

R A Stratton 26/10/99

Abstract

The latest version of the Hadley Centre climate model know as HadAM3 was used to study the impact of changing horizontal resolution between 3.75° to 1.25° longitude and 2.5° to 0.833° latitude. Three integrations were run using AMIP II sea surface temperature forcing for 1979-96. All three integrations had additional vertical resolution in the troposphere. Increasing horizontal resolution improves the simulation of mid-latitude synoptic scale systems. Most of the transient eddy fluxes increase tending to improve agreement with the ECMWF reanalyses. The westerly jets shift polewards and the troposphere warms. The largest benefits coming from doubling the horizontal resolution. Two additional shorter integrations examine the impact of changing orographic resolution.

1. Introduction

As supercomputing power increases in the future it will be possible to consider increasing the horizontal resolution of the atmospheric component of coupled models. Previous studies of atmospheric resolution (Boville 1991; Kiehl and Williamson 1991, Boyle 1993; Phillips et al 1995; Williamson et al. 1995; Deque and Piedelievre 1995; Stendal and Roeckner 1998; Stratton 1996 & 1999) have shown that higher resolution atmospheric models produce a better more realistic simulation of the storm track regions. This study uses the atmospheric part of Hadley Centre climate model, HadAM3 (Pope et al 1999), with the aim of providing guidance on what horizontal resolution to chose for the future. This study intercompares three different horizontal resolutions (table 1), SRES, the standard resolution used for most climate simulations, MRES, a medium resolution and HRES, a high resolution, (until recently equivalent to that used widely for global NWP), each run for at least 10 years using AMIP II style forcing, an improved set of AMIP I forcing (Gates 1992). The study differs from previous work by using a higher vertical resolution in the troposphere (~ 25hPa instead of ~50 hPa in the upper troposphere) for all three integrations (Pope et al. 2000).

HadAM3 is the latest version of the atmospheric component of the Hadley Centre coupled model HadCM3, its formulation is described in Pope et al. (1999). HadAM3 was used for all three integrations with the only differences in the model being those mentioned in Table 1, these are all in coefficients that are resolution dependent. The critical relative humidity used in the parametrization of cloud amount was regarded as resolution dependent and used to tune the model at each resolution to give a roughly similar top of atmosphere radiation balance. This differs from the approach taken in the previous resolution study using HadAM2b (Stratton 1999). All the AMIP II integrations were run using a real calendar year as opposed to the 360 day year used in most Hadley Centre climate integrations. Two HRES resolution integrations were performed, the first (run id abbcm) for 10 years, had noise at 80°N or 80°S for periods of strong winds and the second (run id abbcq) for 17 years, included divergence damping between 45°N/S and the poles to remove the noise. The second HRES integration used a 360 day year as it was also designed to act as a control for a climate change $2xCO_2$ enhanced sea surface temperature HRES run. For most of the results presented

here the first HRES run is used. A comparison of the seasonal means showed no significant differences between the two HRES integrations despite the noise and difference in year length.

A comparison of the global annual means is given in section 2. Details of the seasonal means and their intercomparison and validation against observations are provided in section 3. Section 4 provides an assessment of the models variability. Section 5 attempts to examine the impact of changing orographic resolution on the circulation. In most sections a wide range of figures covering both DJF (December, January February) and JJA (June, July, August) are provided.

Table 1
Differences between the three AMIP II integrations. For the information of people within the Hadley Centre the run ids for the integrations are given in brackets.

	SRES (abbcn)	MRES(abbci)	HRES(abbcm)
Horizontal resolution	2.5 x 3.75	1.25 x 1.875	0.833 x 1.25
approx resolution at mid latitudes (km)	300	150	100
physics time step	15 min	15 min	10 min
dynamics time step	15 min	15 min	5 min
GWD coef gwd lee wave coef	2.0e4 3.0e5	1.7e4 2.55e5	1.6e4 2.4e5
RH crit	0.7	0.75	0.8
diffusion of u,v,θ e-folding time*	∇^6, 12 hours	∇^4, 12 hours	∇^4, 12 hours
diffusion of q e-folding time	∇^6, 12 hours & ∇^4, 4.3 hours above 150hPa	∇^4, 45 hours all levels	∇^4, 50 hours & ∇^4, 12 hours above 90hPa
top level diffusion, ∇^2 e-folding time	1 hour	1 hour	1 hour
length of run	17 yrs 3 mons	17 yrs 3 mons	10 yrs 1 mon

* The e -folding times are for 2, 4 and 6 grid length waves for SRES, MRES and HRES respectively.

2. Comparison of annual means

Means for the first ten years of the AMIP integrations were compared. Table 2 gives a selection of global annual means. These can be assessed in two ways;
a) how successfully the three different resolutions have been tuned to give a similar top of atmosphere (TOA) radiation balance.
b) how the integrations differ.

Table 2. Global annual means for 1979-88 for the three integrations plus an additional SRES integration with the critical relative humidity set to the HRES value.

Quantity (units)	SRES RH_{crit}=.8	SRES	MRES	HRES
Net downward top of atmosphere radiation (TOA) (Wm^{-2})	2.13	-1.92	-0.71	0.58
Outgoing shortwave at TOA (Wm^{-2})	97.3	100.5	98.4	96.8
Outgoing longwave at TOA (Wm^{-2})	242.1	242.9	243.7	244.1
Clear-sky outgoing shortwave at TOA (Wm^{-2})	50.4	50.5	50.4	50.2
Clear-sky outgoing longwave at TOA (Wm^{-2})	261.9	262.2	263.1	263.6
total cloud amount	0.5	0.48	0.48	0.47
total precipitation (mm/day)	3.00	3.01	3.06	3.07
total convective precipitation (mm/day)	2.30	2.27	2.25	2.19
Precipitation - evaporation (mm/day)	-0.0014	-0.0015	-0.0014	-0.0017
total runoff (mm/day)	0.19	0.17	0.19	0.23
total column water vapour (kgm^{-2})	24.11	23.86	24.06	24.36
total cloud water (liquid + ice) (kgm^{-2})	0.081	0.098	0.094	0.09
total cloud ice water (kgm^{-2})	0.050	0.053	0.055	0.057
surface temperature (K)	288.0	287.9	288.1	288.3

The tuning of the top of atmosphere radiation balance was done through adjusting the critical relative humidity in the model cloud scheme to try to keep the cloud amounts at all resolutions similar. Although this has been successful in keeping the total cloud amount similar, the composition of the cloud differs leading to differences in the net top of atmosphere balance of up to $2.5Wm^{-2}$. Note in the HadAM2b AMIP I integrations, where the

critical humidity was not altered with resolution, the net downward top of atmosphere radiation was +2.2 for SRES and -2.5 for HRES. The results suggest that the adjustment of RHcrit value i.e. its increase from 0.7 to 0.8 at HRES was slightly too large thus over compensating for the reduction in the top of atmosphere radiation with resolution.

Despite these differences in the radiation balance it is still possible to draw some conclusions from the global annual means. These are;

1. Precipitation increases with resolution. There is more resolved dynamical precipitation and less parametrized convective precipitation. Note the change in critical relative humidity has almost no impact on total precipitation and would tend to increase convective precipitation at HRES.
2. The total water vapour of the atmosphere increases. Increasing the critical relative humidty with resolution may be partly responsible for this.
3. The total cloud water decreases with resolution but the proportion of ice cloud water increases. The change to critical relative humidity alone would tend to decrease both the total cloud water and the cloud ice water.
4. The total runoff increases. This may indicate that more precipitation occurs as short intense bursts of heavy rainfall rather than continuous light rainfall. Increasing critical relative humidity with resolution does tend to increase the runoff by 0.03mm/day but not by 0.06mm/day seen at HRES.
5. The surface temperature rises which implies that the land surface temperature rises as the sea surface values are prescribed by the AMIP II forcing data. Increasing critical relative humidity has almost no impact on surface temperature.

3. Comparison of seasonal means

The ten year seasonal means from the three integrations are intercompared and are compared against ERA, ECMWF Re-Analyses (Gibson et al 1998) to assess whether any changes due to increased resolution improve agreement with climatology. For some fields difference between ERA and NCEP (National Centre for the Enrivoment and Prediction, Kalnay et al. 1996) are presented to provided some idea of the reliability of the reanalysis climatologies. Difference between ERA and NCEP may partly be due to the differences in the horizontal resolution of the models used for the analyses i.e. T106 and T62 respectively.

3.1 Main dynamical fields

Winds and circulation

The main change to the westerly winds in all seasons is a poleward shift in the mid-latitude westerly jets, Fig 1 shows changes for DJF and JJA. This agrees with the studies of Boville (1991), Williamson et al. (1991) and Stendal & Roeckner (1998). Most of the poleward shift occurs when doubling resolution from SRES to MRES. The shift in the westerly winds is consistent with the changes in the temperature gradients due to increased resolution, see later.

The shift of the jets polewards tends to increase the easterly bias in the upper troposphere, Figs 1(g) &(h). The increased strength of the jet core in the southern hemisphere at around 200 hPa in DJF, Figs 1(c), (e) &(g), is not beneficial when compared with ERA. On the whole the systematic winds errors of the 30 level HadAM3 model are comparable to those from other recent atmosphere climate models.

At mid-latitudes increasing resolution improves the V component of wind at around 200 hPa by increasing the north south flow, Fig 2. The model Hadley circulation is too strong, fig 2(g) and (h). This increases slightly in going from MRES to HRES. Figures 2 (i) and (j) show that far less confidence can be put in the analysis of the v component of wind. Neither analysis supports the strong Hadley circulation i.e. the high model values between 100 and 300hPa over the equator.

Fig 3 shows the changes in vertical velocity on increasing resolution. Associated with the improved north south flow at mid-latitudes, the southern hemisphere cell in DJF increases in strength and in the northern hemisphere around 60°-70°N the ascent increases with resolution in both seasons both giving better agreement with ERA. At all resolutions the model simulations disagree with ERA between 15°N-15°S but there is little agreement between the reanalyses Fig 3 (i) and (j).

Fig 4 shows the velocity potential for 200 hPa for DJF. The main changes in the divergent circulation occur in the tropics where the divergence above the tropical land i.e. Amazona and tropical Africa is increased giving worse agreement with ERA. Note the tropical precipitation also increases above the tropical land tending to increase the model's precipitation bias, see later. Similarly in JJA, Fig 5, there is an increase in the across equator gradient of velocity potential between Africa and the South Atlantic increasing the systematic bias.

Associated with the shift in the westerly jets the mean sea level pressure tends to decrease over the poles and increase at mid-latitudes in all seasons, Fig 6. These changes tend to improve agreement with ERA. In particular the large high pressure bias over the North Pole at SRES in DJF is reduced on increasing resolution, Fig 7. Overall the DJF and JJA mean sea level pressure biases of the HRES run are low relative to other models. One systematic bias which appears to be insensitive to resolution is the underestimation of mean sea level pressure over the tropics.

Looking in more detail at DJF the increase in sea level pressure over the North Pacific does not improve the simulation. To the south of Australia the high pressure bias increases with resolution. In JJA, Fig 8, there remains a low pressure bias over the meditterrean, Eastern Europe and Central USAwhich may be associated with the lack of precipitation see section 3.3. The systematic errors in the 500 hPa geopotential height (not shown) are very similar to those in the mean sea level pressure.

Temperature and humidity

The tropospheric temperature increases on increasing horizontal resolution improving agreement with ERA. The largest increases occur at mid-latitudes, Fig 9. Over the winter pole in the stratosphere the temperature decreases with resolution changing from a large warm bias to a small cold bias. Comparison of HRES and MRES Fig 9(c) shows a decrease in temperature at 200 hPa over both poles and a decrease above 100 hPa around 30° N/S. This may be due to the radiational impact of the additional decrease in specific humidity towards the top of the model, fig 10, when going from MRES to HRES. The increase in tropospheric temperature with resolution is due to increased ascent and descent leading to more latent heat release via condensation. A comparison of spinup temperature tendencies from HRES and SRES for cloud (not shown) supports this. Also the temperature tendencies from large scale precipitation suggest that the HRES resolution model cools less due to re-evaporation of falling precipitation. Dynamical core tests run using the HadAM3 model with simple Held Suarez forcing (Held and Suarez 1994) at the different resolutions suggest that the increased temperature around 200hPa at mid-latitudes may be mainly due to the dynamics.

Figure 11 shows the changes to specific humidity. At the top of the model the specific humidity decreases with resolution, giving worse agreement with climatology. Possible reasons for this are;
(a) differences in the diffusion of specific humidity near the top of the model at different resolutions.
(b) the tendency of the convection scheme to produce very low specific humidity values which can ascend into the stratosphere if not mixed quickly by diffusion with higher values. Note with a higher resolution model and in the case of HRES a shorter timestep there is a higher probability of more low values being produced by convection.

At around 30°-40 N/S in the lower to mid troposphere the specific humidity decreases with resolution. Elsewhere in the troposphere the specific humidity increases with resolution reducing the dry bias in the tropics but tending to increase an upper tropospheric moist bias. This can be seen in fig 12 showing the total column water vapour. One anomalous change is the large increase in the low level moisture between 60°-90° N in JJA at HRES, Fig 11(h) & 12(b), giving worse agreement with ERA. Global plots of the total column water for JJA (not shown) show that this extra moisture is mainly over North East China and the North West Pacific Ocean.

Associated with the increase in temperature and decrease in specific humidity at mid-latitudes there is a decrease in relative humidity, fig 13 , in the troposphere improving agreement with ERA. The cooling seen in HRES around 200 hPa despite the decrease in specific humidity gives an increase in relative humidity. In the tropical troposphere there is a slight increase in relative humidity due to a small increase in specific humidity and to the increase in temperature.

The overall magnitude of the temperature biases in HadAM3 at all resolutions are smaller than those seen in HadAM2b. This may be partly due to this study using more levels in the vertical which tends to reduce the cold bias (Pope et al 2000). Comparisons of semi-lagrangian and Eulerian advection of moisture, Chen & Bates (1996), Rasch & Williamson (1991) suggest that the cold bias over the summer pole is reduced with semi-lagrangian advection. HadAM3 uses Eulerian advection.

3.2 Comparison of eddy flux diagnostics

Previous studies with HadAM2b (Stratton 1999) and spectral models (Boville 1991, Boyle 1993; Williamson et al. 1995; Deque and Piedelievre 1995; Stendal and Roeckner 1998) have shown that transient eddy fluxes tend to increase with horizontal resolution as the model becomes better able to simulate mid-latitude synoptic scale disturbances. For this reason the changes to a wide variety of transient eddy fluxes are examined and compared with ERA. Our knowledge of these fields is far less certain than the mean fields as can been seen from Table 3 which provides peak fluxes from both ERA and NCEP analyses for comparison with the three integrations.

Table 3

Peak transient eddy values for a wide variety of fields in both hemispheres for DJF and JJA. The peak values are evaluated between 15°-65° N or S and between the pressure levels given in the table.

Transient eddy flux	Season	Hem	SRES	MRES	HRES	ERA	NCEP
Kinetic energy	DJF	NH	278	287	298	310	294
		SH	309	345	365	336	222
(600-150hPa)	JJA	NH	199	222	209	236	223
		SH	317	316	324	320	238
Northward momentum	DJF	NH	42	46	50	47	48
		SH	-63	-66	-75	-73	-50
(600-150 hPa)	JJA	NH	28	30	31	35	33
		SH	-70	-79	-86	-76	-58
Northward heat	DJF	NH	16.8	18.1	18.3	20.4	17.8
		SH	-13.8	-15.2	-15.2	-18.0	-13.1
(850-600 hPa)	JJA	NH	8.6	8.8	8.7	9.6	10.4
		SH	-20.7	-20.9	-21.3	-22.5	-19.9
Northward moisture	DJF	NH	6.12	6.24	6.42	5.82	5.48
		SH	-6.15	-6.31	-6.50	-6.42	-6.18
($x10^{-3}$)	JJA	NH	3.39	3.37	3.30	3.99	3.41
(850-150 hPa)		SH	-6.68	-6.49	-6.60	-5.12	-6.12
omega	DJF	NH	0.16	0.20	0.23	0.23	0.18
		SH	0.12	0.15	0.17	0.16	0.12
(600-150 hPa)	JJA	NH	0.09	0.12	0.14	0.14	0.11
		SH	0.15	0.19	0.22	0.21	0.16
omega * v	DJF	NH	-1.31	-1.40	-1.55	-1.63	_
		SH	1.02	1.14	1.28	1.24	_
(600-150 hPa)	JJA	NH	-0.46	-0.51	-0.53	-0.63	_
		SH	1.47	1.64	1.83	1.79	_
omega * T	DJF	NH	-0.21	-0.24	-0.27	-0.37	-0.22
		SH	-0.18	-0.20	-0.20	-0.19	-0.13
(850-150 hPa)	JJA	NH	-0.09	-0.12	-0.11	-0.11	-0.13
		SH	-0.26	-0.31	-0.32	-0.26	-0.24
omega * q ($x10^{-4}$)	DJF	NH	-1.21	-1.46	-1.59	-1.42	-1.16
		SH	-0.98	-1.20	-1.27	-1.15	-0.99
(850-150 hPa)	JJA	NH	-0.70	-0.96	-1.02	-0.84	-0.78
		SH	-0.97	-1.27	-1.39	-1.21	-1.01

Transient vertical velocity.

Transient vertical velocity is a useful diagnostic for assessing the amount of variability in ascent and descent in a model and also for spotting any problems with noise. Higher values of ω' occur at mid-latitudes in the regions of synoptic disturbances and also in the tropics. Figure 14 shows that the variations in ascent and descent increase at mid-latitudes with increasing resolution; larger changes occur between SRES and MRES, improving agreement with ERA. This is confirmed by the peak values in table 3.

The very high values seen at 80°N in DJF and 80°S in JJA indicate noise in the HRES simulation. Divergence damping included in the second HRES simulation (known as abbcq) removes this noise in transient vertical velocity, compare Fig 15(a) and (b) with 14(a) and (b). There may also be some evidence of noise at 60°S in JJA at around 100hPa in the MRES simulation, Fig 14 (f). The increase in transient vertical velocity between SRES and HRES occurs over both land and sea, Fig 15(e), (f), (i) & (j). The larger increases in transient vertical velocity tend to occur over the land in the tropics. The land sea contrast will be referred to again later in section 5, where the figs 15(c), (d), (g) and (h) will be explained.

In the tropics all resolutions lack variability when compared with ERA but there is a large disagreement between ERA and NCEP in the magnitude of transient vertical velocity at all latitudes. NCEP is consistently less than ERA but then the resolution of the model used for NCEP is T62 as opposed to T106. This may partly account for the differences. Note that the peak transient vertical velocity values, in table 3, for NCEP tend to fall between the model values for SRES and MRES, whereas those for ERA are close to the HRES values.

The increase in the distribution of vertical velocity as resolution increases can be used to help explain the increase in temperature in the mid-latitude troposphere. With more rapid ascent water vapour will be more likely to condense releasing heat and so warming the atmosphere. This also helps to explain an increase in large-scale precipitation (see later).

Kinetic energy and the energy cycle

Transient eddy kinetic energy increases with resolution in all seasons at mid-latitudes, (Fig 16 & Table 3) agreeing with the other resolution studies mentioned earlier. The largest increase occurs between SRES and MRES with a further increase from MRES to HRES implying that the peak model eddy kinetic energy value has not converged. The increases in eddy kinetic energy tend to improve agreement with ERA. In addition to the increase in transient eddy kinetic energy there is evidence of a slight polewards shift partiuclarly in the southern hemisphere consistent with the shift in the westerly jets seen earlier.

Looking in more detail, in the stratosphere over the winter pole, increases in transient kinetic energy improve agreement with ERA. Changing resolution has little impact on the excessive eddy kinetic energy at around 150 hPa over the equator present in all seasons which may be connected with the Hadley Circulation being too strong. In the southern hemisphere between 20°-40°S at around 200 hPa the eddy kinetic energy is too high. This may be linked to errors in the simulations of the westerly winds in the southern hemisphere (the model winds tend to be too strong, fig 1(g) & (h)). There is also a large disagreement between ERA and NCEP values in the southern hemisphere. The HRES eddy kinetic energy extends too high up when compared with ERA and may be linked to problems with the model's tropopause height.

Table 4 gives the components of the energy cycle for DJF calculated using the definitions given in Ulbrich and Speth (1991) but using temperature instead of virtual temperature as mean virtual temperature was unavailable. The global mean values for those fields with large values near steep orography may be subject to inaccuracy in the way missing

data was treated. The main point to come out of the analysis is that the energy cycle seems to intensify with resolution. The baroclinic conversion rates between zonal available potential energy APE and transient APE and on to transient KE increase and are higher than ERA. It is interesting to note that the values for NCEP (a lower resolution model) are lower.

The total kinetic energy increases with resolution, the increase coming from the increase in transient eddy kinetic energy. Note there is a large difference between the ERA and NCEP values for the total transient eddy kinetic energy; the model values being in closer agreement with ERA. The zonal kinetic energy is reduced at higher resolutions giving worse agreement with ERA and NCEP. There is little change in the stationary eddy kinetic energy which agrees well with the climatologies. Zonal plots of the stationary eddy kinetic energy (not included) show that the stationary eddy kinetic energy increases slightly with resolution between 45°-90°N improving agreement with ERA.

The ERA and NCEP values for the zonally available potential energy (APE) agree well with those for MRES and HRES. The SRES value is too high probably due to the excessive values of APE over the equator between 300 and 500 hPa related to the tropospheric cold bias. The stationary eddy APE is larger in the model than ERA and NCEP and is due to too much stationary APE between 30°N and 30°S at 200-300 hPa and at 400-600hPa around 50°N. The model values of transient APE fall between those for NCEP and ERA and increase with resolution.

The model values for CZ (conversion of zonal APE to zonal KE) are lower than ERA and NCEP but both ERA and NCEP have high positive values near the surface over the South Pole. Slight errors in masking out values below the land surface could lead to differences. The conversion rates, CE, for stationary APE to KE are in good agreement. Those for the transient waves increase with resolution to values higher than ERA which is higher than NCEP. Conversion rates, CA, from zonal APE to stationary APE agree well; the higher resolution model values being slightly too high. This is consistent with the model having higher stationary APE and lower zonal APE. The transient CA conversion rates of the model again increase with resolution and are higher than ERA. Unfortunately not all the required fields were available from the model runs to calculate the conversion rates CK, from zonal KE to eddy KE. No attempt was made to calculate the generation and dissipation terms.

A large part of the energy of the model is held in the large-scale planetary waves. Fig 17 shows the seasonal cycle of the wave number one amplitude for 300hPa height, a level corresponding to the maxima in kinetic energy. In the northern hemisphere the wave number one amplitude tends to improve agreement with ERA with increasing resolution, particularly through the summer and autumn. In the southern hemisphere during January and February the decrease in amplitude with resolution does not improve the simulation. Also at all resolution the model tends to have too large an amplitude close to the South Pole.

Table 4

Components of the energy cycle for DJF. Calculations were done using mean pressure level data. Values for kinetic energy in brackets were calculated using model level data. kinetic energy and available potential energy are in 10^5 Jm^{-2} . conversion terms are in Wm^{-2}.

Energy component	SRES	MRES	HRES	ERA	NCEP
Zonal KE	7.77 (7.92)	7.40 (7.55)	7.53 (7.68)	7.82	8.02
Stationary eddy KE	1.50 (1.50)	1.58 (1.60)	1.56 (1.59)	1.49	1.51
Transient eddy KE	7.02 (7.19)	7.33 (7.52)	7.53 (7.72)	7.90	6.85
Zonal APE	46.69	44.58	44.73	44.89	44.89
Stationary APE	2.35	2.39	2.20	2.14	2.15
transient APE	4.86	5.13	5.16	6.09	4.63
CZ	0.19	0.14	0.08	0.53	0.79
CE stationary	0.49	0.52	0.52	0.50	0.56
CE transient	2.20	2.50	2.52	2.33	1.80
CA stationary	0.65	0.71	0.70	0.64	0.61
CA transient	2.15	2.26	2.25	2.10	1.69
CK stationary			-	-0.10	-0.08
CK transient	-	-	-	-0.61	-
C ate - ase	-	-	-	-0.52	-0.43
C kte -kse	-0.16	-0.22	-0.21	-0.23	-0.22

Momentum flux and atmospheric torques

Figure 18 shows the relative angular momentum for the three different resolutions. SRES had the largest values in the region of the jet maxima. As the resolution increases the peak relative angular momentum moves polewards with the westerly jets. Conservation of angular momentum implies that the divergence of the northward momentum flux should balance the total torque (Boer & Lazare 1988). A comparison of the model total torque and divergence of northward momentum does not show complete agreement. The total torque from the model tends to be noisy particularly over regions of high orography. Fig 19 shows the components of the total torque for DJF and JJA. The total torque for MRES and HRES is very similar for most latitudes apart from 30°-45°S, where the mountain torque differs probably due to the difference in representation of the Andes; and between 30°-60°S where the surface stress torque increases with resolution. The total torque for SRES differs around 30°-45°N in DJF and between 25° and 60°S in both DJF and JJA. The differences around 25°S may be due to the low resolution of the Andes (the only significant orography at that latitude).

The source of angular momentum in DJF in the tropics is similar in HRES and MRES and slightly less than SRES. The transport of the angular momentum polewards between 30° -60° increases with resolution, fig 20, the increase coming from an increase in the transient and stationary eddies. But the transport polewards between 0° and 30° decreases. The net result is a higher relative angular momentum at lower resolution.

Figure 21 shows the transient eddy northward momentum flux for DJF and JJA. The strength of the flux increases with resolution, Table 3 and Fig 21 (c)-(f) giving a better agreement with ERA at mid-latitudes. All three resolutions have too much southward/northward momentum flux at around 150hPa over the equator in DJF/JJA, the same location as the excessive transient eddy kinetic energy.

Heat fluxes

A significant part of the total poleward transport of heat at mid-latitues is via eddies rather than the zonal component of vT. There is evidence that the poleward transport of heat via eddies increases with increasing horizontal resolution in good agreement with ERA, fig 22. NCEP values are weaker in the southern hemisphere , Figs 22(i) and (j), and near the surface agree better with the three model simulations. At higher resolution the northward heat flux increases in the stratosphere improving agreement with ERA.

The upward transient eddy heat transport occurs mainly at mid-latitudes, fig 23, and increases with resolution particularly between SRSE and MRES, Table 3 and figs 23(e) and (f). This change is consistent with the increase in magnitude of ascent and descent and the greater release of heat due to condensation. Figures 23 (i) & (j) show that there is less confidence in the analysis of this field with the magnitude of the differences between NCEP and ERA being similar to those between the model simulations and ERA. In fact the model would look better if compared with NCEP rather than ERA.

Moisture fluxes

Like the heat transport most of the mid-latitude poleward transport of moisture is via eddies and tends to increase with horizontal resolution, Fig 24. This increase does not improve agreement with ERA or NCEP though Figs 24 (i) & (j) indicates there are large uncertainties in the analysis of v*q. The model transport of moisture polewards is too high in the winter hemisphere. In the tropics the across equatorial flow of moist associated with the Hadley Circulation increases.

The vertical transient eddy transport of the moisture also increases with resolution, Fig 25, particularly between 30° and 60° N/S. This increase improves agreement with ERA around 60°N/S but is too large nearer the equator where even the values at SRES were too large when compared with ERA and NCEP. At all resolutions the model lacks vertical transient eddy transport of moisture upwards over the equator instead the moisture seems to ascend either side of the equator. Problems with the tropical eddy transport of moisture may be linked to problems with the tropical circulation.

3.3 Precipitation

Table 2 indicates that there is a slight increase in the global mean precipitation with resolution. A greater proportion of the precipitation is resolved large scale rather than parametrized convective. These changes are consistent with the increased variability in vertical velocity leading to more condensation of moisture mentioned earlier. Associated with the shift in the westerly winds and storm tracks there is a polewards shift in the mid-latitude precipitation but little change in magnitude. This shift is most noticeable over the oceans Figs

26 & 27. There is less precipitation over Europe between 40°-60°N and in the central USA between 40°-60°N in both DJF and JJA. This tends to improve agreement with the CMAP (CPC Merged Analysis of Precipitation for 1979-1996) Xie & Arkin (1997) in DJF but not in JJA, as in DJF the precipitation over the land is too large relative to CMAP at all resolutions. In JJA the poleward shift of the storm track over land is not sufficient to explain the reduction in precipitation over central Europe as the resolution increases. As elsewhere, over central Europe the convective precipitation is reduced as the resolution increases but unlike other regions this is not compensated by increases in the large scale precipitation.

In the tropics the precipitation over land increases with resolution with associated decreases over the Indian ocean in DJF and the Pacific and Atlantic in JJA. The increase precipitation over tropical land does not improve agreement with CMAP. The tropical changes are consistent with the changes in velocity potential mentioned earlier i.e. there is more divergence over the regions of higher tropical precipitation. The additional SRES run with increase critical relative humidity, i.e. using the HRES value, also shows increased precipitation over the tropical land. This suggests that the tropical changes seen on increasing resolution may be due mainly to the change in the critical relative humidity. A comparison of two SRES runs with physics timesteps of 15 and 30 minutes suggests that decreasing timestep does not account for any increase in precipitation over tropical Africa and could only account for a very small percentage increase over the Amazon. An examination of daily timeseries for points in Africa and the Amazon suggests that there is more precipitation overnight as the resolution increases. Note, at all resolutions the diurnal cycle of convective precipitation over land is not very realistic as the model tends to have a maximum in convective precipitation just after dawn rather than a peak in the afternoon. Over the tropical ocean the depth of the convection reduces with resolution accounting for the fall in precipitation. It maybe that the change over the ocean, particularly the large reduction over the southern part of the Indian Ocean forces the changes elsewhere in the tropics.

3.4 Clouds and radiation

The total cloud amount varies little with resolution as each different resolution has been tuned using the critical relative humidity of the cloud scheme to give approximately the same total cloud. This approach is similar to that taken in many of the previous resolution studies mentioned earlier. The actual type of cloud present does vary with resolution giving rise to large differences in the radiative properties of the cloud. Fig 28 shows that there is sightly more layer cloud present at higher latitudes (> 60°) in the troposphere with slightly less in the boundary layer. Fig 29 shows that convective cloud decreases at mid-latitudes. The large increase in convective cloud in the tropics in going from MRES to HRES is probably mainly due to the change in physics timestep from 15 to 10 minutes (Stratton 1999).

Fig 30 shows that the amount of cloud liquid water decreases with increasing resolution particularly in the model's boundary layers though the total layer cloud at the same levels remains approximately constant. This change is associated with the change to the RH_{crit} value, a higher value results in more higher level cloud ice water and less cloud liquid water. Fig 31 shows the changes in cloud ice water, this increases in the mid-troposphere but decreases in the lower troposphere.

Although the global annual mean top of atmosphere net downward radiation is within $2.5 Wm^{-2}$ it is not identical in all runs (table 2) and Fig 32. As the resolution increases the model reflects less of the incoming solar radiation, Fig 33, tending to improve agreement with ERBE in the southern hemisphere, make the tropics (15°N-15°S) worse, and have mixed results in the northern hemisphere. The amount of low level bright water cloud (a high

reflector of SW) decreases to be replaced by higher cloud with more ice water. The decrease in relative humidity with resolution at mid-latitudes results in an increase in outgoing longwave radiation, Fig 34, tending to increase the model bias everywhere except the tropics and from 60°-90°S. Also the land surface warms at higher resolution (see section 3.5) so more longwave radiation will be emitted from the surface. In the tropics the reverse is true, the relative humidity increases with resolution while land surface temperatures do not increase significantly.

On the whole the changes to the cloud composition on increasing resolution do not improve the shortwave cloud forcing, Fig 35 or the longwave cloud forcing Fig 36. Over northern hemisphere land in JJA the lack of cloud at higher resolution gives an under estimate of both shortwave and longwave cloud forcing. Over the tropics, in both DJF and JJA, the fall in shortwave cloud forcing with resolution is due reductions in the shortwave cloud forcing over land. All resolutions tend to have too much shortwave cloud forcing in the storm track regions over the oceans. In the warm pool over Indonesia all resolutions lack shortwave and longwave cloud forcing. The behaviour of the model shortwave cloud forcing over sea ice disagrees with ERBE. The differences in the longwave cloud forcing between 30°-45°S in DJF correspond to the poleward shift in the storm track with increasing resolution. The differences around 30°S in JJA correspond to a slight reduction in precipitation in the SPCZ, Fig 27.

3.5 Land surface

In AMIP climate integrations the land surface temperature is free to vary but the ocean surface is forced to follow the prescribed sea surface temperatures. As the resolution increases the land surface temperatures rise particularly at higher latitudes figures 37 and 38. This is consistent with the warming seen in the troposphere.

In DJF the warming over Northern hemisphere land improves agreement with the Legates and Willmott climatology (Legates and Willmott 1990) over Europe but increases the warm bias over Alaska, northern Canada and North East Asia. In JJA the temperature rise with increasing resolution in the northern hemisphere tends to increase the warm bias throughout Europe, Northern Asia and the USA. The areas which warm most in JJA correspond to those where the cloud cover and the precipitation decrease with increased resolution.

Fig 39 shows the zonal mean total soil moisture and canopy water for DJF and JJA. In JJA in the northern hemisphere between 40°-60°N HRES has less soil moisture than the other resolutions. This is probably due to the reduction in precipitation particularly in the central USA and Eastern Europe, Fig 40(b) & Fig 27. In the northern hemisphere between 45°-70°N the canopy water decreases with resolution. It has been suggested (Richard Jones, personal communication) that the fall in canopy water with increased resolution is linked to the fact that the convective precipitation is assumed to fall over just a fraction of the gridbox. A drier canopy means less water is available for re-evaporation. This may be true between 30°-45°N but not further north, Fig 40(d) where the evaporation increases with resolution.

In the tropics around the equator SRES has less soil moisture and less precipitation. Canopy water is similar at all resolutions apart from SRES in JJA which is lower. Figs 40 (e) and (f) show the total runoff at all resolutions. Over the tropics where the soil moisture and precipitation increase with resolution the runoff is higher. This may partly be due to the precipitation falling as more intense bursts at higher resolution.

3.6 Ocean surface

The surface wind stress over the oceans increases slightly in the storm track latitudes with resolution, fig 41. The peak in the wind stress also shifts polewards. These changes are associated with the shift in the westerly winds (section 3.1) and an increase in the intensity of the storms (section 4.2.1). In the tropics there is almost no change apart from in JJA between 10°and 30°N due to changes in the monsoon.

Fig 42 shows the net annual mean surface heating over the oceans compared with the Da Silva climatology (Da Silva et al. 1994). On the whole the agreement is good considering that the estimated errors in the surface fluxes are of order +/- 20Wm^{-2}. One of the largest biases occurs over the equator where the model has too much surface heating, and the bias increases with resolution. This increase is due to shortwave heating at the surface increasing, fig 43(a), due to changes in the tropical cloud ie a reduction in the bright low level water cloud over the ocean. In the sub-tropics the net heating is too low when compared with da Silva. Increases in the near surface winds at higher resolution lead to higher latent heat fluxes, Fig 43(d) which are partly balanced by an increase in the shortwave fluxes.

Between 30° and 50°N the net annual mean heating increases with resolution making agreement with climatology worse. The differences in resolution appear to occur during JJA rather than DJF, Fig 42(b) & (c) and are due to a combination of changes in all four components forming the net surface heat flux. The sensible heat flux is reduced as the atmosphere is warmer at higher resolution. The latent heat flux is reduced, the longwave flux increases while the shortwave changes are mixed.

At high latitudes over the North Pole the models do not agree with the climatology but north of 80°N vary little with resolution. The biggest differences with da Silva seem to be in the sensible heat fluxes. Note this region consists mainly of Arctic sea ice.

Overall, increasing resolution does not reduce the model biases in surface heat fluxes. The differences in the net heat fluxes at mid-latitudes and the tropics suggest that a coupled model may behave different when using a higher resolution atmosphere.

4. Variability

4.1 Blocking

Ten years is a short period when considering the climatology of blocking and therefore results from this intercomparison must be treated with some caution. Blocking indices for 1979-88 calculated using a slightly modified form of the Tibaldi and Molteni (1990) blocking index are given in fig 44. In DJF, fig 44(a), increasing horizontal resolution improves the North Atlantic blocking removing the spurious peak around 60°W. All the models lack blocking around 90°E possibly due to problems modelling the flow over the Himalayas. Compared with simulations from HadAM2b, (Stratton 1999), all model resolutions have reasonable values for the blocking in the Pacific; MRES being slightly too low. This improvement in the blocking is thought to be due to a better simulation of the precipitation over Indonesia in HadAM3 Pope et al (1999). In MAM, Fig 44(b), MRES has too much blocking in the western Pacific. Blocking in the eastern part of the Pacific decreases with resolution. In JJA, Fig 44(c), blocking increases with resolution over the Pacific improving agreement with ERA. In SON, Fig 44(d), both MRES and HRES have too much blocking over the Atlantic; SRES is in better agreement with ERA.

In the southern hemisphere, Fig 45, the blocking tends to decrease with resolution in all seasons improving agreement with ERA. This change may be related to the polewards shift in the westerly winds.

4.2 Variability in 500 hPa height.

4.2.1 Storm tracks - band pass

A band pass Blackmon filter (Blackmon et al 1977) selecting time scales of 2.5 to 6 days was used to assess storm tracks. The main change on increasing resolution is the polewards shift and strengthening of the storm tracks which improves agreement with ERA, Figs 46 DJF and Fig 47 JJA. The improvement in the simulation of storms with increasing resolution is expected as at SRES the model grid length is relative large compared with the size of most storms. The improvement in the storm tracks is consistent with improvements in all the transient eddy fluxes mentioned in section 3.2. The increase in band pass filtered 500 hPa heights with resolution in DJF agrees with the finding for ECHAM4 (Stendal & Roeckner 1998). In SRES the storm tracks tend to be too weak, and in the southern hemisphere too near the equator. When compared with the previous HRES HadAM2b simulation the peaks tend to be slightly lower in the HadAM3 case.

One region which remains a problem in DJF independent of resolution is around New Zealand (180° in the southern hemisphere) where the storm track is too far equatorward in the model. In DJF over Northern Canada the model storm track is too weak at all resolutions. The northward turning of the Atlantic storm track in DJF is well captured by HadAM3 at all resolutions.

4.2.2 Low pass

The low pass filter used selects variability on time scales of 10-90 days, with high values tending to occur at the end of the storm tracks. Low pass filtered 500 hPa heights tend to agree better with ERA as the horizontal resolution increases agreeing with Stendal & Roeckner (1998). In DJF, fig 48, the strength of the variability over the North Pacific and Alaska increases at HRES and is in better agreement with ERA than that from the HadAM2b HRES simulation. The variability over Northern Europe is higher at HRES and MRES in DJF agreeing with ERA. In JJA, Fig 49, the variability at HRES is higher over the North Pole.

In the southern hemisphere the pattern of variability improves in the southern Pacific. The excessive variability in JJA, fig 49, in the southern Indian Ocean, SRES, is reduced, but in DJF this is increased.

4.3 Intraseasonal oscillation

The tropical intraseasonal oscillation was investigated for all three resolutions using methods similar to those described in Slingo et al. (1996). In additional the analysis was also performed on a 19 level SRES simulation, aawei and on an additional SRES 30 level run with a longer timestep to help intercomparison with the HadAM2b study (Stratton 1999).

Table 5
Details of the seasonal and intraseasonal amplitude of variations in the 200 hPa U component of wind. Values are for the 17 years 1979-96 with values for the first 10 years in brackets.

Run	Horizontal resolution	vertical resolution	timestep in minutes	Seasonal amplitude	intra-seasonal amp
ERA	T106	31		4.0 (4.0)	1.4 (1.4)
aawei	SRES	19	30	4.6 (4.7)	1.3 (1.4)
abcda	SRES	30	30	3.6 (3.8)	1.7 (1.6)
abpad	SRES RH_{crit} as HRES	30	15	(3.9)	(1.7)
abbcn	SRES	30	15	3.7 (4.0)	1.8 (1.8)
abbci	MRES	30	15	4.1 (4.2)	1.6 (1.7)
abbcm	HRES	30	10	(5.1)	(1.5)
abbcq	HRES	30	10	(5.1)	(1.4)

Comparing aawei and abcda the addition of extra levels in the vertical reduces the seasonal amplitude improving agreement with ERA and increases the intraseasonal amplitude making it too high relative to ERA. A comparison of the aawei values with those from HadAM2b suggests that HadAM3 has improved the seasonal and intraseasonal amplitudes reducing them from 6.0 and 1.8 respectively.

Reducing timestep in HadAM3 has little impact on the seasonal amplitude but increases the intraseasonal amplitude (the reverse behaviour to HadAM2b) giving worse agreement with ERA.

Increasing horizontal resolution increases the seasonal amplitude (the reverse to HadAM2b) giving worse agreement with ERA and reduces the intraseasonal amplitude (in agreement with HadAM2b) improving agreement with ERA. Fig 50 shows the wave-number one power spectra for 200hPa velocity. There is some evidence that HRES has more energy at lower frequencies than MRES and SRES in better agreement with ERA. All the model runs with 30 levels have too much energy at higher frequencies. The additional SRES run with RHcrit=0.8, fig 50(b), also has more energy at low frequencies suggesting that the improvments seen at HRES may be due more to changes in the cloud and precipitation than to resolution. As mentioned in section 3.3 the tropical changes in precipitation on increasing resolution are partly due to the change in critical relative humidity.

4.4 Response to SST forcing

In an earlier study (Stratton 1999) using HadAM2b any change in the response of the model with resolution to the SST forcing was assessed by looking at the interannual variability of clear-sky outgoing longwave radiation. The observed values were compared with CLERA (Clear-sky Longwave ERA) data (Slingo et al 1998) which covers the 15 years

of the ERA analyses. The same analysis has been repeated for the HadAM3 simulations which 17 instead of 10 years. Fig 51 shows results for the NINO3 region (5°N-5°S 90°-150°W); the HRES results being for the run abbcq. When the sea surface temperatures increase the clear-sky OLR is reduced as there is more convection resulting a moister atmosphere. All model resolutions respond to the El Nino events in 1982-83 , 1986-87 and 1991-92. There is no clear evidence of any resolution dependence in the model's response to the SST anamolies in the NINO3 region.

At mid-latitudes as the sea temperature warms the clear-sky OLR tends to increase ie the reverse of the tropical behaviour. Fig 52 shows the behaviour for an area covering the North Atlantic from 40°-55°N, 10°-50°W. CLERA and the models respond to the dip in sea surface temperatures during 1985-1987. Fig 53 shows an area in the North East Pacific. All three models respond to the change from a cold to a warm anomaly through 1987-91. It is difficult to see any strong signal of changing response to sea surface forcing at mid-latitude with resolution.

4.5 Interannual variability of mean sea level pressure

The interanual variability of the model was examined by looking at the standard deviation of mean sea level pressure. In DJF, fig 54, the greatest variability occurs in the northern hemisphere over the North Pole and the Atlantic and Pacific oceans. All three resolution fail to reproduce the high variability over the North Pole. As the resolution increases and the mean circulation improves (see section 3) the interannual variability also improves over the Pacific and Atlantic oceans. In the southern hemisphere the interannual variability around Antarctica falls with increasing resolution improving agreement with ERA. In the tropics difference plots (not shown) indicate that the model has less variability than ERA over the Eastern Pacific, Amazona and Central Africa.

Fig 55 shows JJA, as in DJF, the interannual variability around Antarctica decreases with resolution improving agreement with ERA. Variability in the northern hemisphere is lower in JJA and in reasonable agreement with ERA.

5. Impact of orography on the simulations

As the model resolution is increased the surface elevation and land sea mask are also altered. In the main AMIP II runs described above the resolution of the orography is increased. None of the model resolution studies mentioned earlier have attempted to look at the impact of changing orography on the simulation. Two additional shorter runs, Table 6, were done to try to assess the impact of changing the orography. Common sense suggests that in fields like precipitation and 1.5m temperature small scale details over steep orography will change as the orography changes. It is more difficult to say whether the small scale local changes will lead to larger scale circulation changes. In the additional integrations only the surface elevation was altered, all other orographic fields such as the standard deviation of orography in the NS and WE directions used in the gravity wave drag parametrization, were left at the values normally used at each resolution.

There are arguments to suggest that the orography currently used in the UM at each resolution has more detail than can be resolved by the model (Webster, 1999) and should be smoothed eg using a 1-2-1 filter. The approach taken in this study is to take the orography used at SRES and interpolate to the other higher resolution grids with the aim of seeing if it has an impact on the large scale circulation in the higher resolution simulations.

Table 6

A list of the integrations used to look at the impact of orography.

Run	Resolution	Description	length
abbcn	SRES	Control SRES orography	10 yr 3 mon
abbci	MRES	Control MRES orography	17 yr 3 mon
abbch	MRES	SRES interpolated to MRES	10 yr 3 mon
abbcq	HRES	Control HRES orography (similar to abbcm)	17yr 3mon
abbcp	HRES	SRES interpolated to HRES	5 yr 3 mon

5.1 Mean climatology

To determine whether the addtional integrations differed from original higher resolution orography integrations multi-annual seasonal means were intercompared. Fig 56 shows the changes in mean sea level pressure at MRES between abbci and abbch, i.e. the impact of using a smoother orography in a MRES run. There are some small significant changes at mid-latitudes in the large scale circulation e.g. 2 hPa over the UK in DJF. In JJA there is a 2hPa significant change South East of Africa. In both seasons the changes are relatively small and so no more will be said about this run.

The difference in orography between the HRES integrations is larger as the same SRES orography has been interpolated to the HRES grid. Fig 57 gives an example of the difference by showing the orography for North America. The orography for abbcp resembles that for SRES whereas the original HRES orography has far more detail and slightly higher peaks. Fig 58 shows the difference in mean sea level pressure for DJF and JJA. In this case there is more evidence that the difference in orography between the runs is having a

significant impact on the large scale circulation. The run with the orography closer to that used at SRES in DJF, Fig 62(a), has lower pressure between 30°-60°N and higher pressure over the North Pole which corresponds to the differences seen in Fig 7. This implies that a small part of the change in mean sea level pressure seen between SRES and HRES may be due to the change in the representation of the orography i.e. better resolution of the Rockies, Greenland and the Himalayas in the northern hemisphere and the Andes in the southern hemisphere. The reduction of pressure over the UK and North Pacific in the smoother orography run is partly benefical but too large, taking the model from a high pressure bias to a low pressure bias. The increase of pressure near the North Pole does not improve the simulation. In JJA, fig 58(b) there are significant reductions in pressure around the southern hemisphere between 30° and 45°S. which tend to correspond with the changes seen between HRES and SRES, fig 8.

Transient vertical velocity is a field which is likely to be altered by changing the orography. Looking back to Fig 15(c), (d), (g) and (h), show the differences over land and over sea between the values in the HRES runs abbcq and abbcp. As expected most of the changes in ω' occur over the regions of steep orography i.e over the land and ω' is lower in the smoother orography run abbcp. Comparison of figures 15(c) & (e), and (d) and (f) suggest that some of the very large increases in ω' over the land in going from SRES to HRES are due to the increase in the resolution of the orography eg between 40°and 50°N there are the Himalyas and Rockies and between 30°and 50°S there are the Andes. Any changes in ω' over the sea must be due to indirect affects i.e. changes in the circulation leading to changes in the regions of synoptic disturbance. The changes over the sea are, apart from the region 60°-80°N, very small, Figs 15(g) and (h), relative to those seen between SRES and HRES, Figs 15(i) and (j). Changes in the variability of vertical velocity near steep orography will alter the generation of high frequency waves. These high frequency waves interact in some unexplained way to alter the large scale planetary waves. Some of the high frequency waves generated in the original run over the orography may be better regarded as noise and their removal improves the simulation whereas others may be realistic and help improve the flow.

The presence of mountains contributes towards the waves in the atmosphere. Fig 59 shows a cross section of the amplitude of wave number one in geopotential height for DJF. The largest amplitudes occur in the northern hemisphere in the region of the westerly jet. The cross section for the integration with the smoother orography, abbcp, is significantly different in the northern hemisphere and tends to resemble that for SRES. The HRES integration, abbcq, agrees better with ERA than SRES. Figures 59 (e) and (f) show that the differences in the wave number one amplitude between HRES (abbcq) and HRES(abbcp) and between HRES (abbcq) and SRES show many similarities in the northern hemisphere upper troposphere. This suggests that the form of the orography used in the simulation is having an impact on the atmospheric waves.

5.2 Variability

Section 5.1 has shown that changing the resolution of the orography at HRES has some impact on the mean circulation. Impact on the variability has been examined by looking at 500 hPa heights. Figure 60 shows the band pass and low pass fields for abbcp i.e. 5 years as opposed to the 10 years shown in figs 46-49. Comparing fig 60 (a) and (b) with fig 46 for band pass DJF it is clear that abbcp is closer SRES than HRES in both hemispheres. This suggests that some of the features are due to the orographic forcing and not the resolution. In JJA, Figs 60 (c) and (d) and Fig 47, abbcp in the south Pacific is closer to SRES though

the South Atlantic and Indian ocean are close to the original HRES.

The low pass filtered heights for abbcp figures 60(e) & (f) are different from the other runs, figure 48, particularly between 0°-60°W in the southern hemisphere. Figures 60(g) and (h) for JJA, and figure 49 show a greater similarity between SRES and abbcp in the southern Pacific.

Conclusions

On the whole increasing the horizontal resolution of the model improves agreement with climatology. The main changes and improvements come at mid-latitudes in the region of the storm tracks. At the higher resolutions the model is better able to resolve synoptic scale disturbances. As the depressions are better resolved the transient eddy fluxes increase in magnitude tending to improve agreement with ERA. The amount of ascent and descent increases, more moisture condenses increasing the latent heat release, the troposphere warms and the relative humidity falls. As might be expected there is more large-scale resolved precipitation and less parametrized convective precipitation as the resolution of the model increases. The tropospheric warming is not uniform and therefore the equator to pole temperature gradient alters, which together with changes in the northward transport of angular momentum helps account for poleward movement of the westerly jets. The polewards shift of the westerly jets in accompanied by changes in the mean sea level pressure which reduce the high pressure bias over the north pole. Many of the changes in the mean fields agree with the earlier study using HadAM2b and 19 levels (Stratton 1999) suggesting that the increase in vertical resolution and changes to some of the physical parametrizations have not significantly altered the models response to increased horizontal resolution.

Not only the mean fields improve with resolution. The northern and southern hemisphere blocking improves as does the simulation of the storm tracks and low frequency variability. This study shows that there is some indication that the simulation of the intraseasonal oscillation may be improved by increases resolution though changing the physics of the model i.e. HadAM2b to HadAM3 has an impact. Although the HadAM3 simulations are longer i.e. 17 years there is still no clear evidence of any resolution dependence in the models response to the SST forcing.

Changes in the ocean surface fluxes in the tropics and mid-latitudes, see section 3.6, suggest that a coupled model using a higher resolution HadAM3 atmosphere may behave in a different way. Most of the biases in the ocean heat fluxes have not improved with resolution and therefore without further tuning a coupled model using the higher resolution atmosphere may well give a worse simulation. On the other hand the wind stresses have improved at mid-latitudes.

Orography and it impact on atmosperic simulations is a complex subject. Results from this study suggest that changing orography as the resolution is increased has only a small impact on the large scale circulation, but that small impact is significant and may in a small way account for some of the differences seen between HRES and SRES. In particular in DJF in the northern hemisphere the reduction of pressure over the pole and the increase in pressure over the Atlantic and Pacific may be partly due to the increase in resolution of the orography. The mechanisms by which small changes in the orography give rise to the large scale changes in the circulation seen in this study cannot be fully explained. It is also possible that some of the extra detail in the HRES orography is generating undesirable high frequency noise which may contribute to a worse large scale circulation.

Based on the results of this study there is clear evidience that SRES does not fully resolve synoptic scale systems. Moving to MRES gives an significant improvement in this area, reducing biases in the main dynamical fields like wind and temperature, and in variability. MRES also has less problem with resolving the Andes, see figs 19(c) & (d) showing the mountian torque. HRES provides further small improvements in many fields but the additional computing cost due to more gridpoints and a smaller timestep is probably not justified. More complex parametization schemes or even more vertical resolution may provide

a greater benefit. A further resolution half way between SRES and MRES i.e. 1.66° x 2.5° is currently being investigated to see whether this will provide most of the benefits of MRES but at less computional cost.

Acknowledgements

S Wilson for obtaining the NCEP climatological data from various sources. V D Pope for her comments on earlier version of this work. This work was funded by the Public Meteorological Service Research and Development Programme.

References

Barkstrom, B., Harrison, E., Smith, G., Green, R., Kibler, J. and Cess, R., 1989. Earth Radiation Budget Experiment (ERBE) archival and April 1985 results. Bull Am. Met Soc., 70, 1254-1262.

Blackmon, M. L., Wallace, J.M., Lau, N-C. and Mullen, S.L., 1977. An observational study of the northern hemisphere wintertime circulation. J. Atom. Sci. 34, 1040-1053.

Boer G J, Lazare M (1988) Some results concerning the effect of horizontal resolution and gravity-wave drag on simulated climate. J Clim 1: 780-806.

Boville, B.A., 1991, Sensitivity of simulated climate to model resolution. J. Clim. 4, 469-485.

Boyle, J.S., 1993, Sensitivity of dynamical quantities to horizontal resolution for a climate simulation using the ECMWF (cycle 33) Model. J. Clim. 6, 796-815.

Chen M, Bates J R (1996) A comparison of climate simulations from a semi-Lagrangian and an Eulerian GCM. J Clim 9:1126-1149.

Da Silva, A.M., Young, C.C. and Levitus, S., 1994, Atlas of surface marine data 1994. Volume 1: Algorithms and procedures. NOAA Atlas NESDIS 6.

Deque, M. and Piedelievre, J.P., 1995, High resolution climate simulation over Europe. Clim Dyn. 11, 321-339.

Gates W L (1992) AMIP: the atmospheric Model Intercomparison Project. Bull Am Meteorol Soc 73: 1962-1970.

Gibson J K, Kallberg P, Uppala S, Nomura A, Hernadez A, Serrano E (1997) ERA description, ECMWF re-analysis project report series 1, ECMWF, Reading , UK.

Hack J J, Kiehl J T, Hurrell J W (1998) The hydrostatic and thermodynamic characteristics of the NCAR CCM3. J Clim 11: 1179-1205.

Harrison, E. F., Minnis, P., Barkstrom, B.R., Ramanathan, V., Cess, R.D. and Gibson, G.G, 1990. Seasonal variation of cloud radiative forcing derived from the Earth Radiation Budget Experiment. J. Geophys. Res., 95, 18687-18703.

Hellerman, S. and Rosenstein, M (1983) Normal wind stress over the world ocean with error estimates. J. Oceanog 13: 1043-1104.

Held I M and Suarez M J, 1994, Aproposal for the intercomparison of dynamical cores of atmospheric general circulation models. Bull Am Met Soc 75: 1825-1830.

Hurrell J W, Hack J J, Boville B A, Williamson D L, Kiehl J T (1998) The dynamical simulation of the NCAR community climate model version 3 (CCM3). J Clim 11: 1207-1236

Jones, R. G., Murphy, J. M. and Noguer, M., 1995. Simulation of climate change over Europe using a nested regional-climate model. I: Assessment of control climate, including sensitivity to location of lateral boundaries. Q.J.R. Meteorol. Soc. 121, 1413-1449.

Kalnay, E, Kanamitsu, M, Kistler R, Collins W, Deaven D, Gandin L, Iredell M, Saba S, White G, Woollen J, Zhu Y, Leetmaa, A, Reynolds R, Chelliah M, Ebisuzaki W, Higgins W, Janiwiak J, Mo K C, Popelewski C, Wang J, Jenne R, Joseph D (1996) The NCEP/NCAR 40-year reanalysis project. Bull Am. Met Soc 77:437-471.

Keihl, J.T. and Williamson, D.L., 1991, Dependence of cloud amount on horizontal resolution in the national centre for atmospheric research community climate model. J. Geophys. Res. 96, 10955-10980.

Legates, D.R. and Willmott, C.J., 1990b. Mean seasonal and spatial variability in global surface air temperature. Theor. and Appl. Clim. 41, 11-21.

Phillips, T.J., Corsetti, L.C. and Grotch S.L., 1995, The impact of horizontal resolution on moist processes in the ECMWF model. Clim dyn 11: 85-102.

Pope V D, Gallani M L, Rowntree P R, Stratton R A (1999) The impact of new physical parametrizations in the Hadley Centre climate model -HadAM3. Submitted to Clim Dyn.

Pope V D, Jackson D R, Pamment JA (2000) The effects of increasing vertical resolution on the simulation of the tropospheric climate in a global GCM. In preparation

Rasch P J, Williamson D L (1991) The sensitivity of a general circulation model climate to the moisture transport formulation. J Geophys Res 96: 123-137.

Slingo A, Pamment J A, Webb M J (1998) A 15-year simulation of the clear-sky greenhouse effect using ECMWF - re-analyses : Fluxes and comparisons with ERBE. J Clim 11:690-708.

Slingo J M, Sperber K R, Boyle J S, Ceron J-P, Dix M, Dugas B, Ebisuzaki W, Fyfe J, Gregory D, Guereny J-F, Hack J, Harzallah A, Inness P, Kitoh A, Lau W K-M, McAvaney B, Madden R, Mathews A, Palmer T N, Park C-K, Randall D, Renno N (1996) Intraseasonal oscillations in 15 atmospheric general circulation models: results from an AMIP diagnostic sub-project. Clim Dyn 12:325-357.

Stendal M, Roeckner E (1998) Impacts of horizontal resolution on simulated climate statistics in ECAM4. MPI report no 253.

Stratton R A (1996) A high resolution AMIP run using the Hadley Centre model HadAM2b. UK Met Office, CRTN 77.

Stratton R A (1999) A high resolution AMIP integration using the Hadley Centre model HadAM2b. Clim Dyn 15:9-28.

Tibaldi, S. and Molteni, F., 1990, On the operational predictability of blocking. Tellus 42A, 343-365.

Ulbrich U and Speth, P. (1991) The global energy cycle of stationary and transient atmospheric waves: results from ECMWF analyses. Meteorol Atmos Phys 45: 125-138.

Webster S, 1999, Report on smooth orography. Hadley Centre internal report. UK Met Office.

Williamson, D.L., Keihl, J.T. and Hack, J.J., 1995, Climate sensitivity of the NCAR community climate model (CCM2) to horizontal resolution. Clim. Dyn. 11, 377-397.

Xie P, Arkin P A, (1997) Global precipitation: a 17-year monthly analysis based on gauge observations, satellite estimates, and numerical model output. Bull Am Met Soc 78: 2539-2558.

Figures

1. Zonal mean cross-sections of the U component of wind for; HRES (a) DJF, (b) JJA; HRES minus MRES (c) DJF, (d) JJA; MRES minus SRES (e) DJF, (f) JJA; HRES minus ERA for (g) DJF, (h) JJA; NCEP minus ERA for (i) DJF, (j) JJA. Contours every 5 or 2 m/s.
2. As fig 1 but for the V component of wind. Contours every 0.5 or 0.2 m/s.
3. As fig 1 but for vertical velocity. Contours every 0.005 or 0.002 Pa/s.
4. Velocity potential at 200 hPa for DJF (a) HRES, (b) HRES minus ERA, (c) HRES minus MRES, (d) MRES minus SRES. Contours every 2 or 1 .
5. As Fig 4 but for JJA.
6. Zonal mean sea level pressure for all resolutions and ERA (a) DJF, (b) JJA.
7. Mean sea level pressure for DJF (a) HRES, (b) HRES minus ERA, (c) HRES minus MRES, (d) MRES minus SRES. Contours every 4 or 2 hPa.
8. As Fig 7 but for JJA.
9. As fig 1 but for temperature. Contours every 10 or 1 K
10. Zonal mean specific humidity for the top model levels. (a) HRES for DJF, (b) HRES for JJA, (c) HRES minus MRES for DJF, (d) HRES minus MRES for JJA, (e) MRES minus SRES for DJF, (f) MRES minus SRES for JJA. Contours every 0.2e-6.
11. As fig 1 but for specific humidity. Contours every 0.001 or 0.0002 kg/kg.
12. Zonal mean model minus ERA total column water for (a) DJF , (b) JJA
13. As fig 1 but for relative humidity. No ERA NCEP comparison plotted. Contours every 5 or 2 %.
14. As fig 1 but for transient vertical velocity. Contours every 5 or 2 m/s.
15. Zonal mean transient vertical velocity for (a) HRES (abbcq) DJF, (b) HRES (abbcq) JJA, (c) HRES (abbcq) minus abbcp over land DJF, (d) HRES (abbcq) minus abbcp over land JJA, (e) HRES minus SRES over land DJF, (f) HRES minus SRES over land JJA, (g) HRES (abbcq) minus abbcp over sea DJF, (h) HRES (abbcq) minus abbcp over sea for JJA, (i) HRES minus SRES over sea for DJF, (j) HRES minus SRES over sea for JJA.
16. As fig 1 but for eddy kinetic energy.
17. The seasonal cycle of wave number one for 300hPa geopotential height, (a) SRES, (b) MRES, (c) HRES, (d) ERA.
18. Zonal mean relative angular momentum (a) DJF, (b) JJA.
19. Zonal mean components of the total torque. Surface stress torque (a) DJF, (b) JJA. Mountain torque (c) DJF (d) JJA. Gravity wave drag torque (e) DJF (f) JJA.
20. Zonal mean integrated northward momentum flux for DJF (a) &(b) total, (c) & (d) zonal, (e) & (f) stationary, (g) & (h) transient.
21. As fig 1 but for transient eddy momentum (uv) flux.
22. As fig 1 but for transient eddy VT
23. As fig 1 but for transient eddy wT
24. As fig 1 but for Transient wq
25. As fig 1 but for Transient vq
26. Precipitation for DJF (a) HRES (b) HRES - MRES, (c) MRES - SRES, (d) HRES - CMAP.
27. As figure 26 but for JJA.
28. Zonal mean layer cloud. (a) HRES for DJF, (b) HRES for JJA, (c) HRES minus MRES for DJF, (d) HRES minus MRES for JJA, (e) MRES minus SRES for DJF, (f) MRES minus SRES.

29. As fig 28 but for zonal mean convective cloud.
30. As fig 28 but for zonal mean cloud liquid water.
31. As fig 28 but for zonal mean cloud ice water.
32 Zonal annual mean downward radiation at the top of the atmosphere model minus ERBE.
33. Zonal mean model minus ERBE for albedo (a) DJF , (b) JJA.
34. As fig 33 but for top of the atmosphere outgoing OLR.
35. As fig 33 but for shortwave cloud forcing.
36. As fig 33 but for longwave cloud forcing.
37. 1.5m temperature for DJF (a) HRES (b) HRES - MRES, (c) MRES - SRES, (d) HRES - Legates & Willmott.
38. As 37 but for JJA.
39. Zonal means over land for; canopy water (a) DJF (b) JJA, soil moisture (c) DJF (d) JJA.
40. Zonal mean over land for; precipitation (a) DJF, (b) JJA, evaporation (c) DJF, (d) JJA, runoff (e) DJF, (f) JJA.
41. Zonal mean wind stress over the ocean for (a) u component for DJF (b) u component for JJA, (c) v component for DJF, (d) v component for JJA.
42. Zonal mean net downward surface heating (a) annual mean, (b) DJF, (c) JJA.
43. The four components of the annual mean surface heating over the oceans (a) shortwave, (b) longwave, (c) sensible heat and (d) latent heat.
44. Northern hemisphere blocking index for (a) DJF, (b) MAM , (c) JJA, (d) SON.
45. Southern hemisphere blocking index as fig 44.
46. Band pass filtered 500 hPa heights for DJF (a) HRES northern hemisphere, (b) HRES southern hemisphere, (c) MRES northern hemisphere, (d) MRES southern hemisphere, (e) SRES northern hemisphere, (f) SRES southern hemisphere, (g) ERA northern hemisphere, (h) ERA southern hemisphere,
47. Same format as figure 46 but for JJA.
48. Same format as figure 46 but for DJF low pass filtered 500 hPa heights.
49. Same format as figure 46 but for JJA low pas filtered 500 hPa heights.
50. Space-time spectra for wave-number one in 200hPa velocity potential meaned between 5°N-5°S for (a) the three different resolutions and ERA, (b) ERA and different integrations at SRES.
51. Twelve month running mean anolmalies for the NINO 3 area for (a) SST, (b) clear-sky outgoing longwave radiation for CLERA and the model runs.
52. As fig 51 but for an area in the North Atlantic covering 40°-55°N, 10°-50°W.
53. As fig 51 but for an area in the North East Pacific covering 40°-50°N, 180°-210°E.
54. Standard deviation of mean sea level pressure for DJF covering the period 1979-88 for (a) HRES, (b) MRES, (c) SRES & (d) ERA.
55. As fig 54 but for JJA.
56. Mean sea level pressure difference for run abbch minus abbci with area of significant differences shaded. (a) DJF (b) JJA.
57. Orography for North America (a) HRES original, (b) HRES abbcp, (c) SRES.
58. Mean sea level pressure difference for run abbcp minus abbcq with area of significant differences shaded. (a) DJF (b) JJA.
59. Latitude pressure cross sections of wave amplitude 1 in geopotential height for DJF. (a) HRES run abbcq (b) HRES run abbcp, (c) SRES, (d) ERA, (e) abbcq minus abbcp (f) abbcq minus SRES.

60. Band pass and low pass 500 hPa heights for the HRES run abbcp for (a) & (b) band pass DJF, (c) & (d) band pass JJA, (e) & (f) low pass DJF, (g) & (h) low pass JJA.

Fig 1 Zonal mean cross-section of U

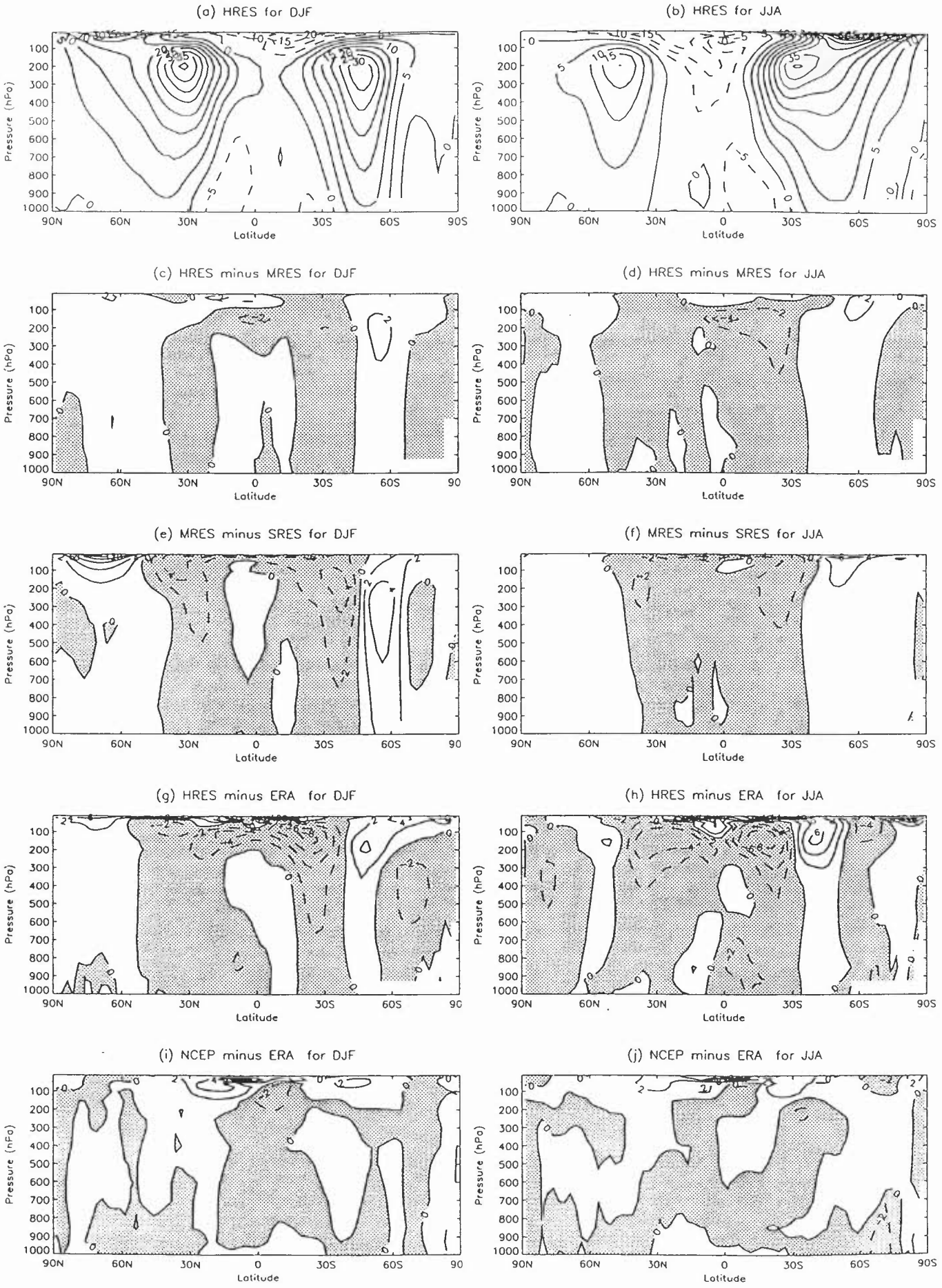

Fig 2 Zonal mean cross-section of V

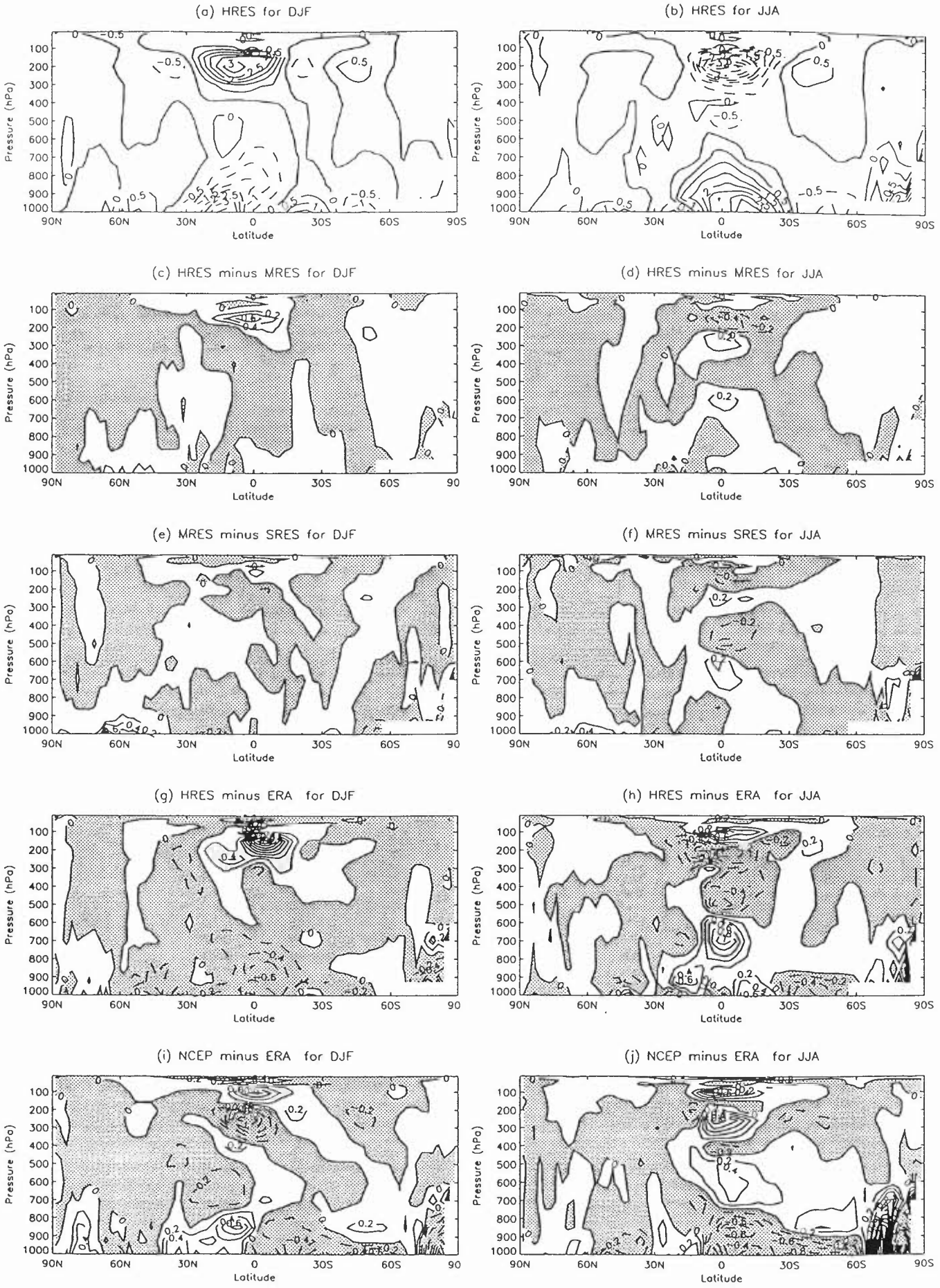

Fig 3 Zonal mean vertical velocity

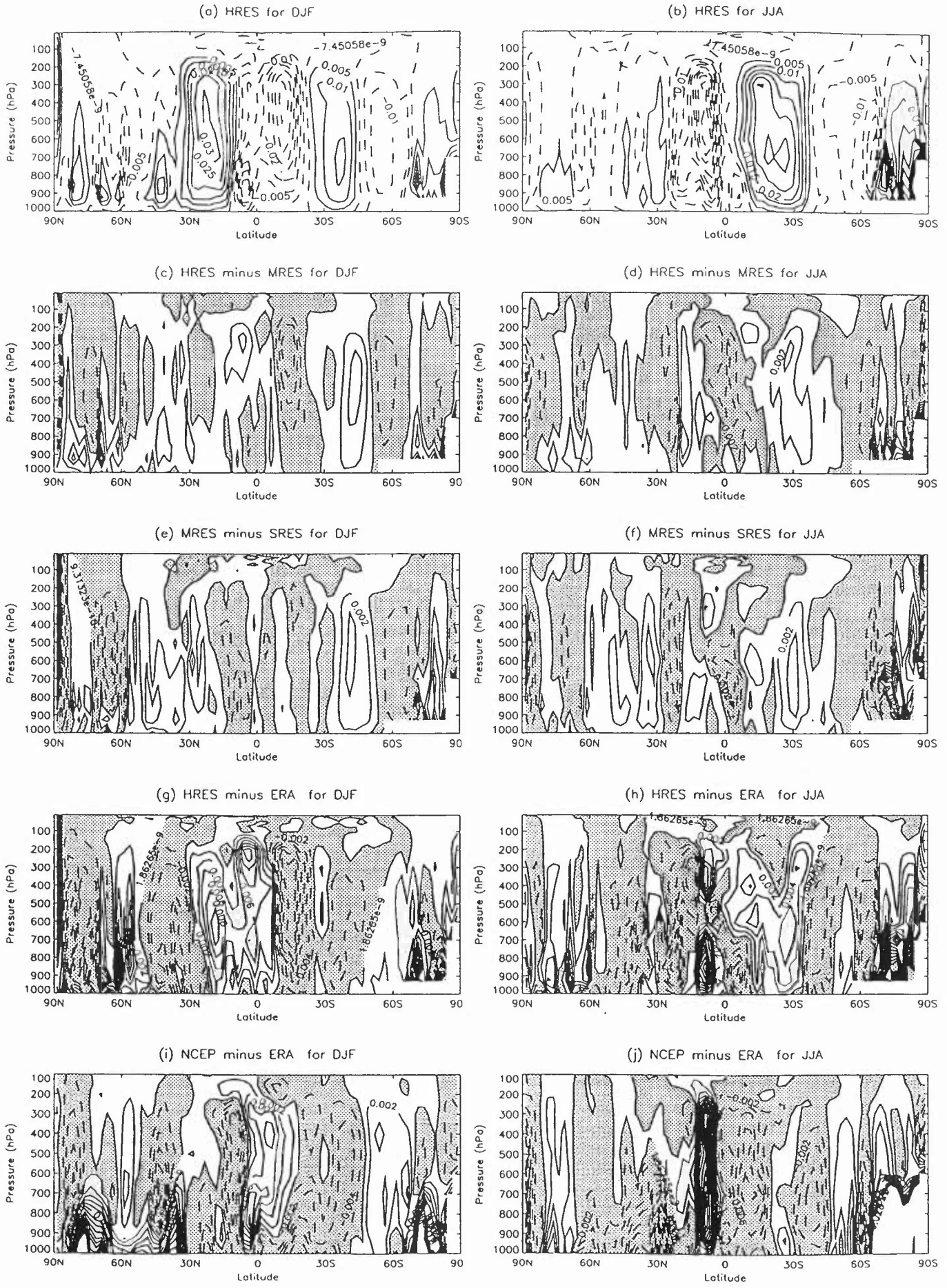

Fig 4 Velocity potential at 200.hPa from mean winds for djf

(a) HRES

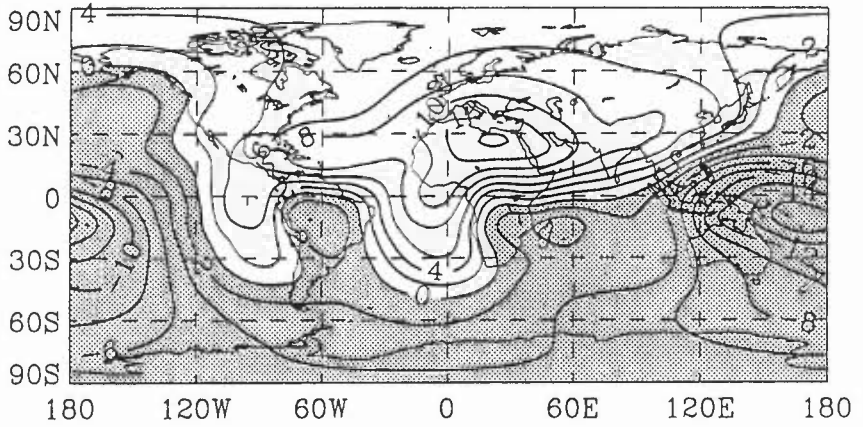

(b) HRES minus ERA

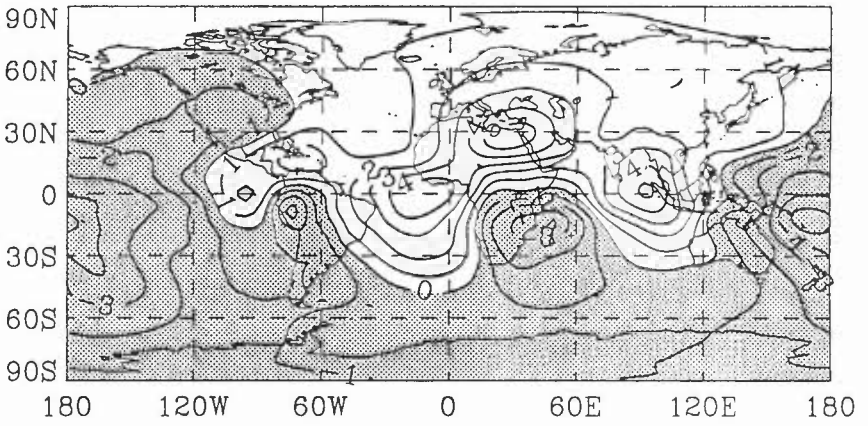

(c) HRES minus MRES

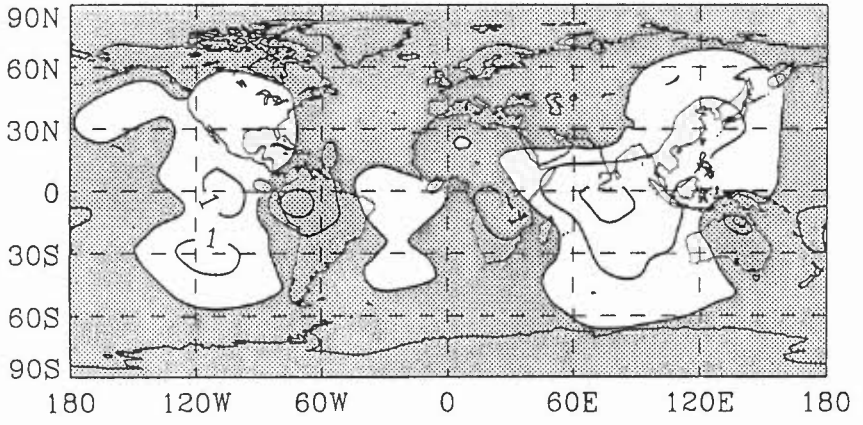

(d) MRES minus SRES

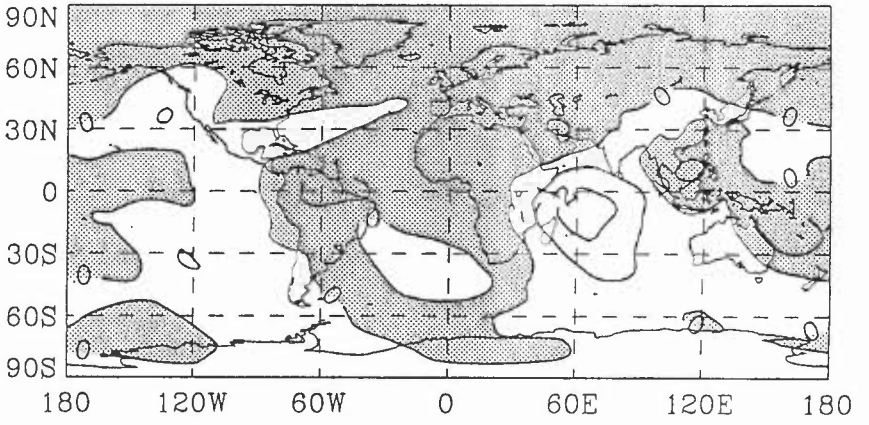

Fig 5 Velocity potential at 200.hPa from mean winds for jja

(a) HRES

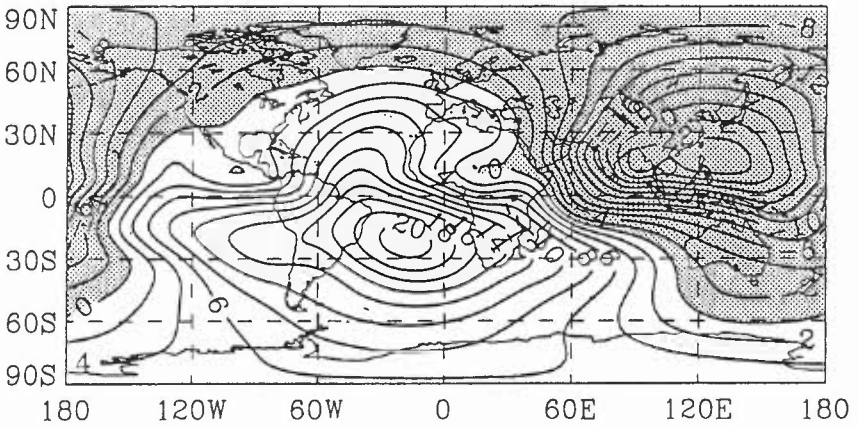

(b) HRES minus ERA

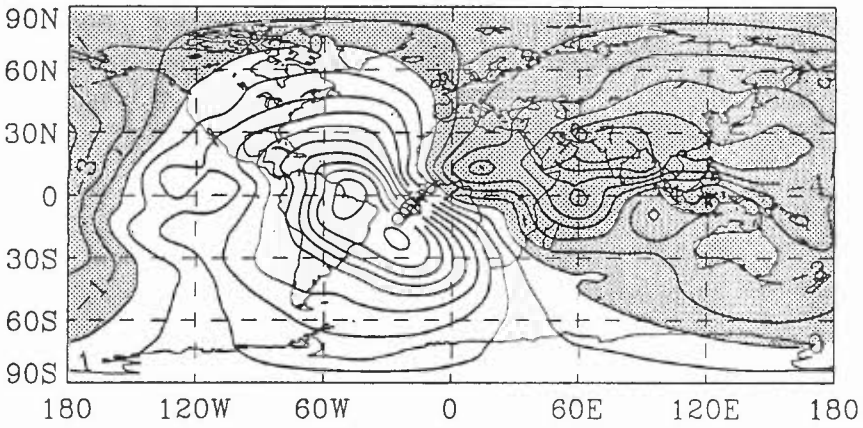

(c) HRES minus MRES

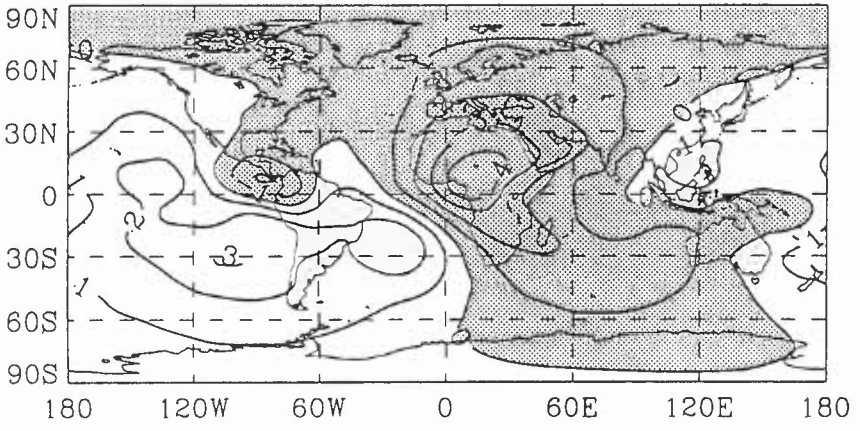

(d) MRES minus SRES

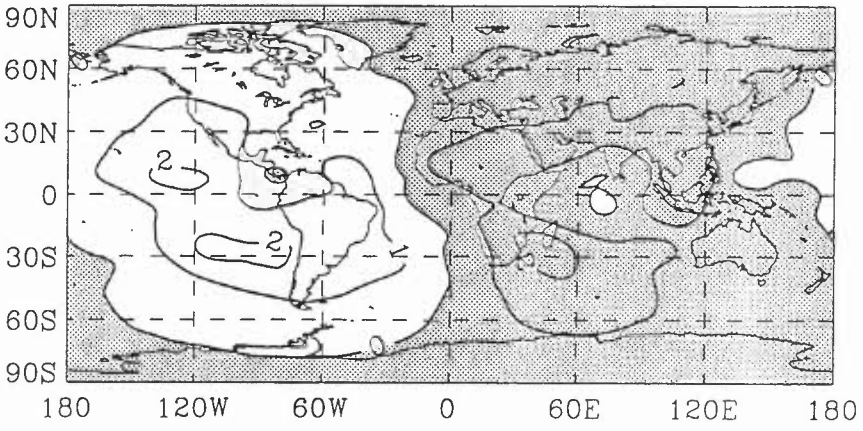

Fig 6 Zonal mean of mean sea level pressure

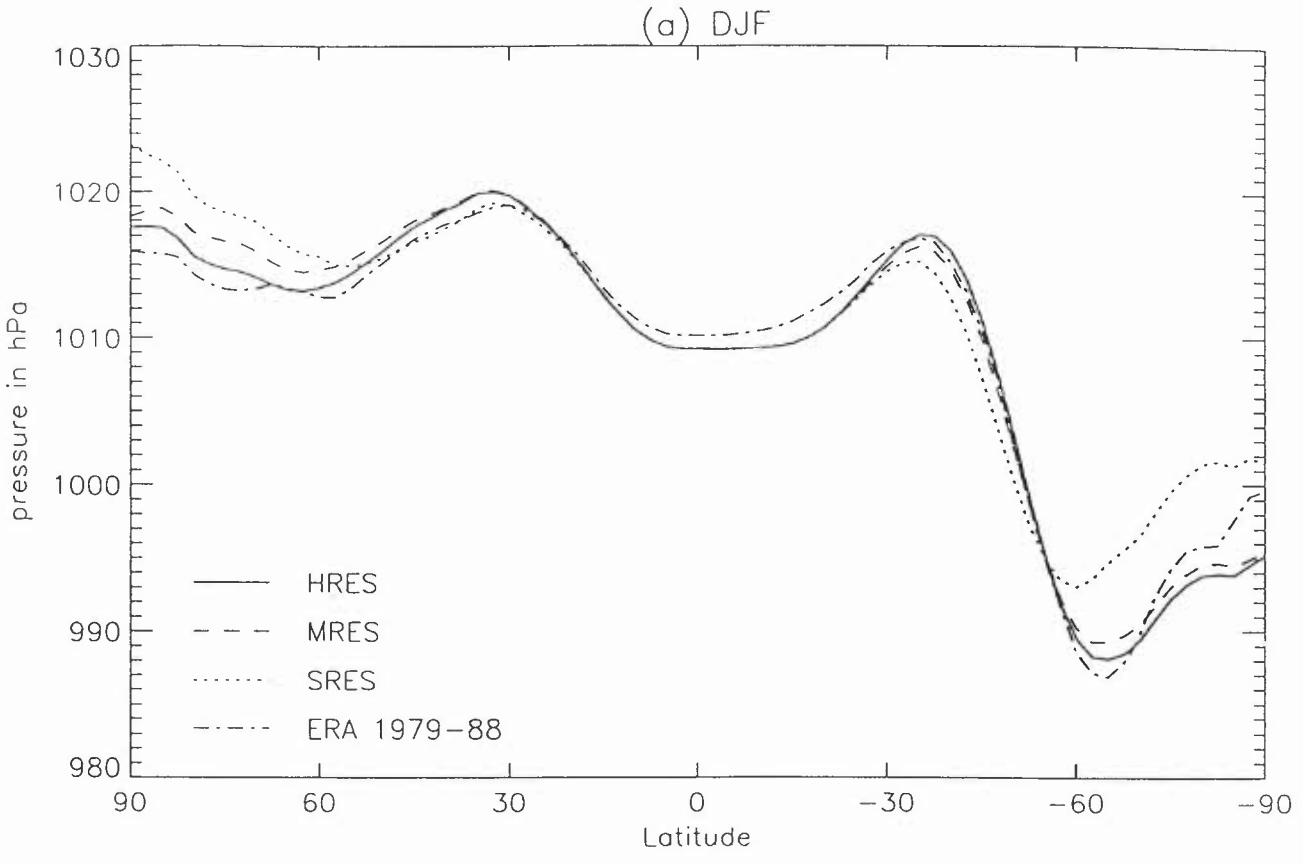

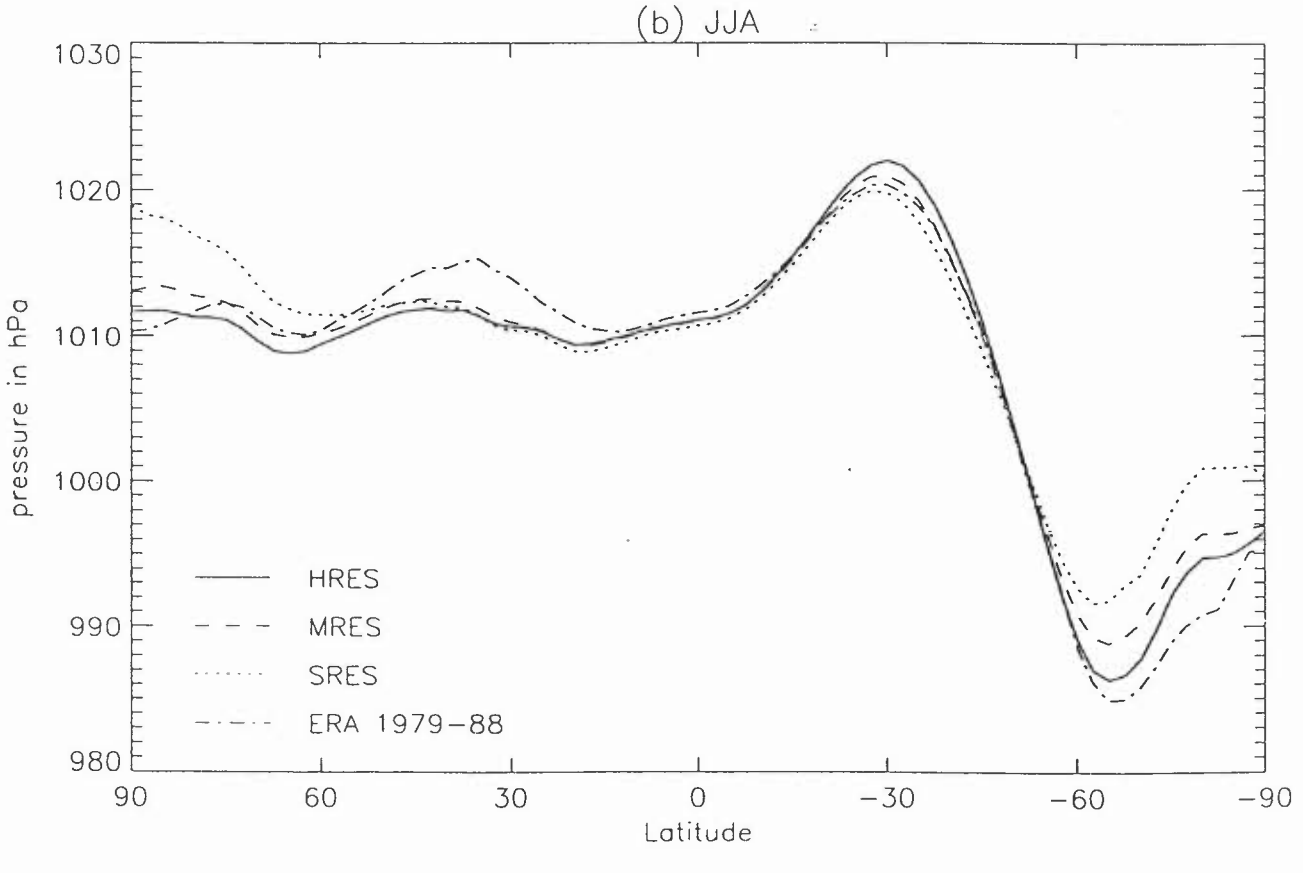

Fig 7 Mean sea level pressure for djf

(a) HRES

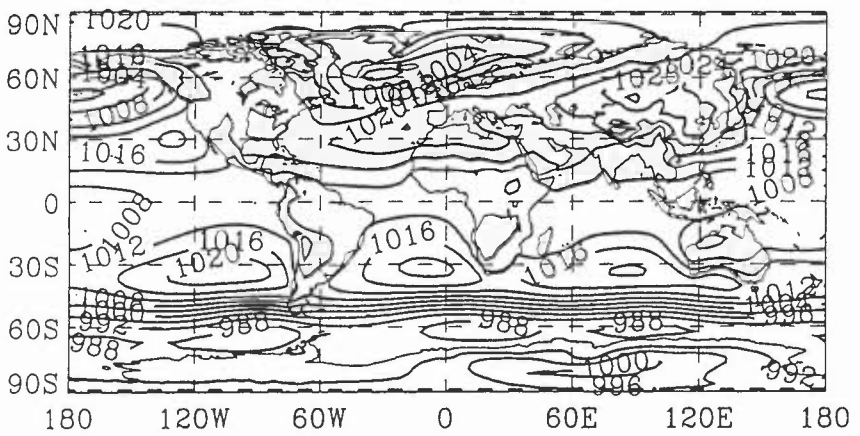

(b) HRES minus ERA 1979–88

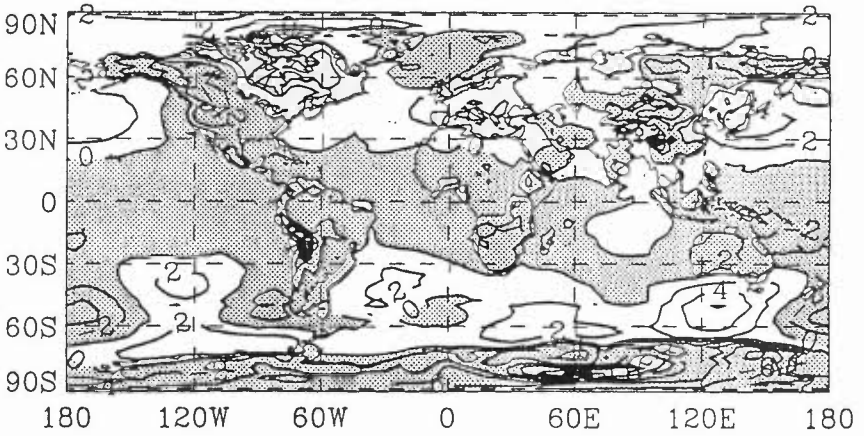

(c) HRES minus MRES

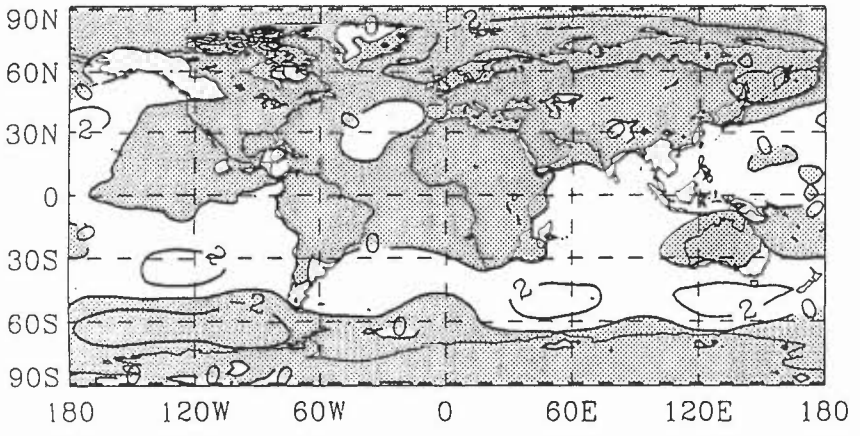

(d) MRES minus SRES

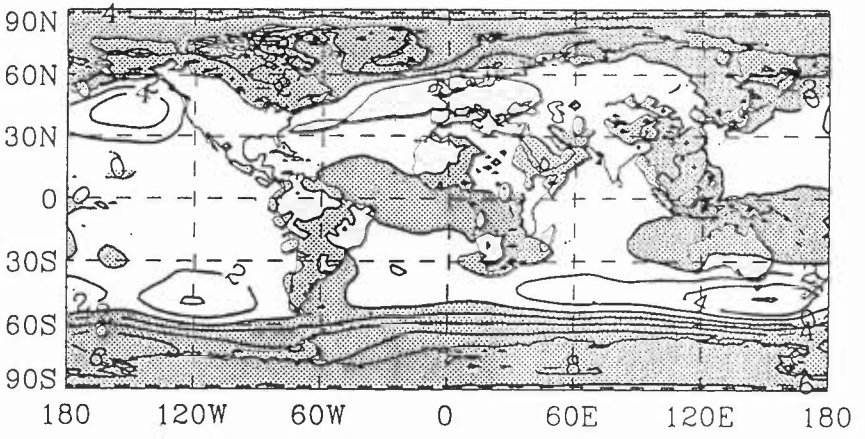

Fig 8 Mean sea level pressure for jja

(a) HRES

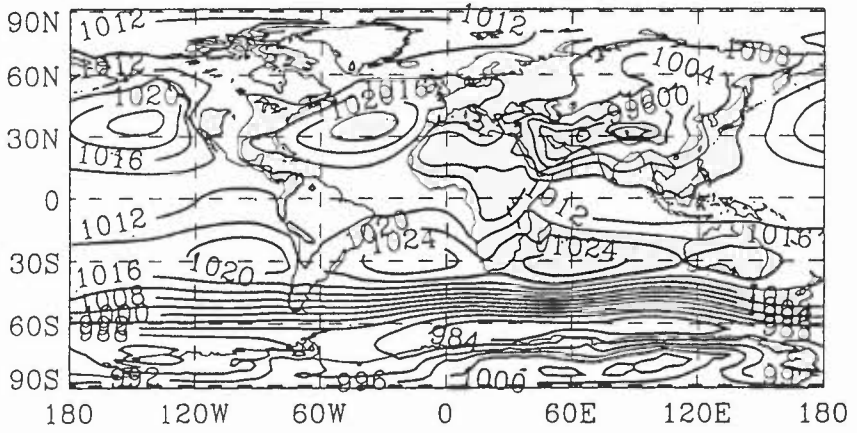

(b) HRES minus ERA 1979–88

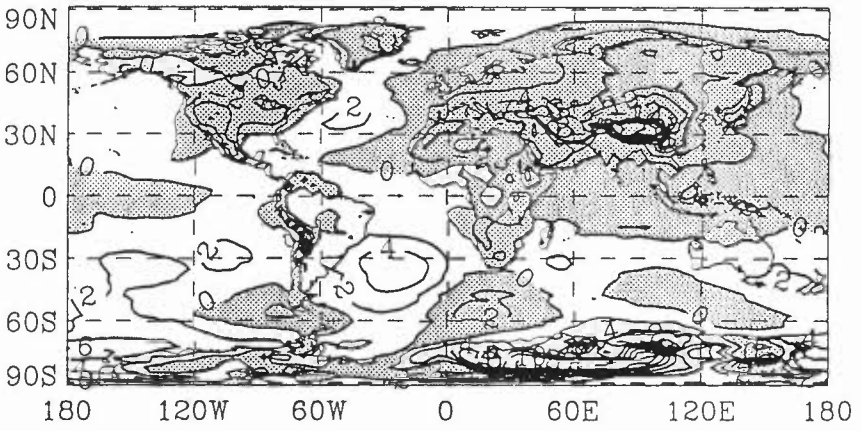

(c) HRES minus MRES

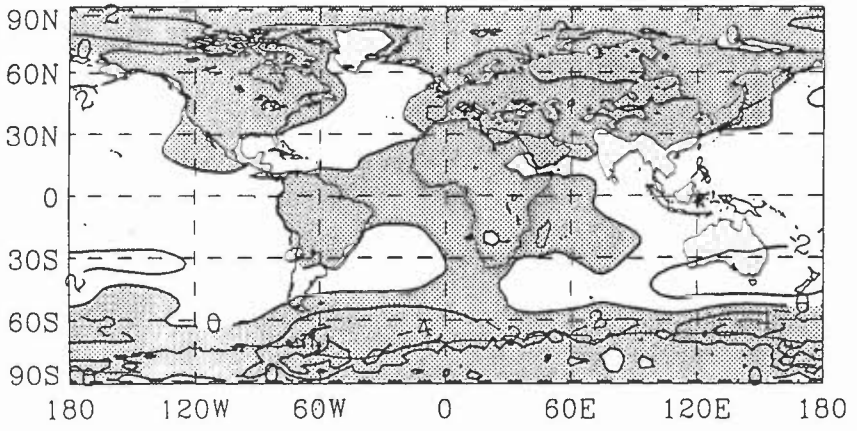

(d) MRES minus SRES

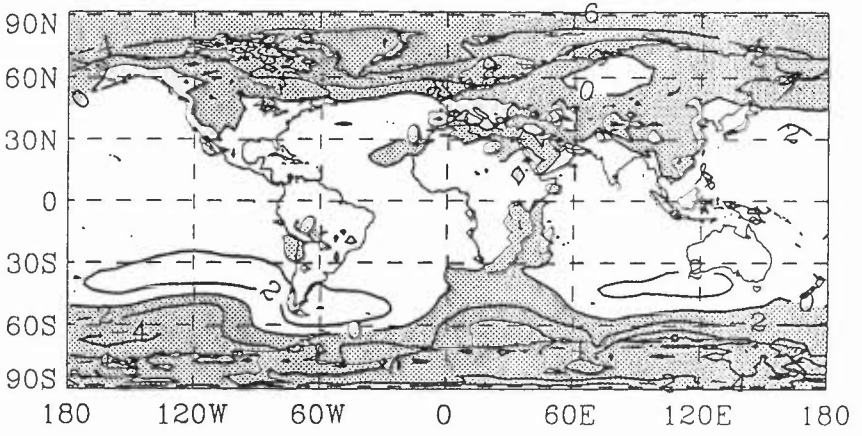

Fig 9 Zonal mean cross-section of temperature

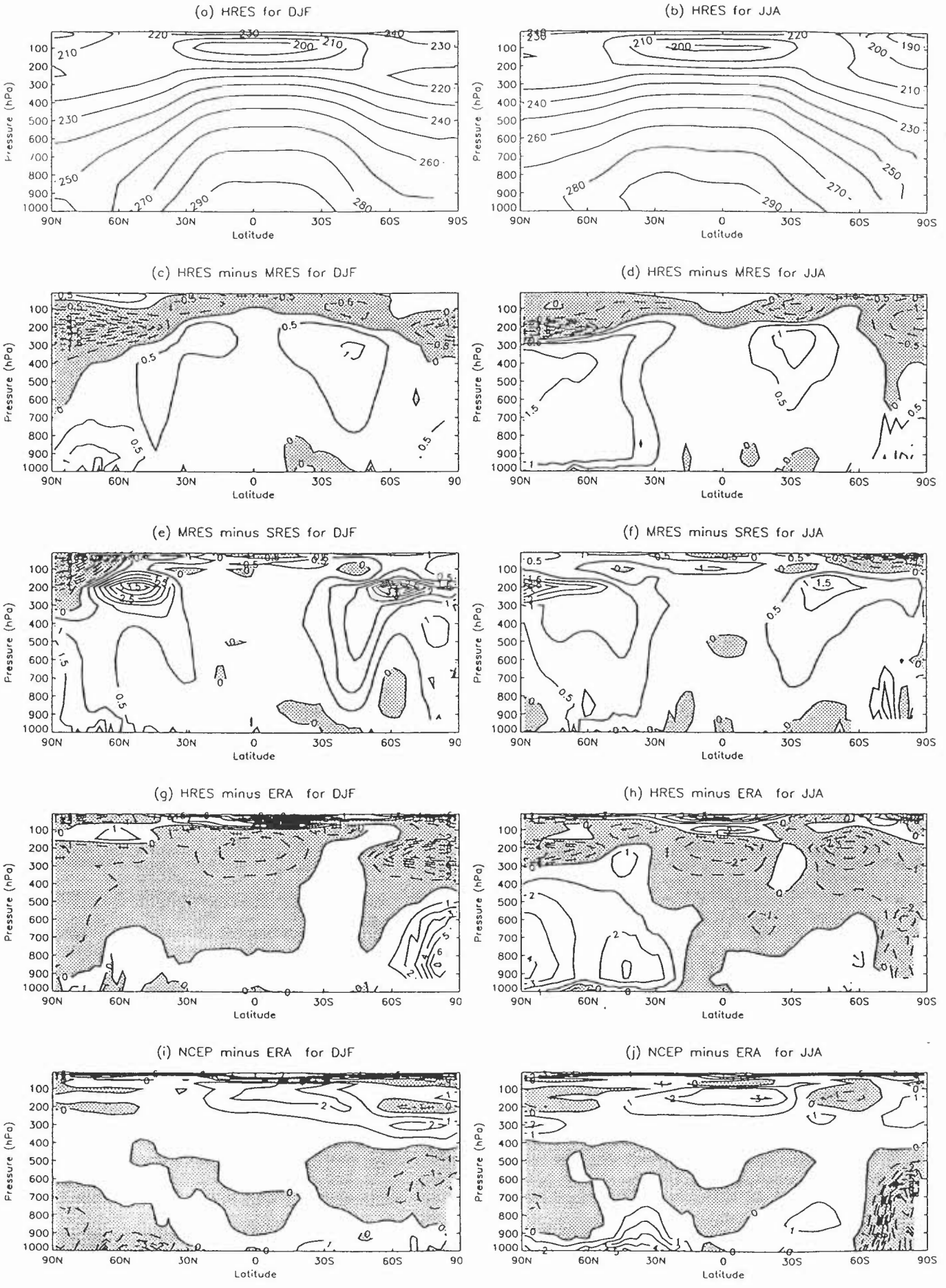

Fig 10 specific humidity

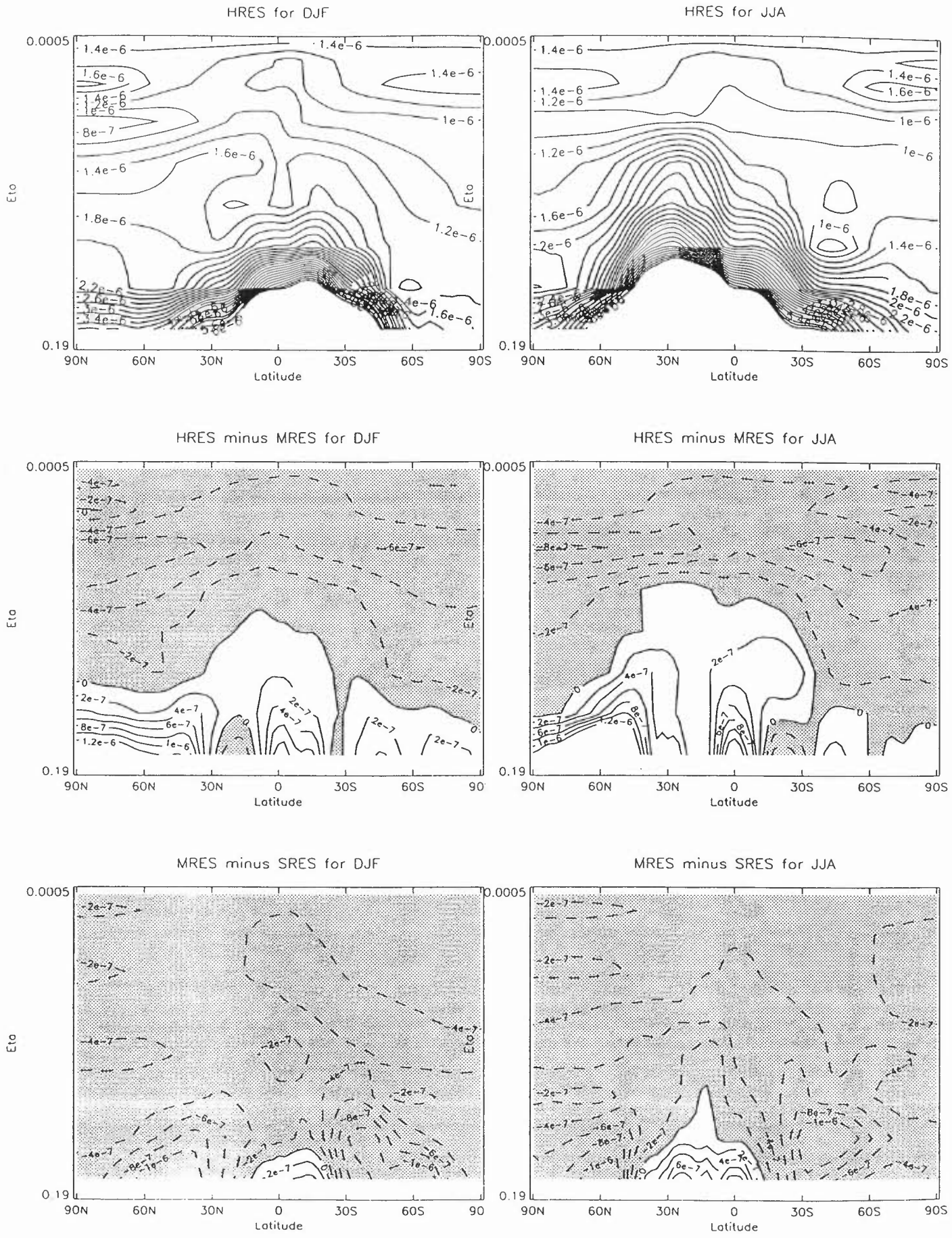

Fig 11 Zonal mean specific humidity

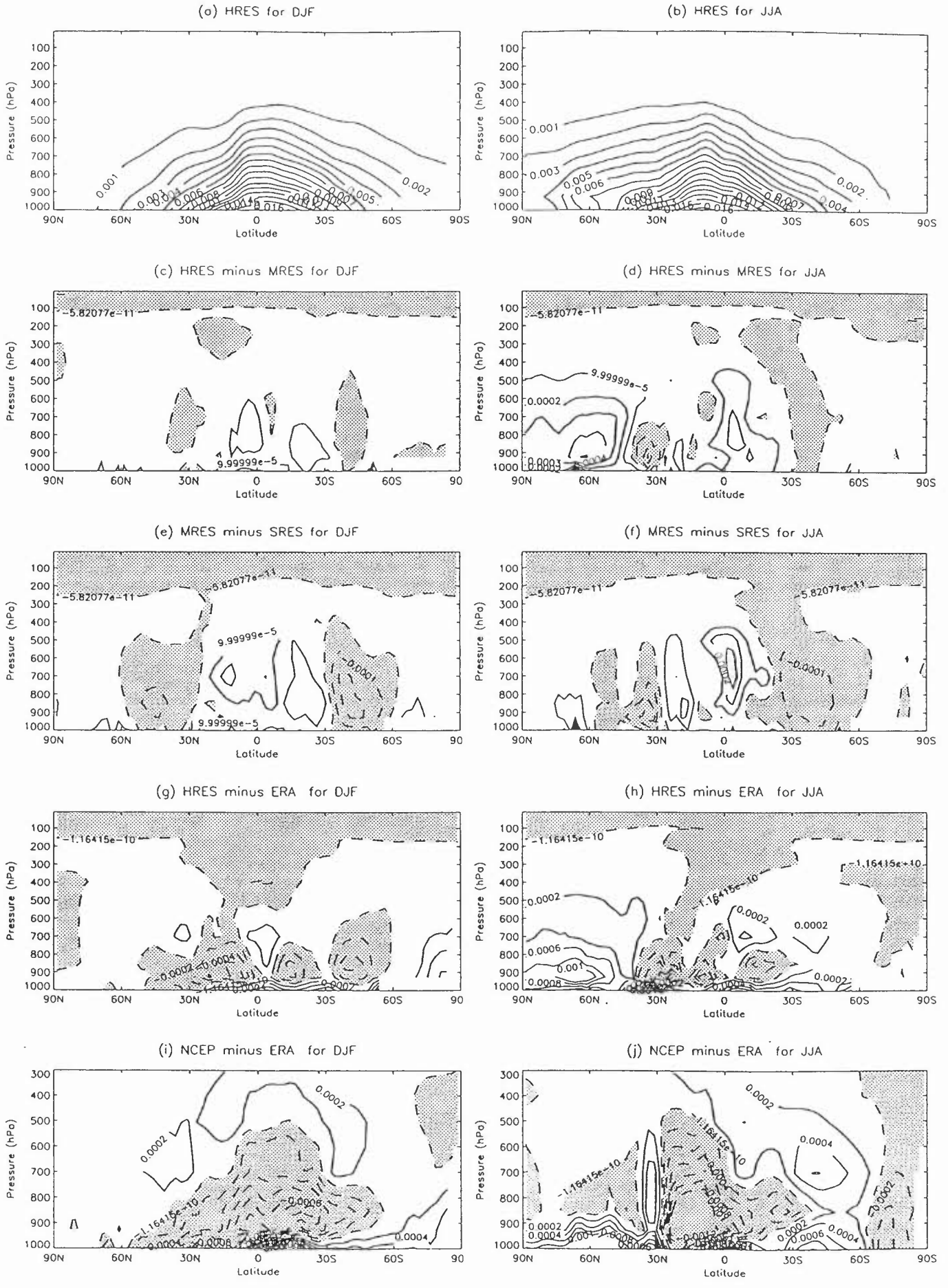

Fig 12 Total column water for

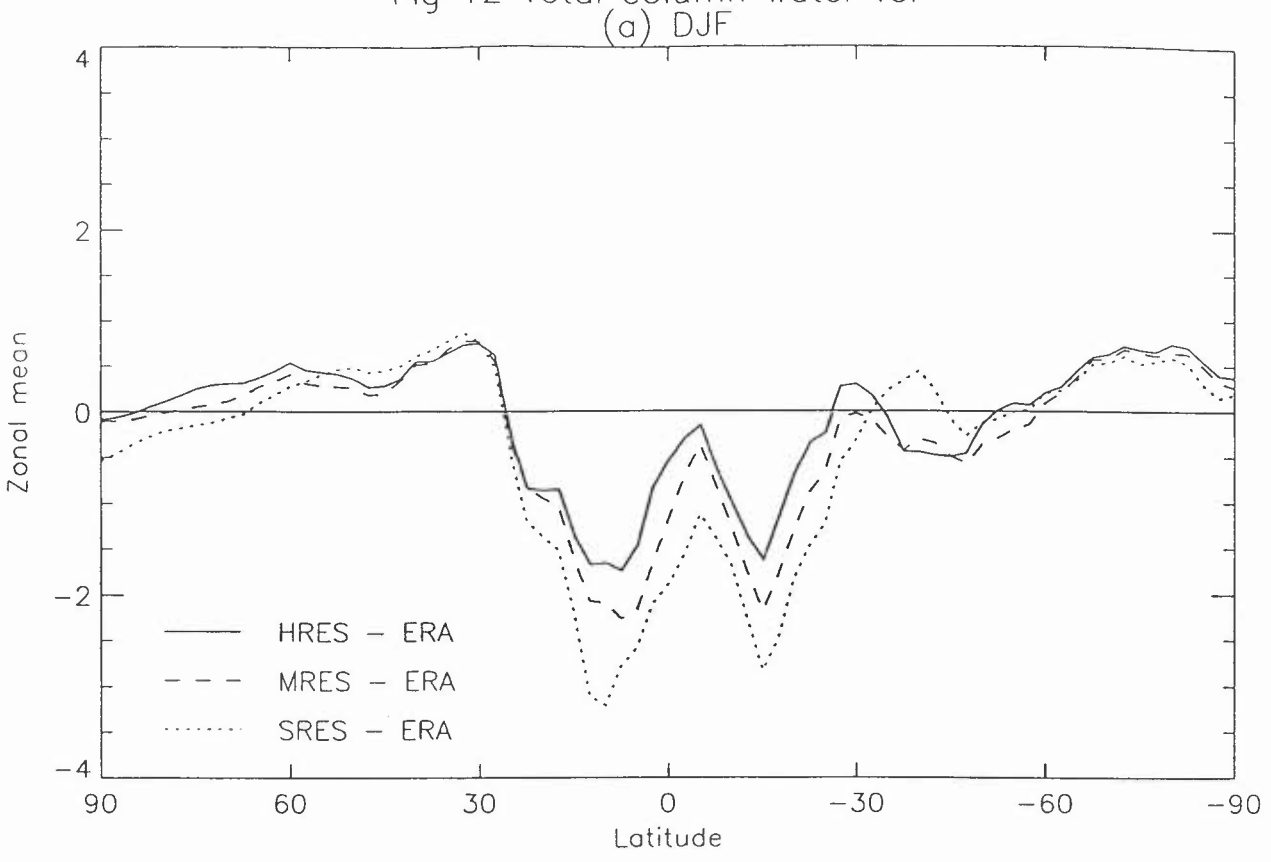

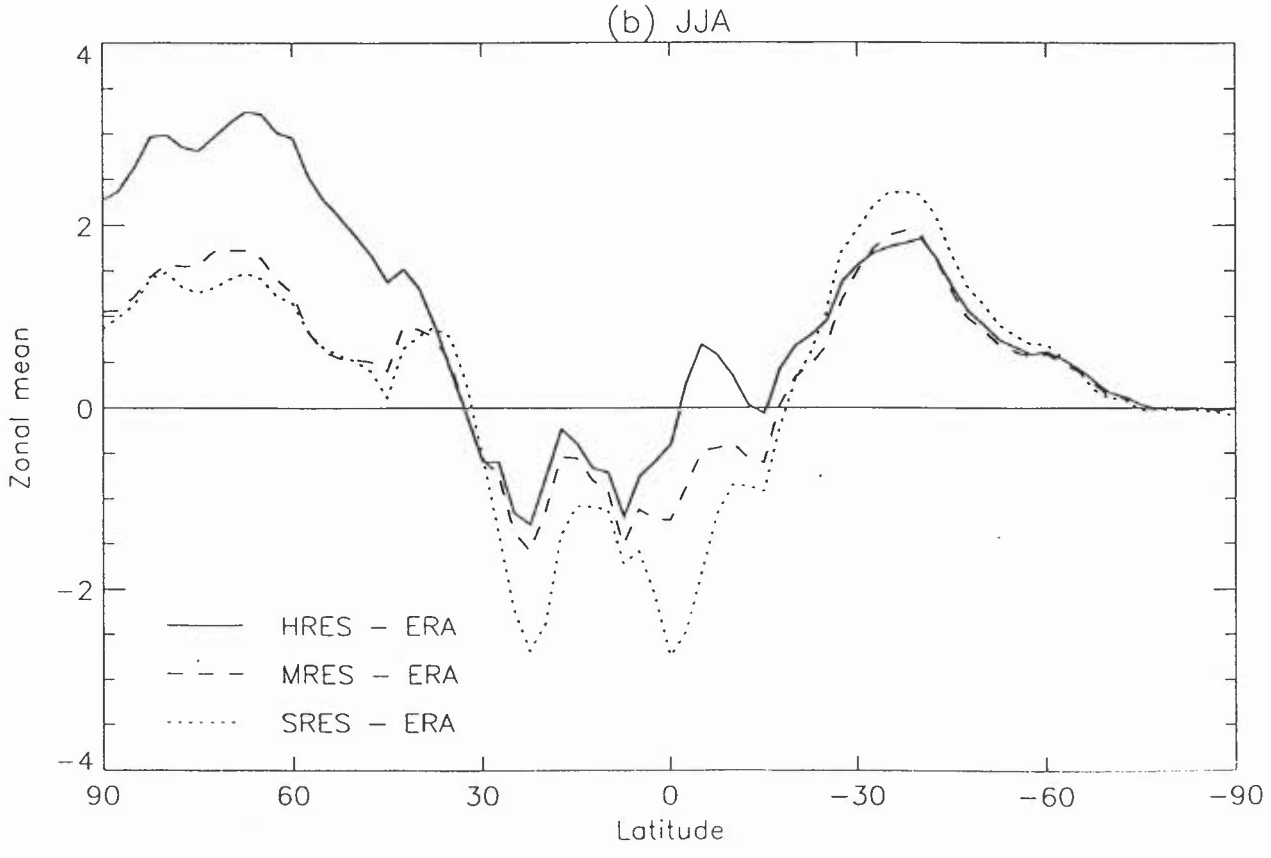

Fig 13 Zonal mean relative humidity

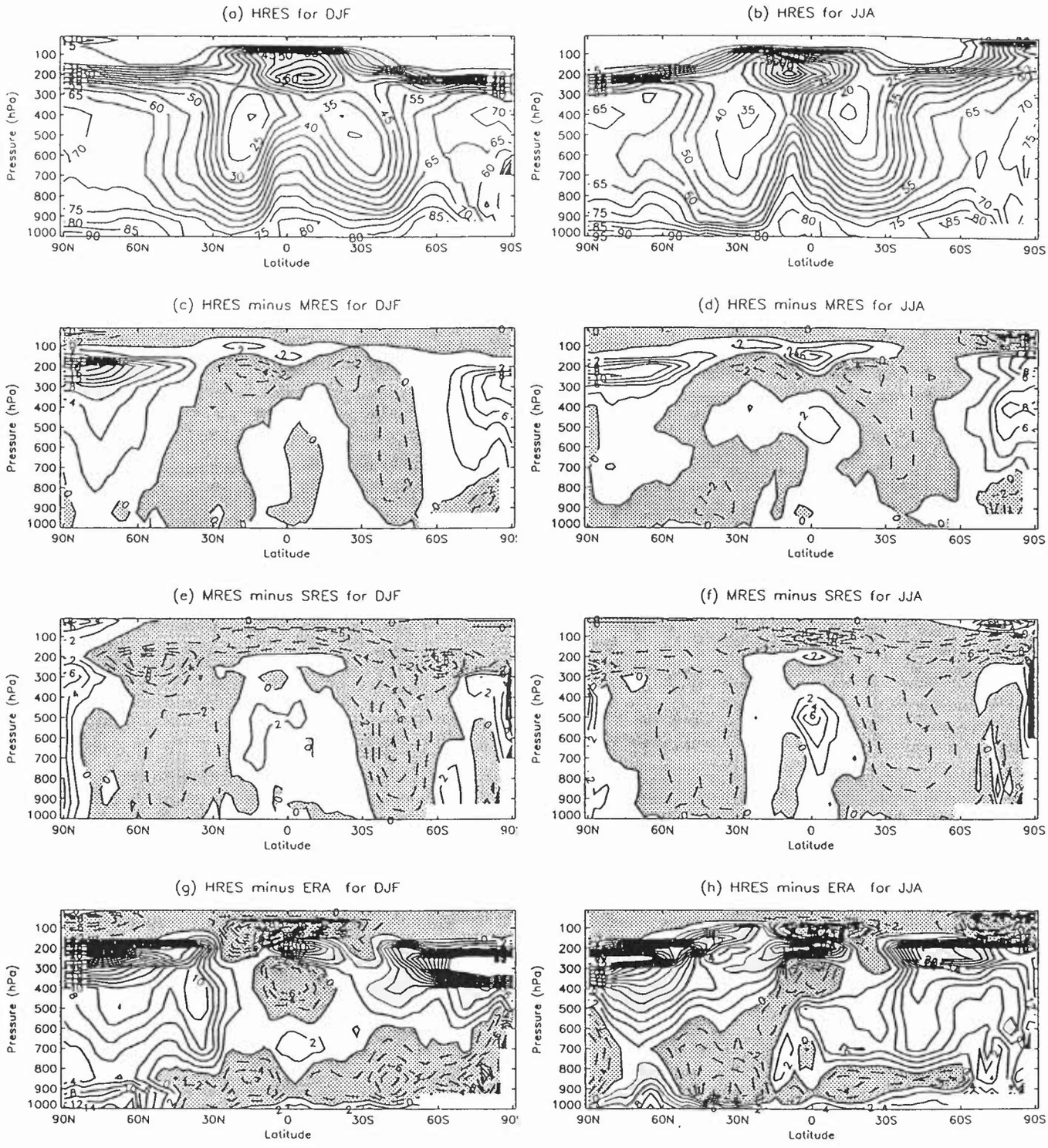

Fig 14 transient w

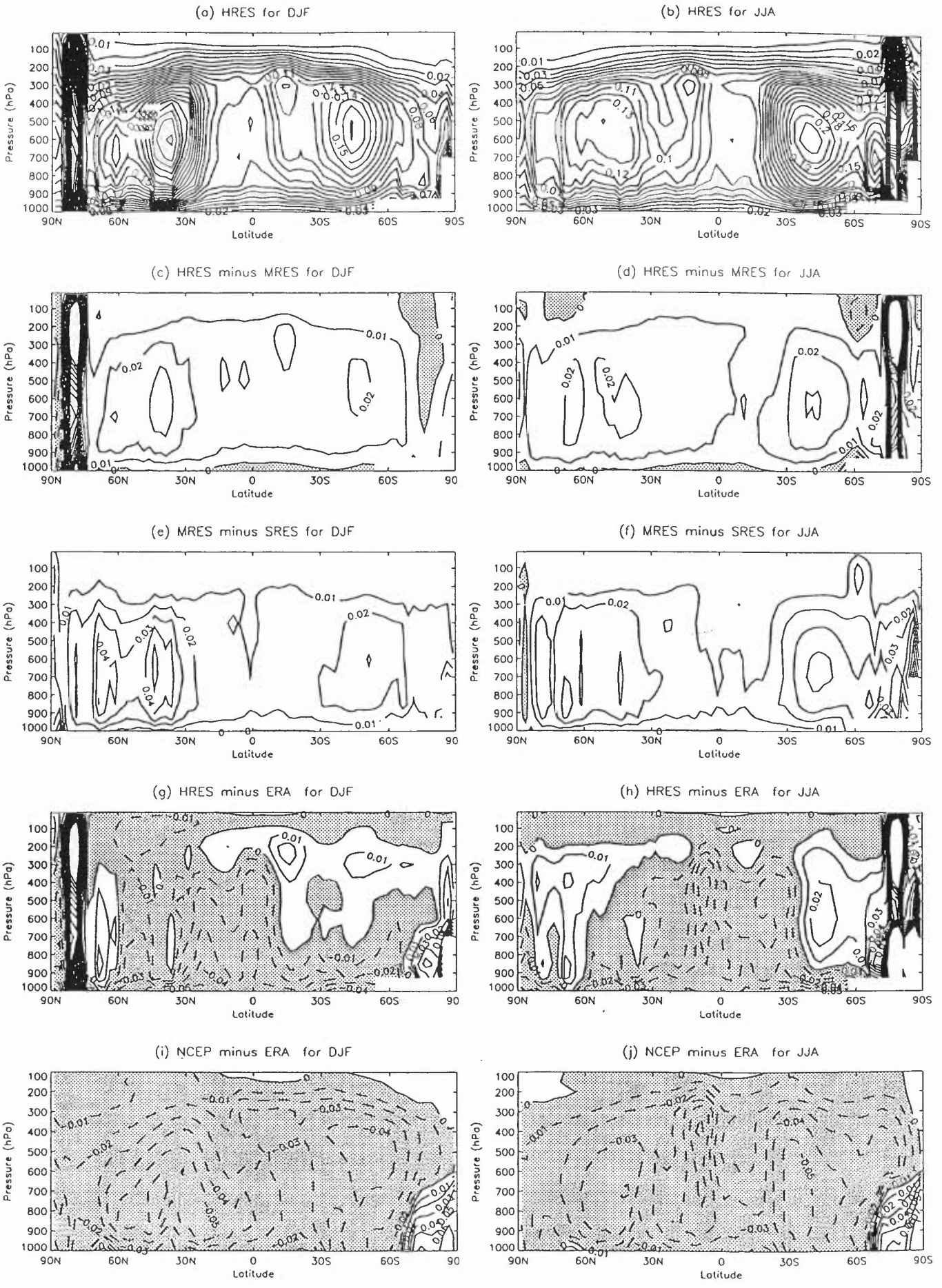

Fig 15 transient w

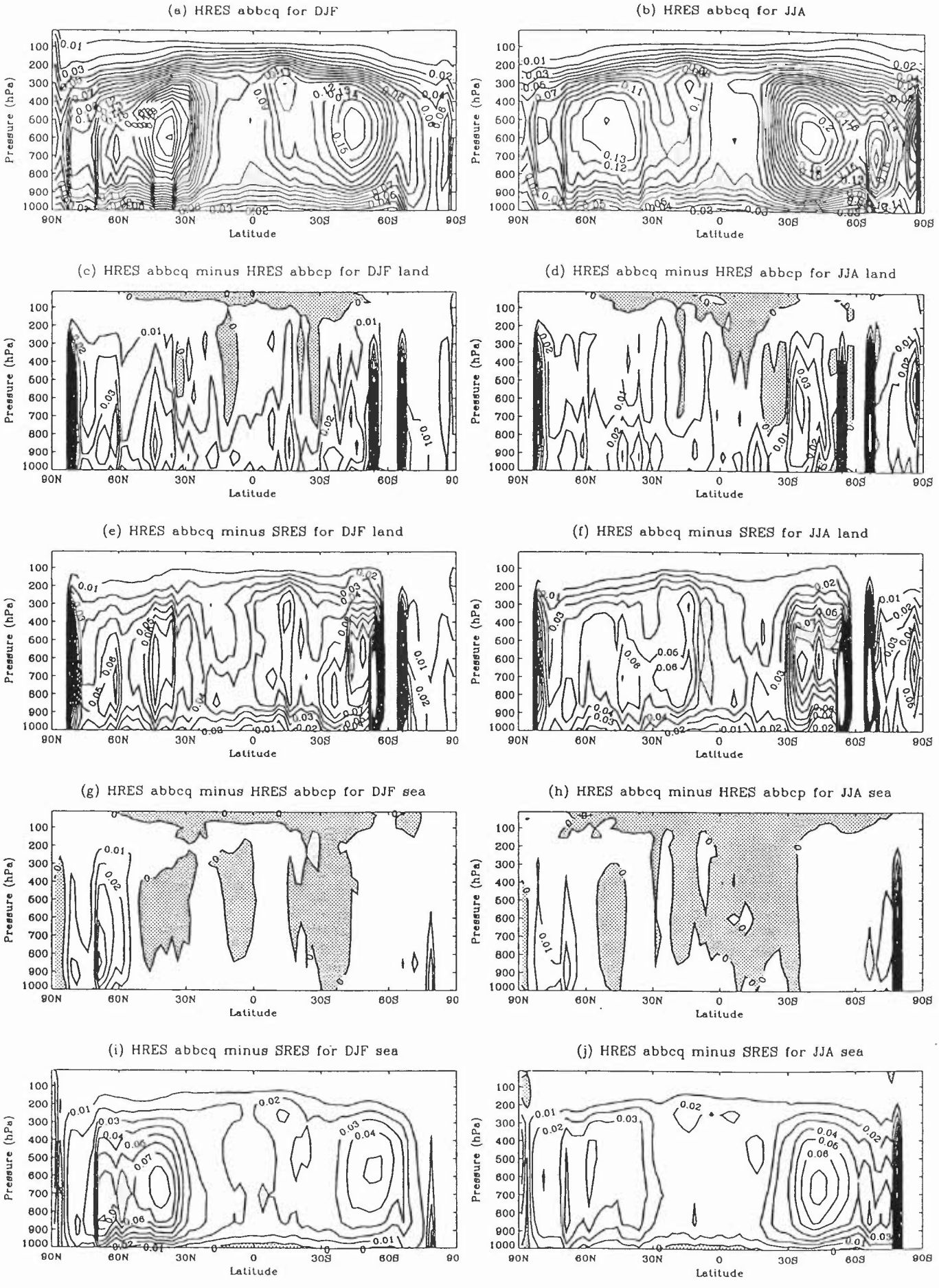

Fig 16 Transient eddy kinetic energy

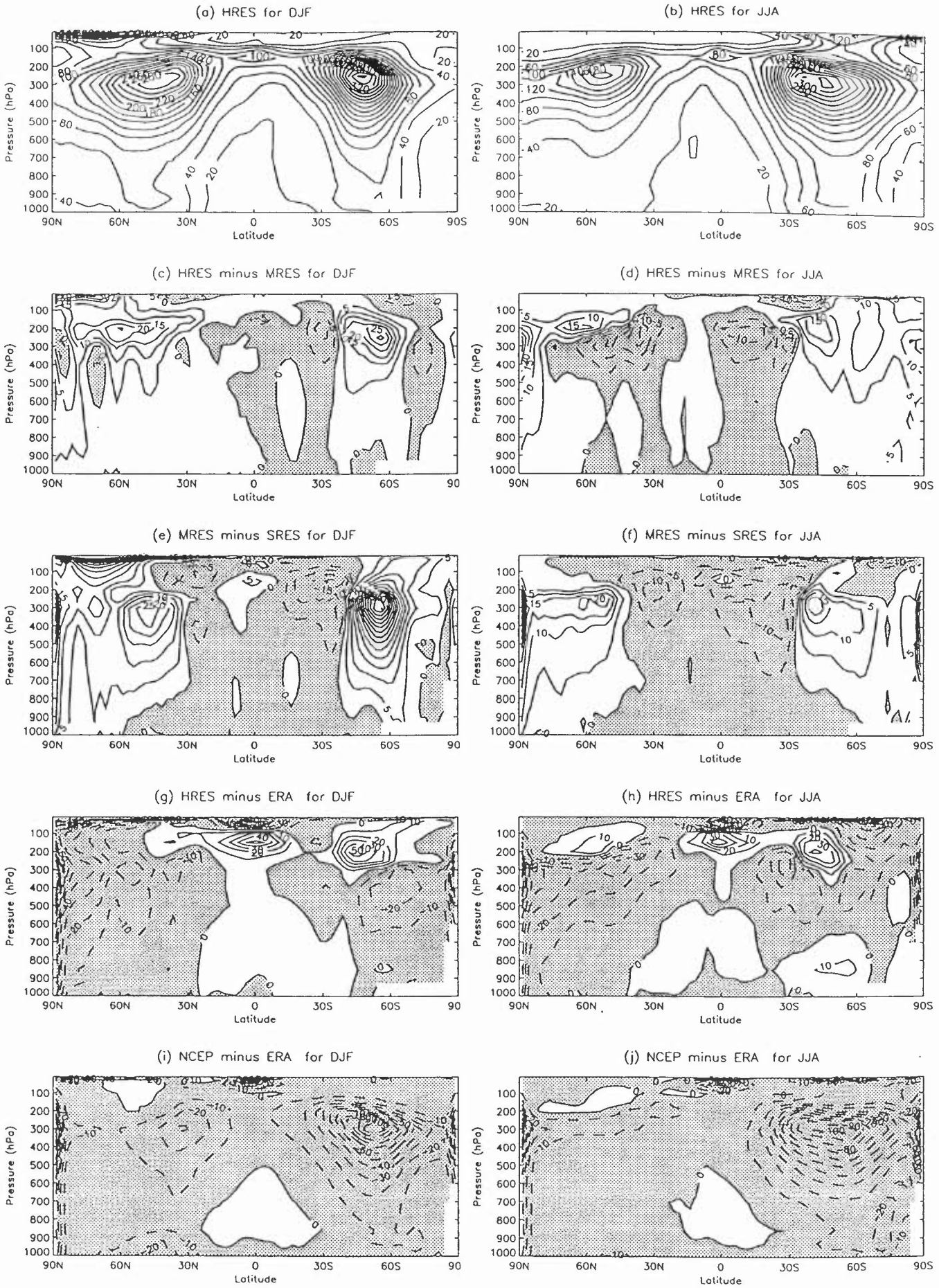

Fig 17 Wave number 1 300.hPa height

(a) SRES

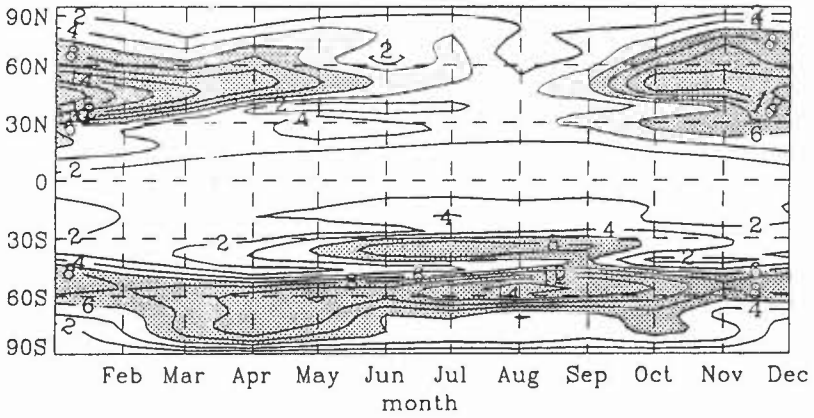

(b) MRES

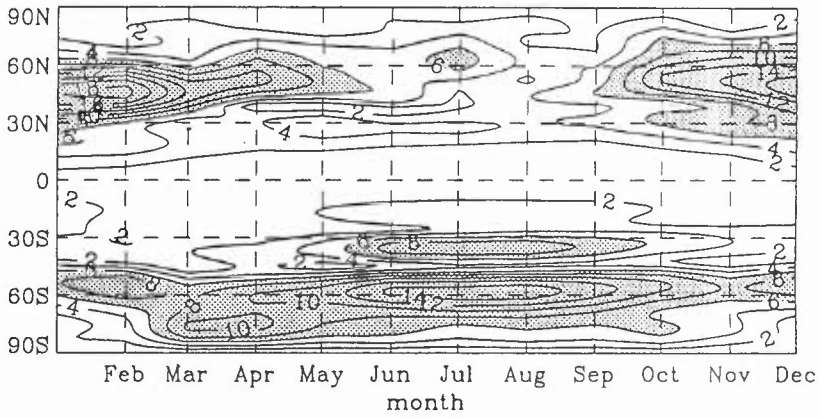

(c) HRES

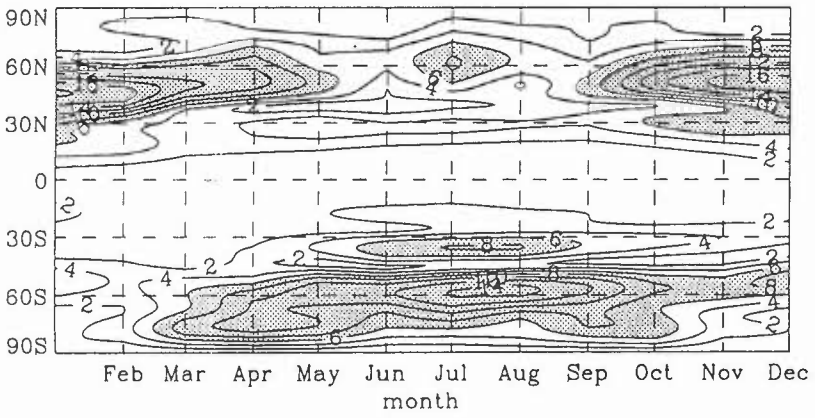

(d) ERA 1979-88

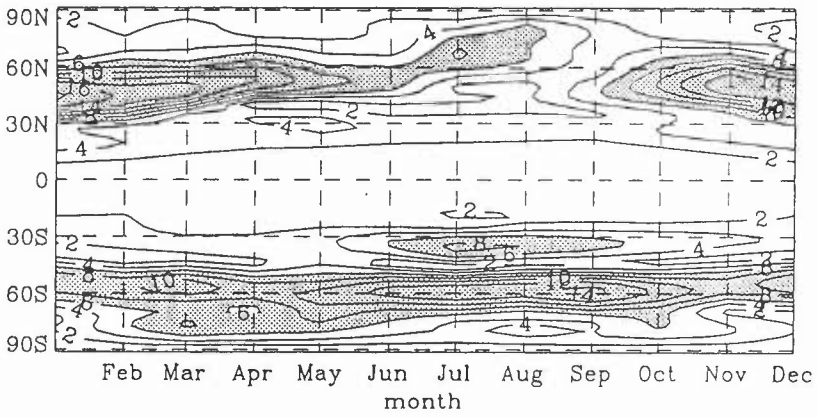

Fig 18 Relative angular momentum

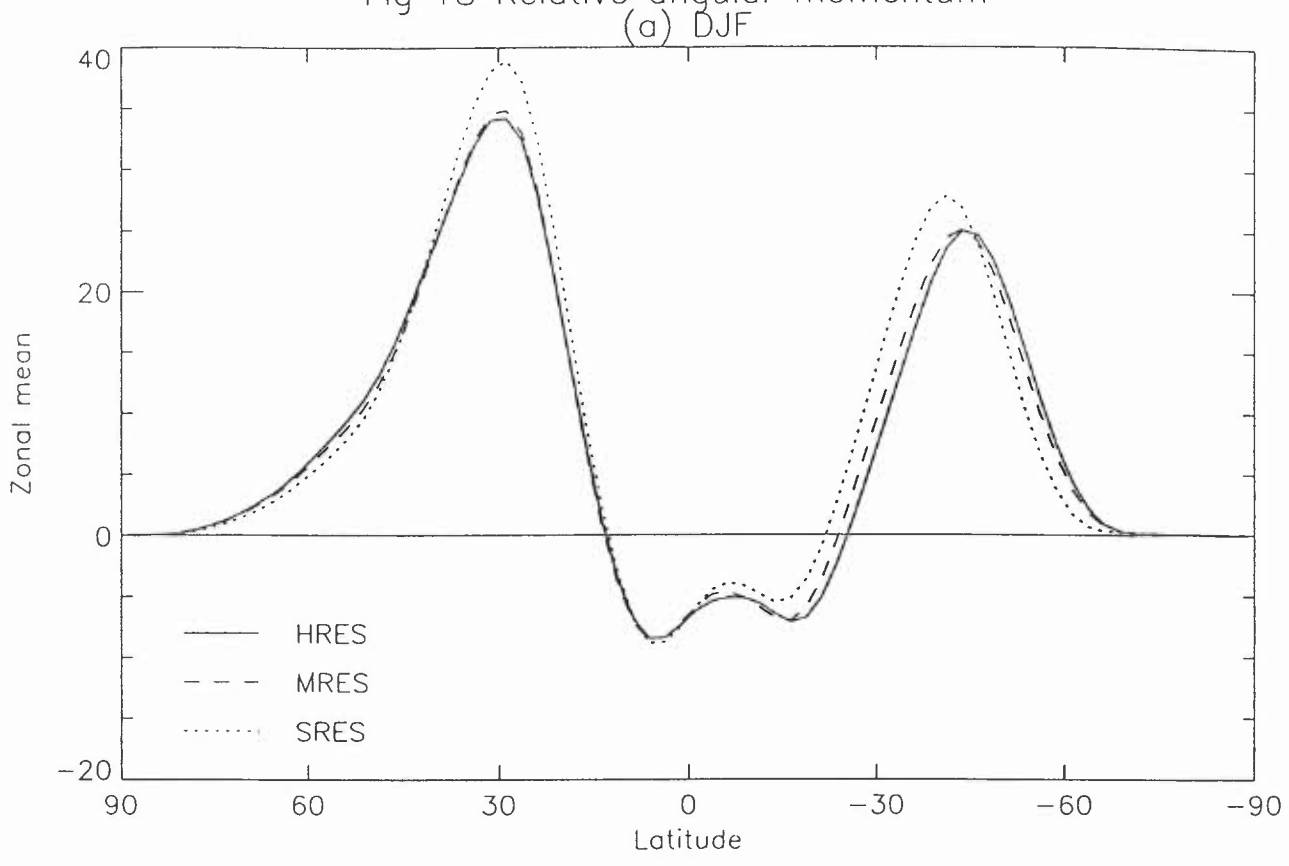

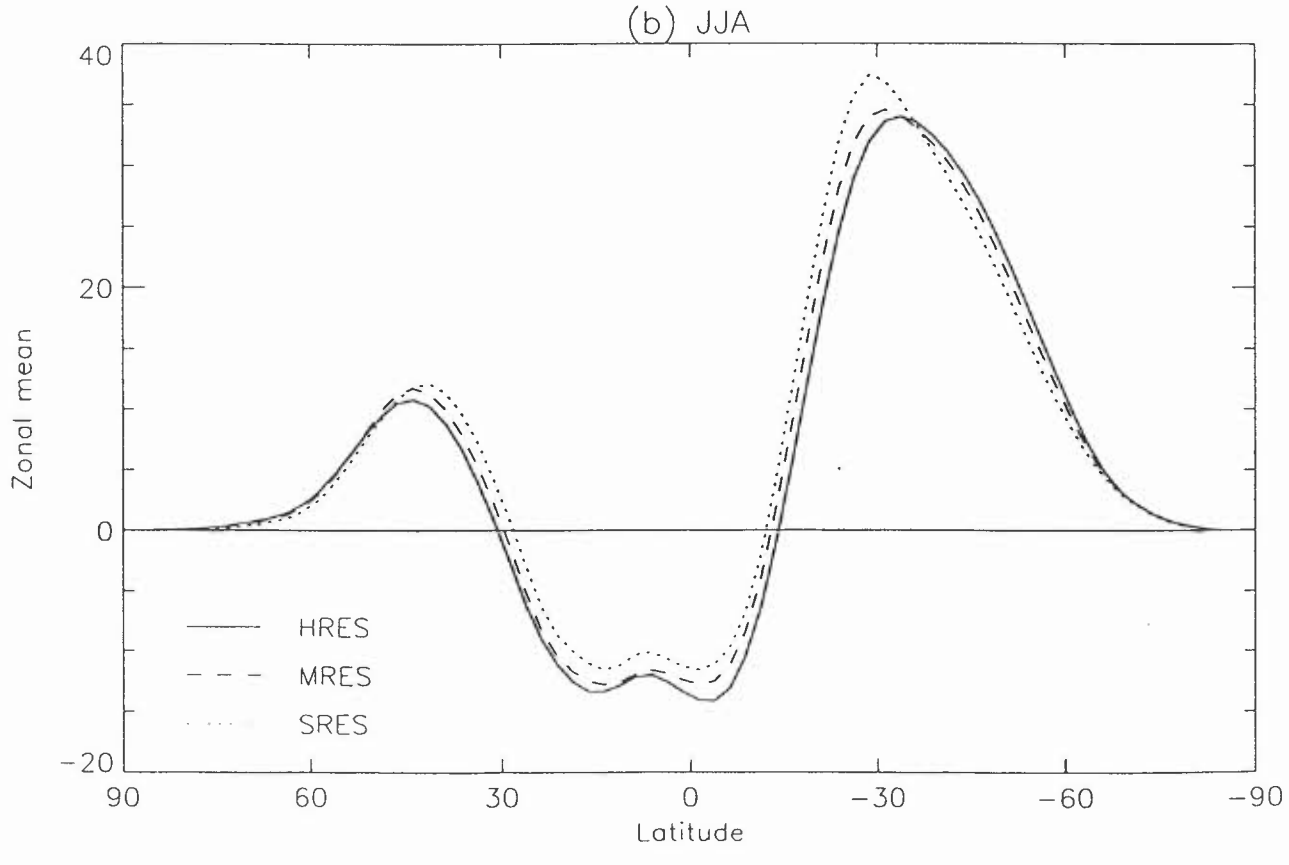

Fig 19 Components of the total torque

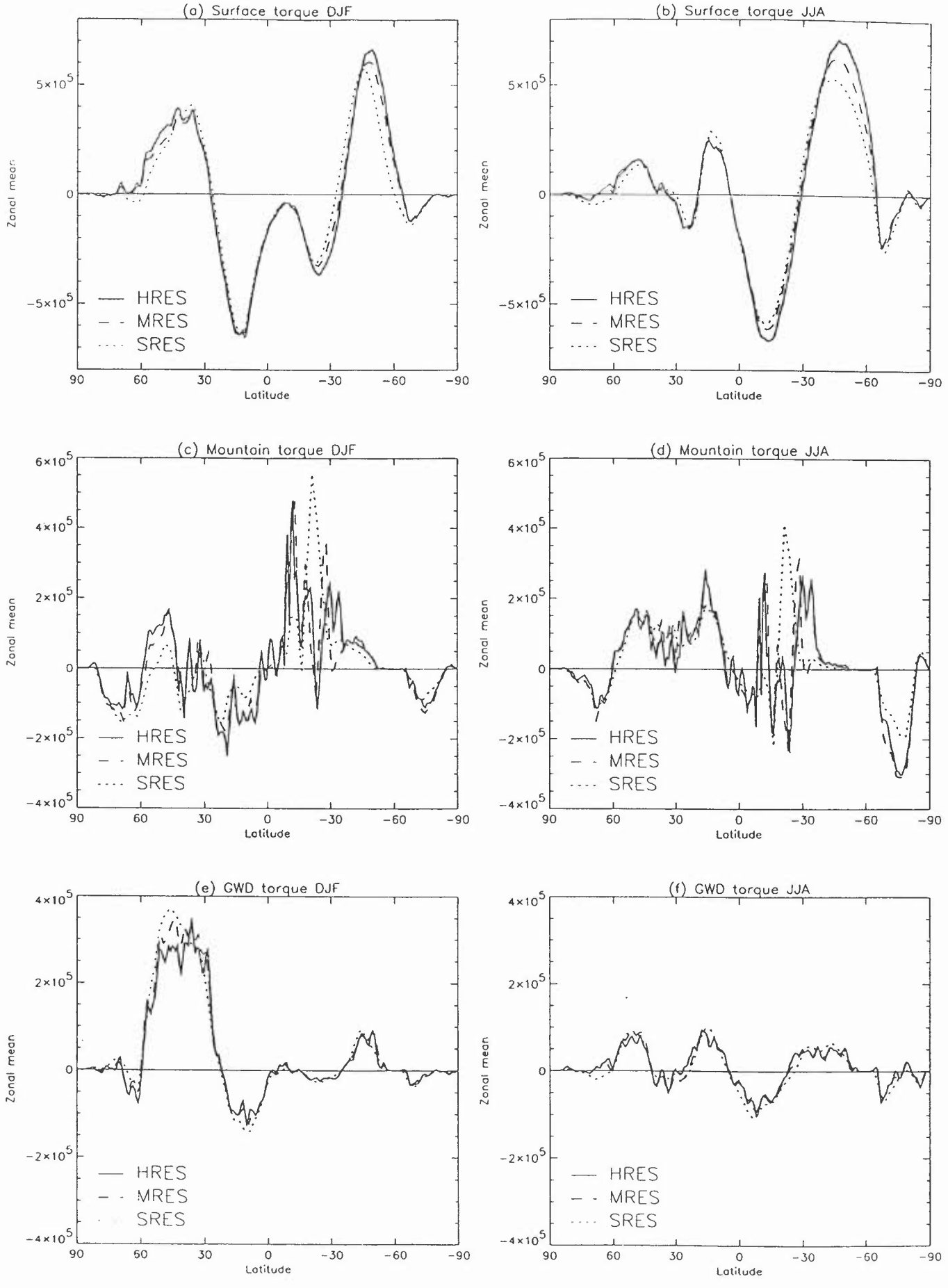

Fig 20 Fluxes of uv for djf

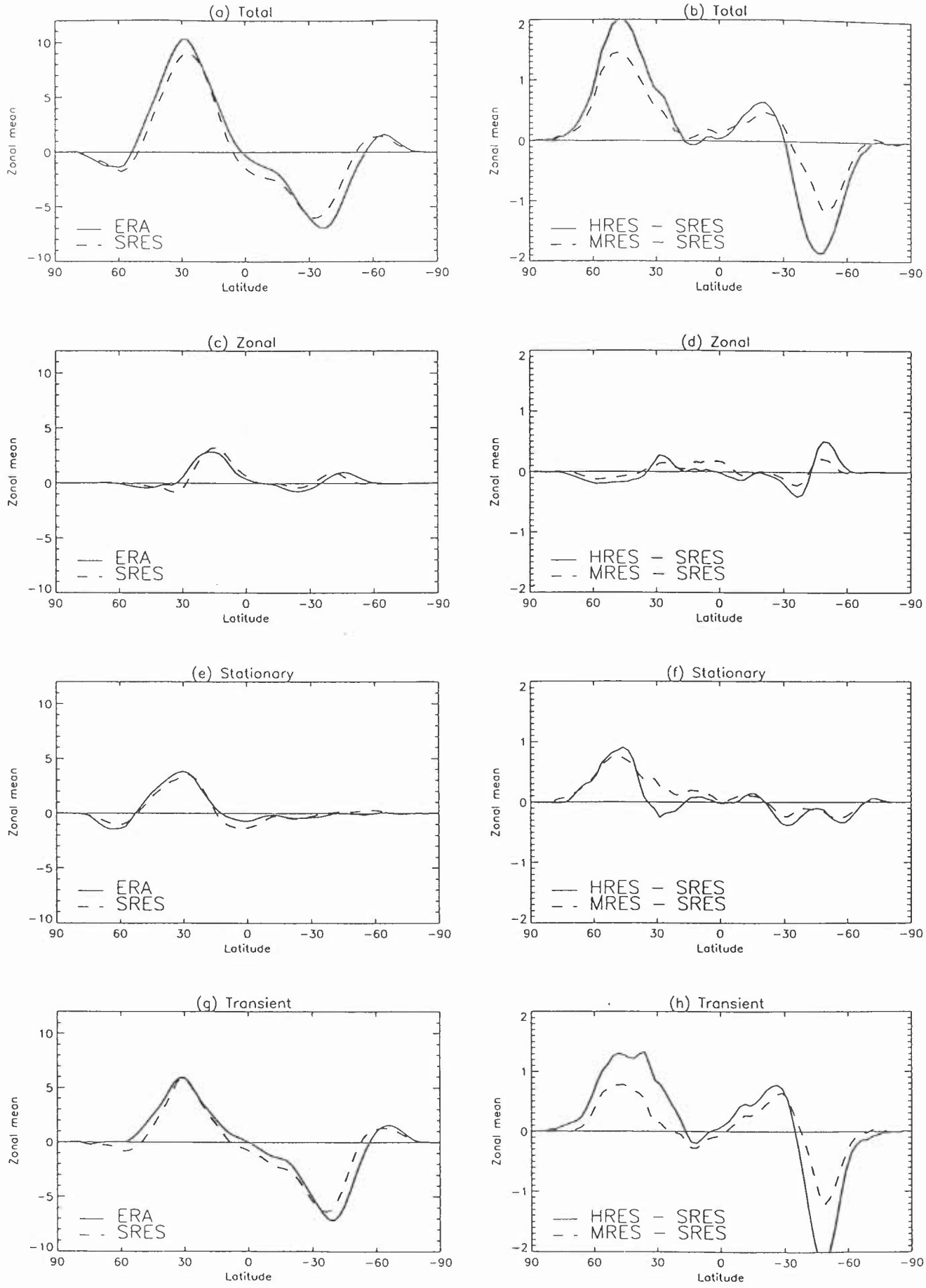

Fig 21 Transient flux UV

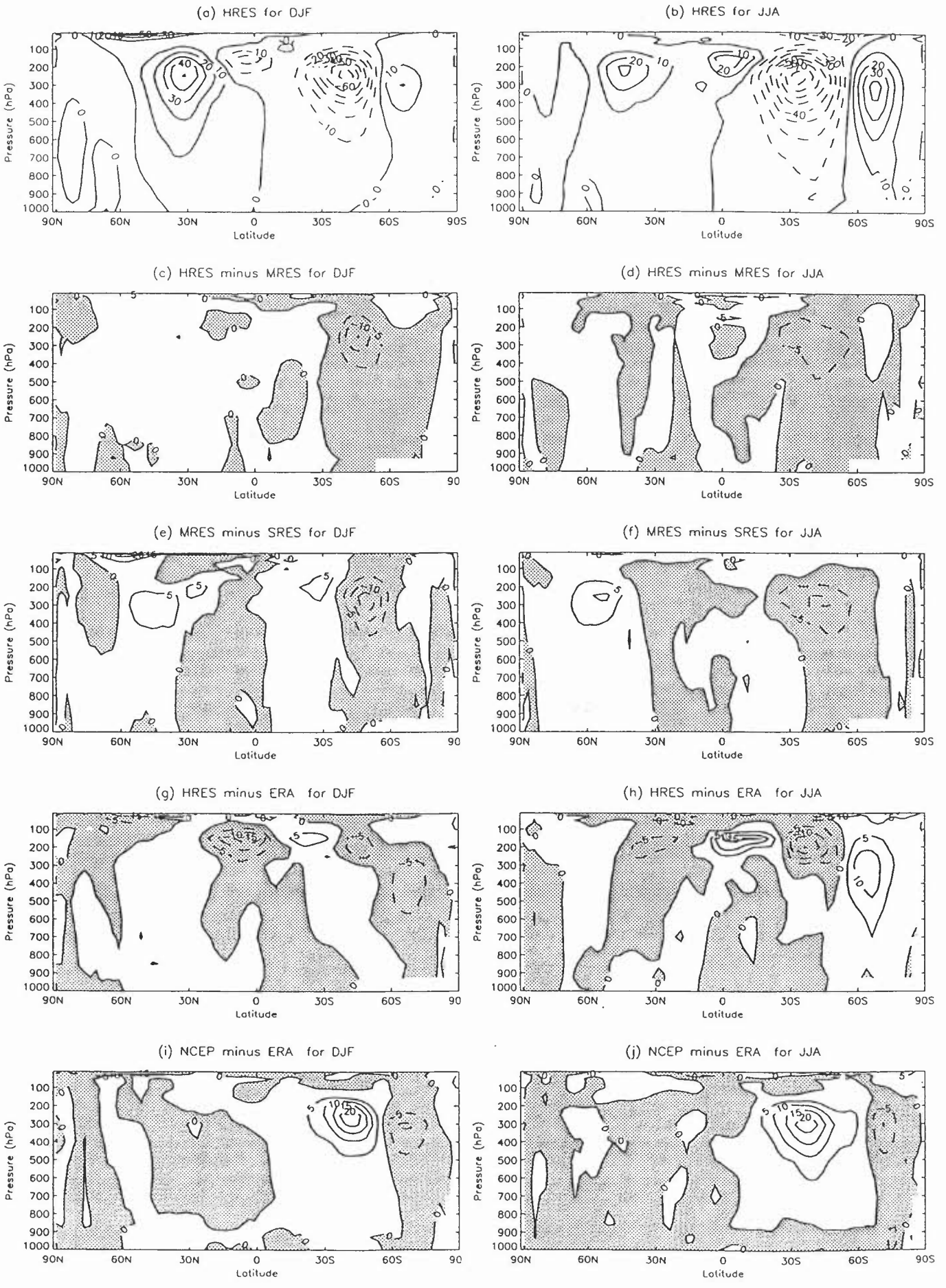

Fig 22 Transient flux VT

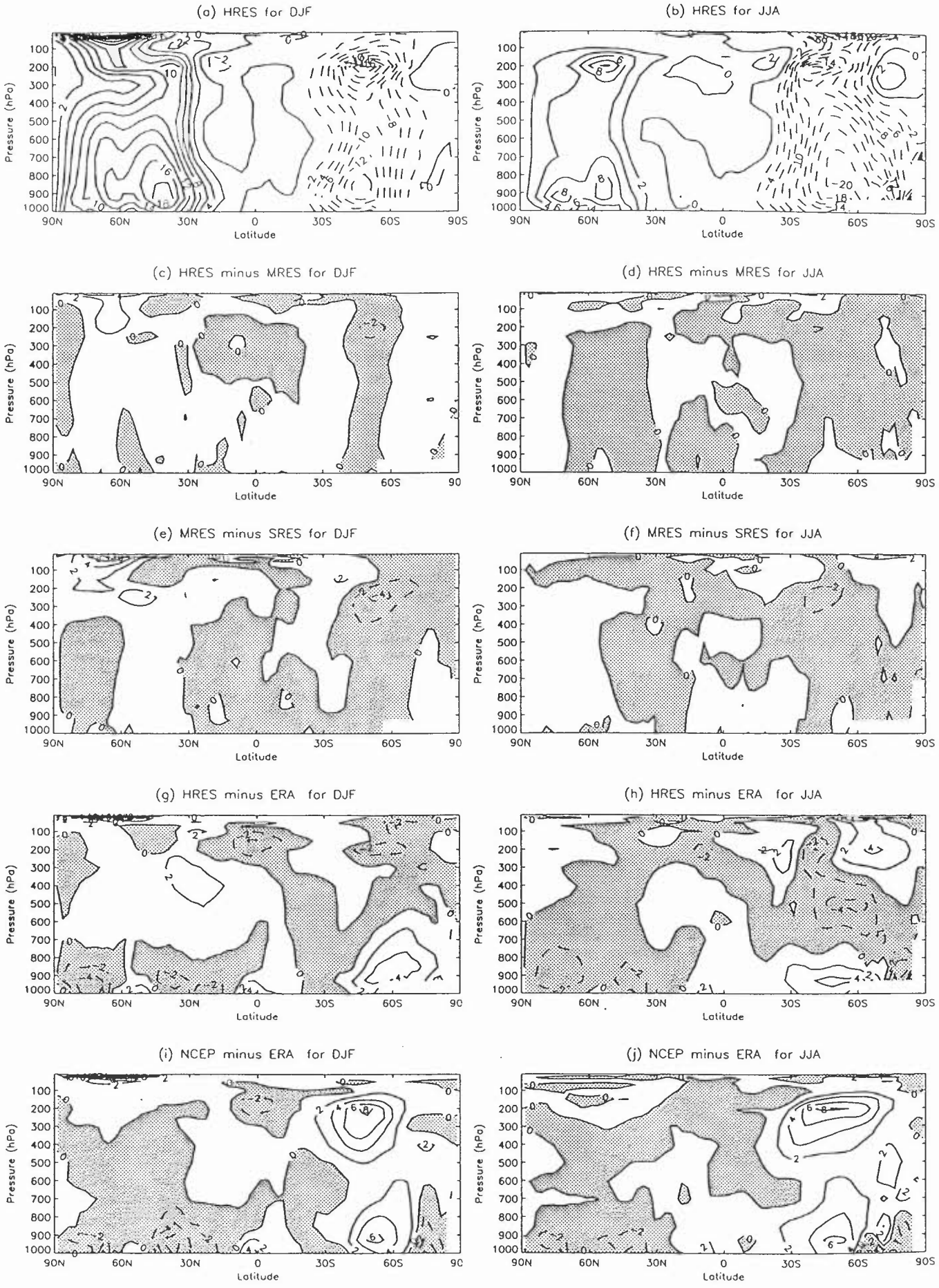

Fig 23 Transient flux wT

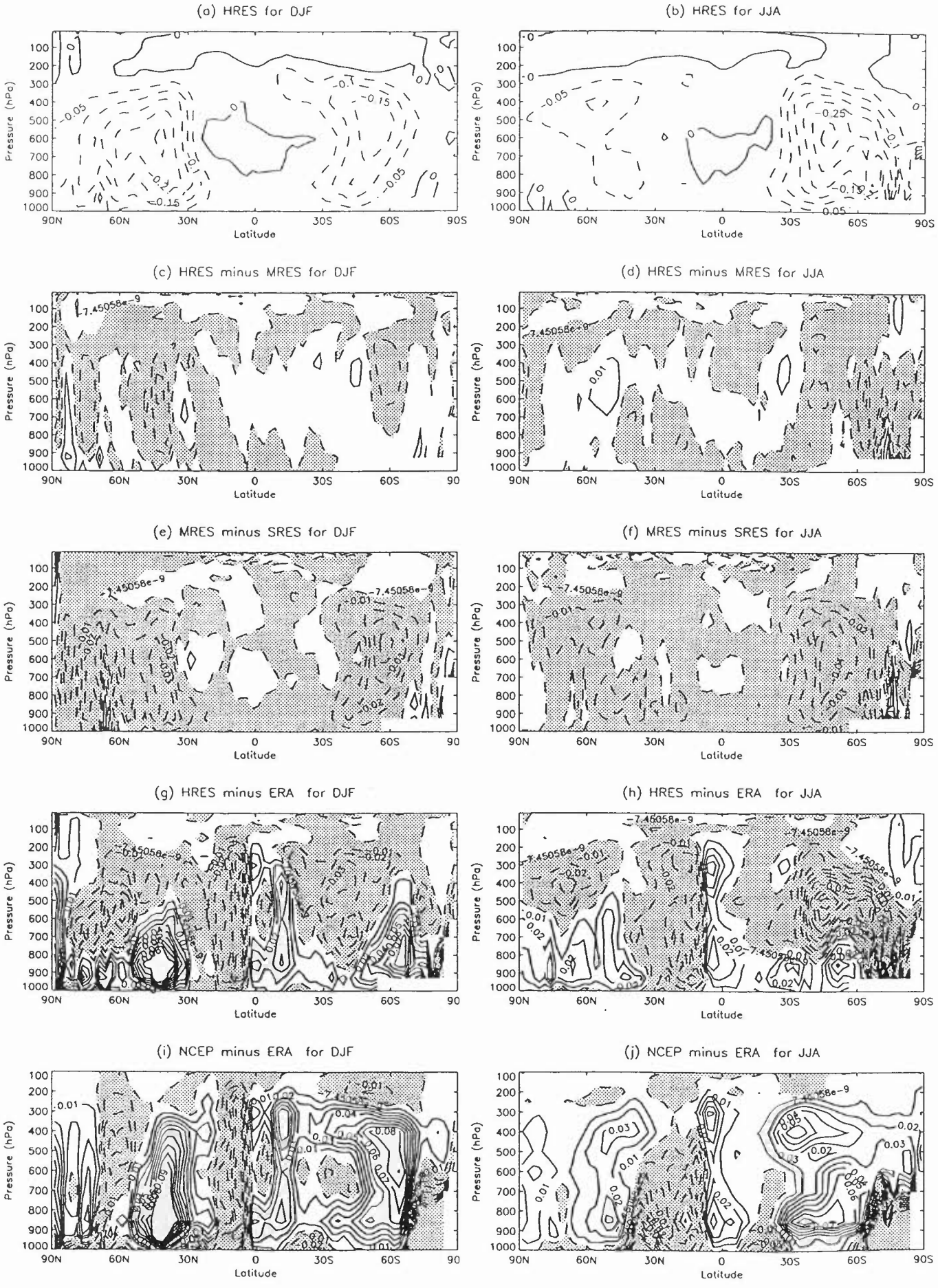

Fig 24 Transient flux Vq

(a) HRES for DJF

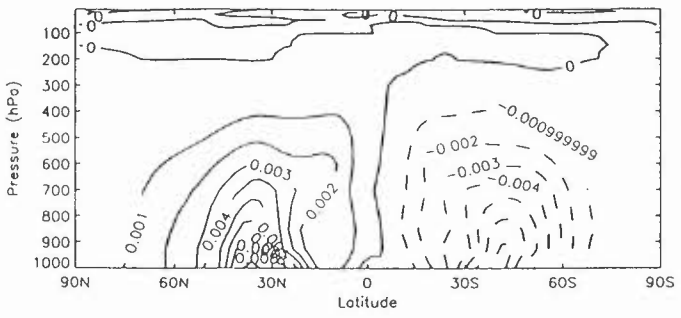

(b) HRES for JJA

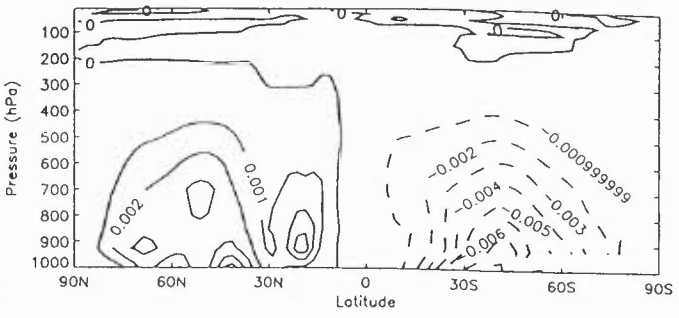

(c) HRES minus MRES for DJF

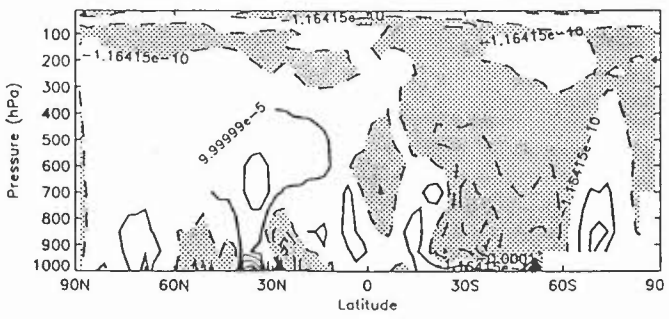

(d) HRES minus MRES for JJA

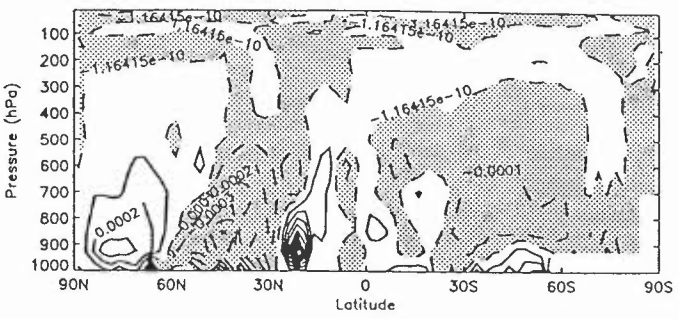

(e) MRES minus SRES for DJF

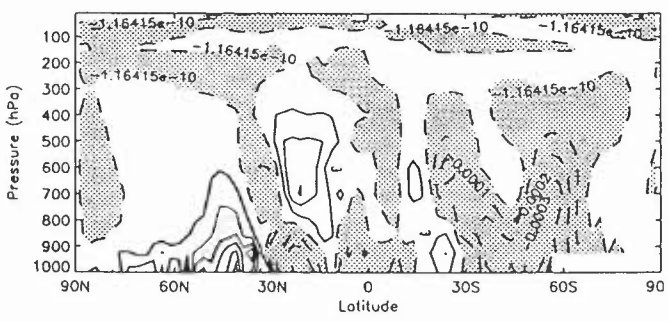

(f) MRES minus SRES for JJA

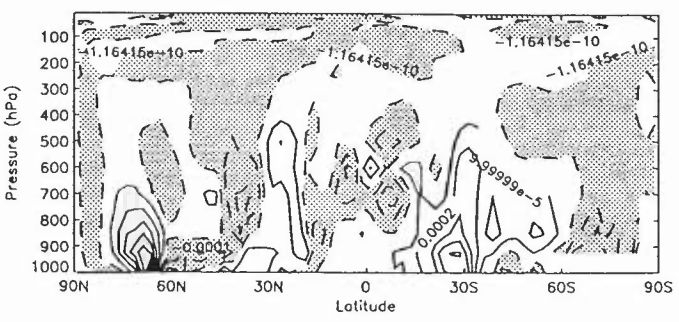

(g) HRES minus ERA for DJF

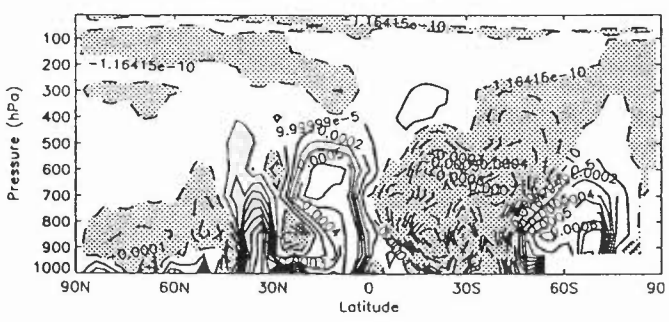

(h) HRES minus ERA for JJA

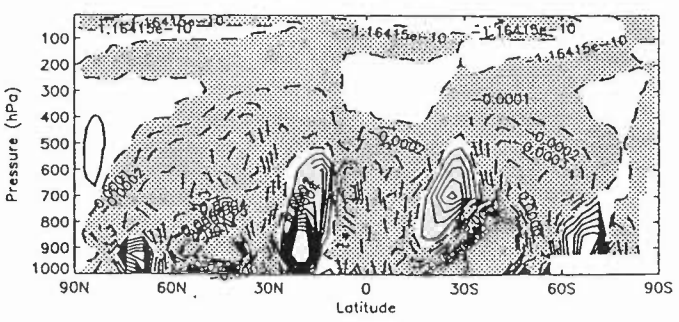

(i) NCEP minus ERA for DJF

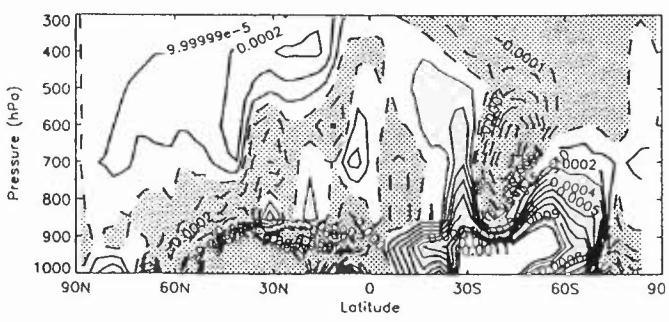

(j) NCEP minus ERA for JJA

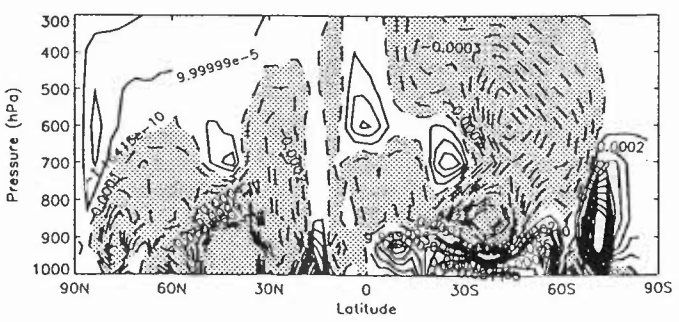

Fig 25 Transient flux wq

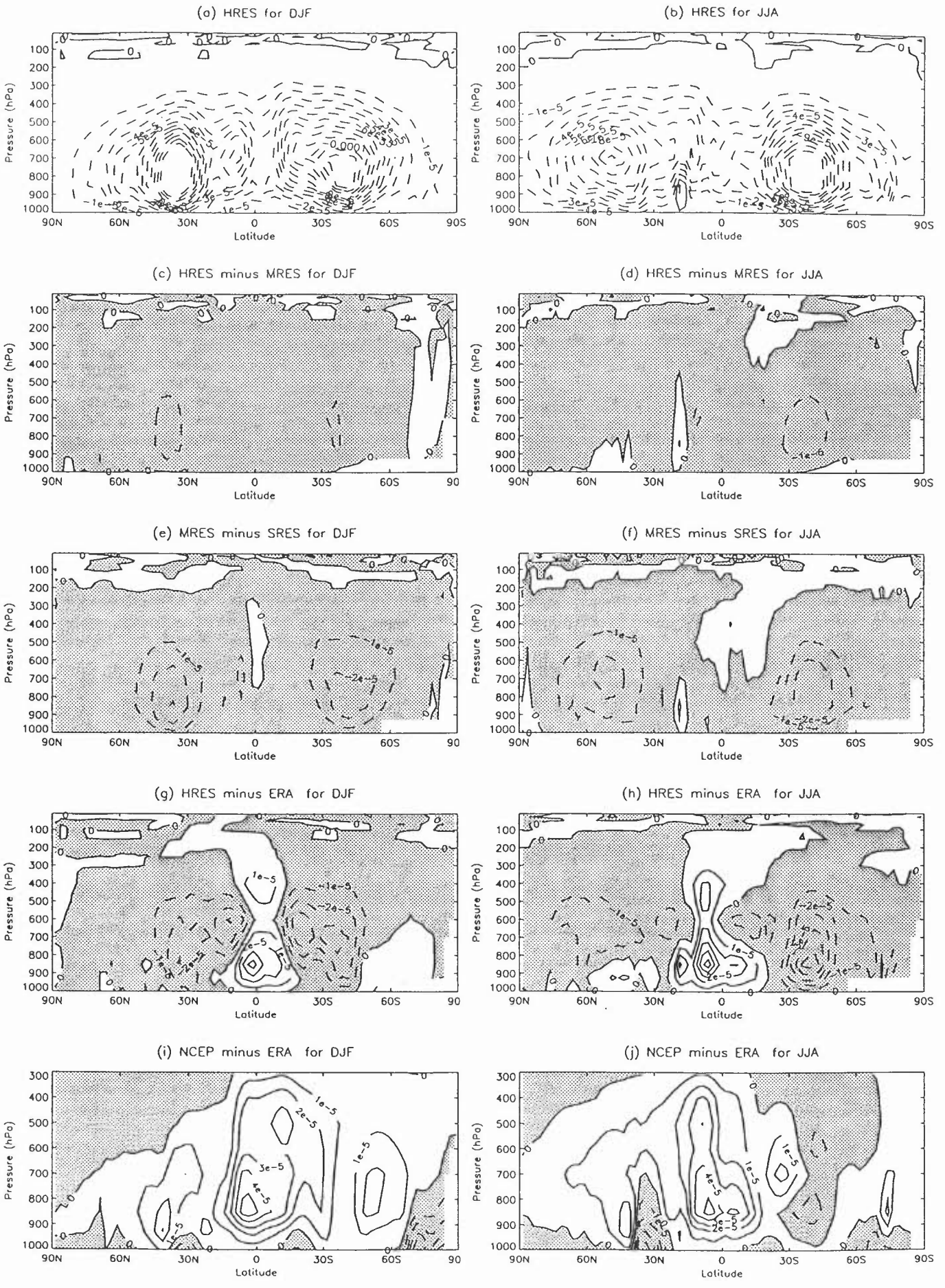

Fig 26 Precipitation for djf

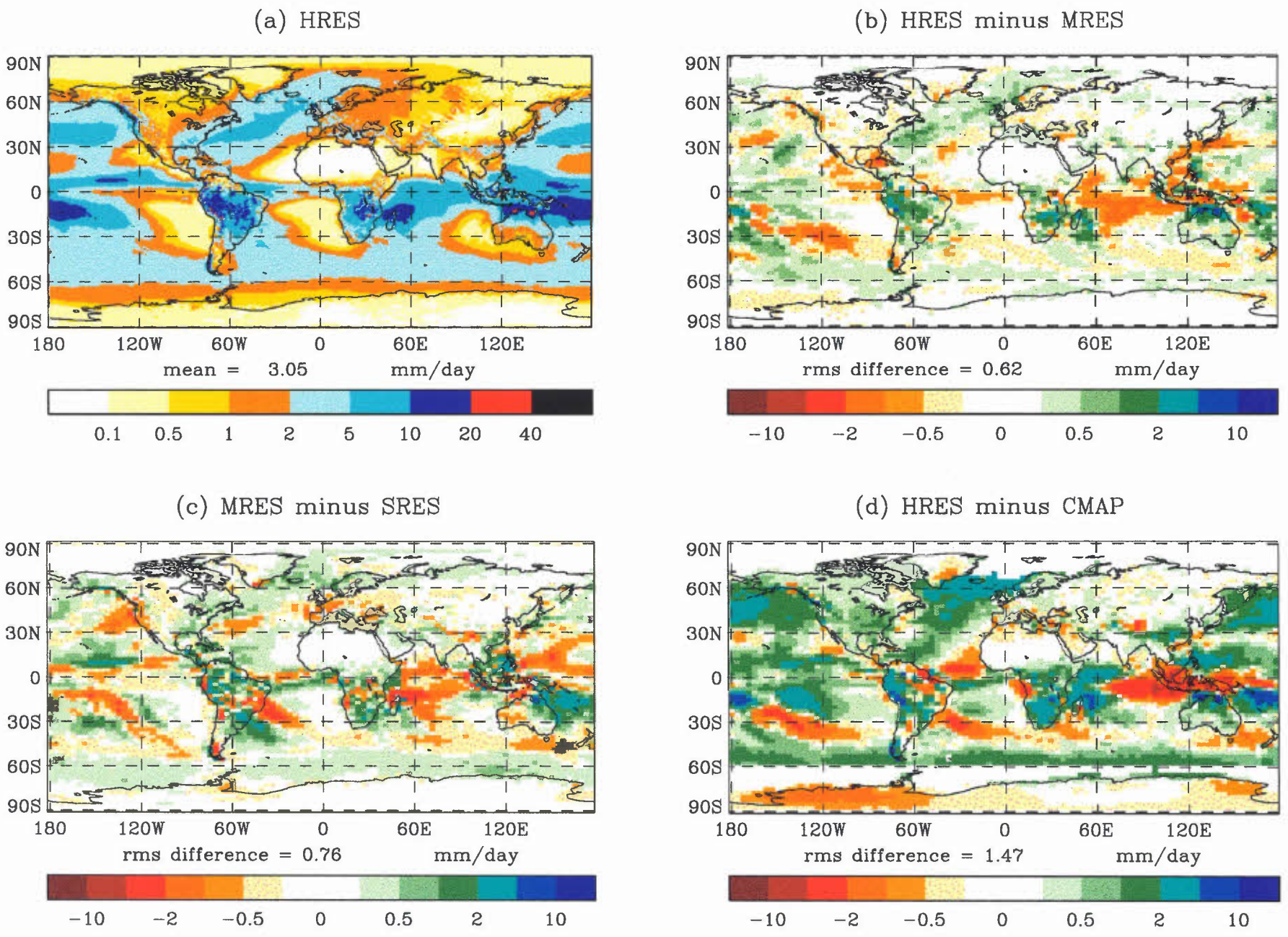

Fig 27 Precipitation for jja

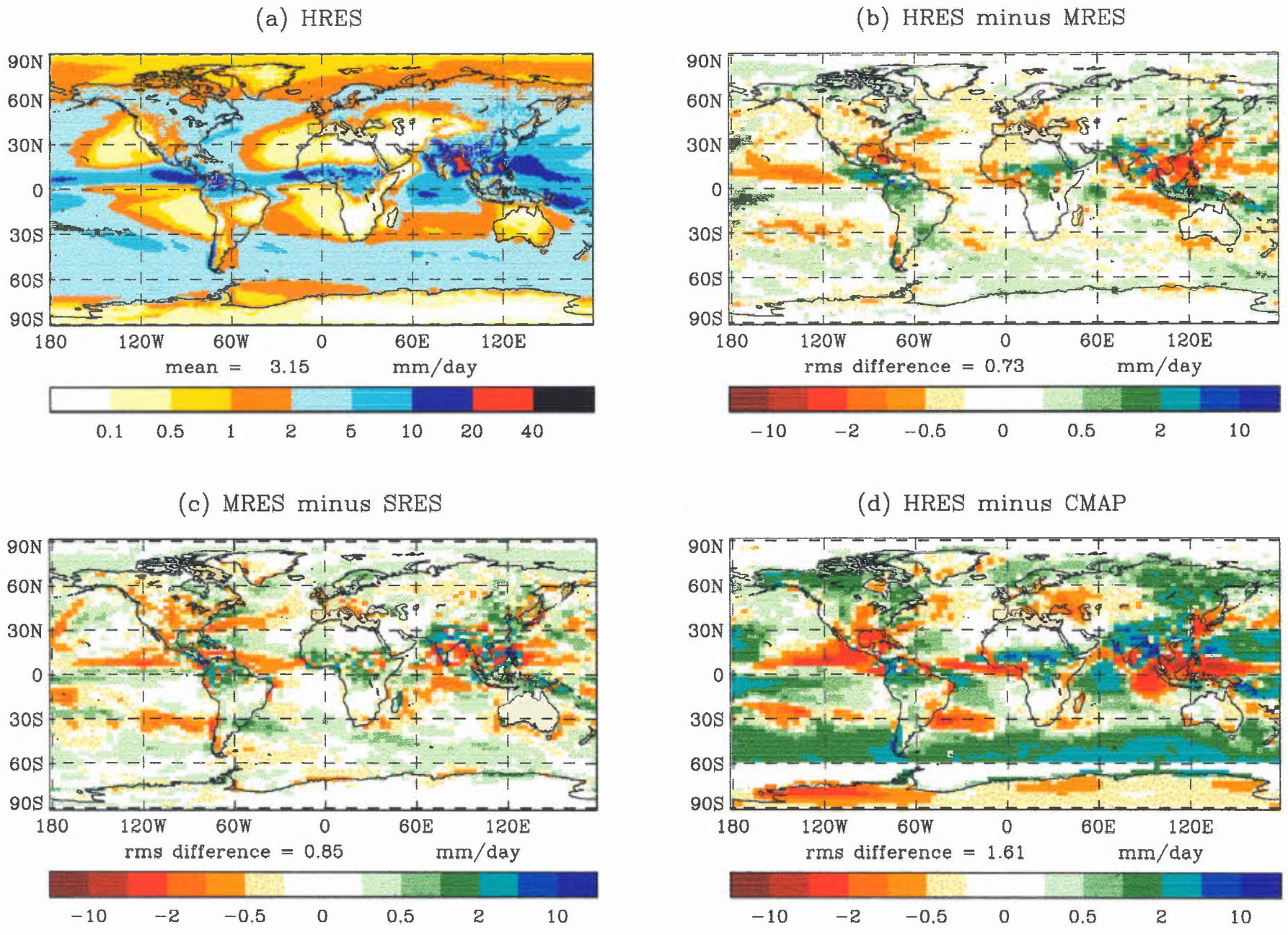

Fig 28 Layer cloud amount

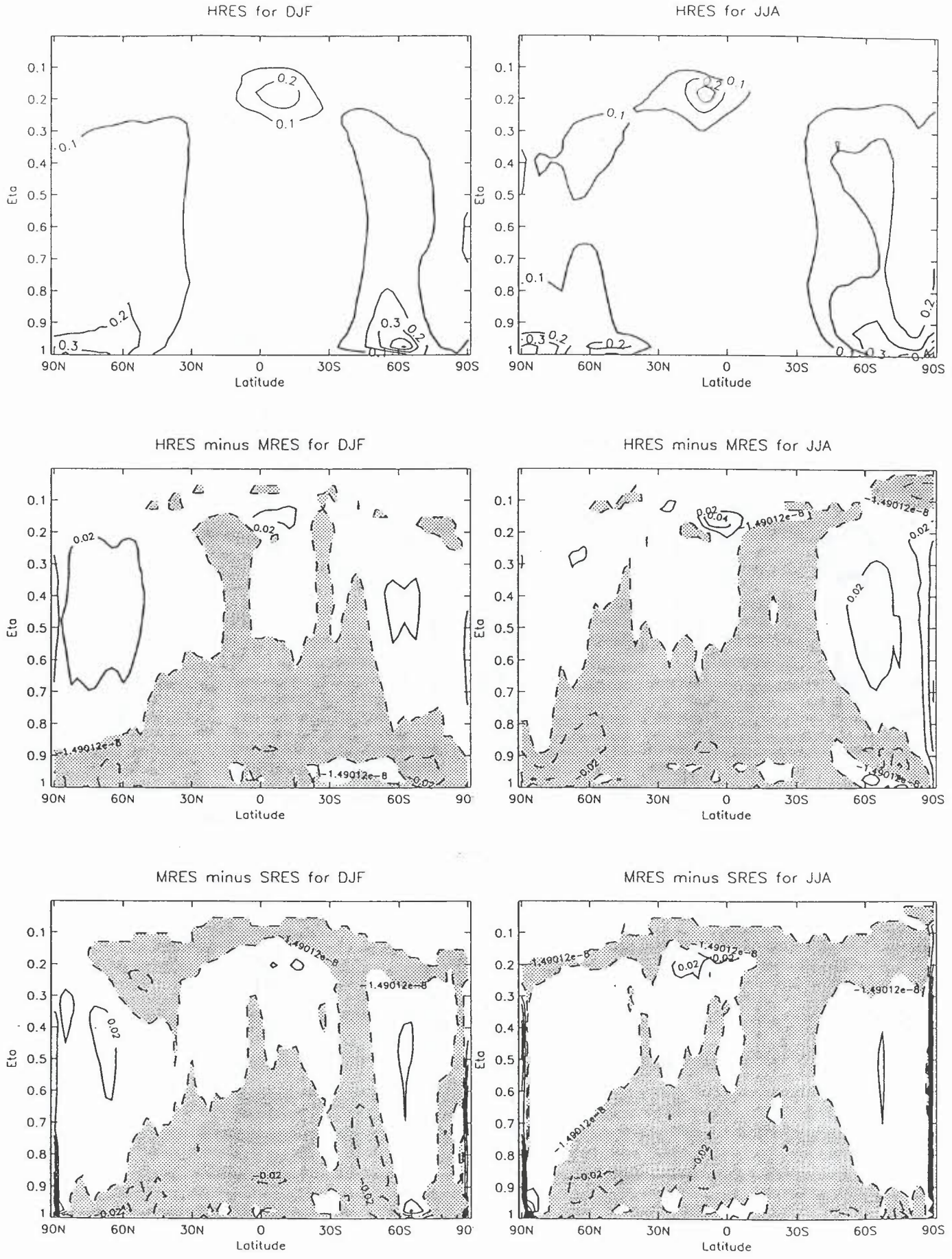

Fig 29 Convective cloud amount

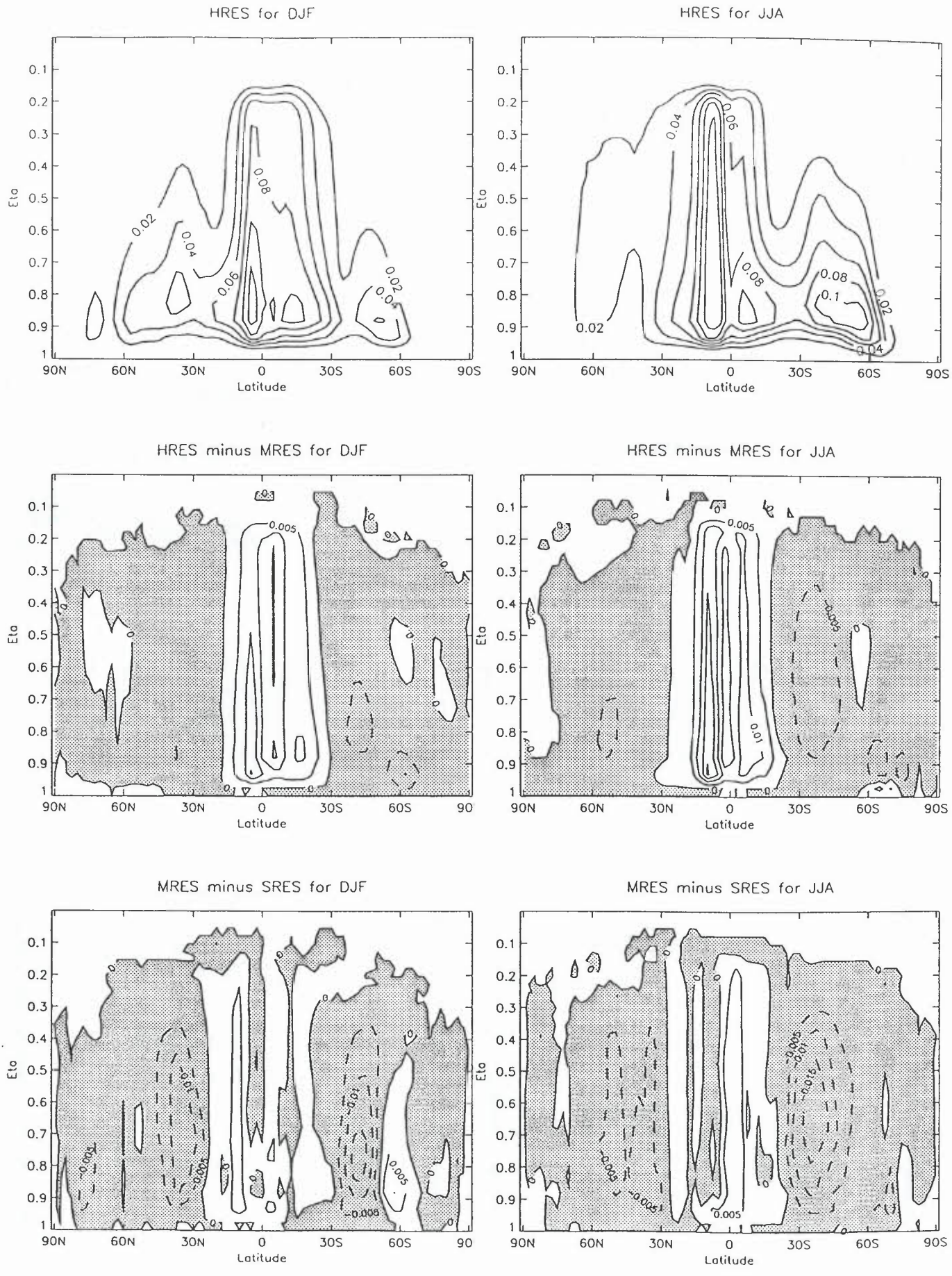

Fig 30 Cloud liquid water

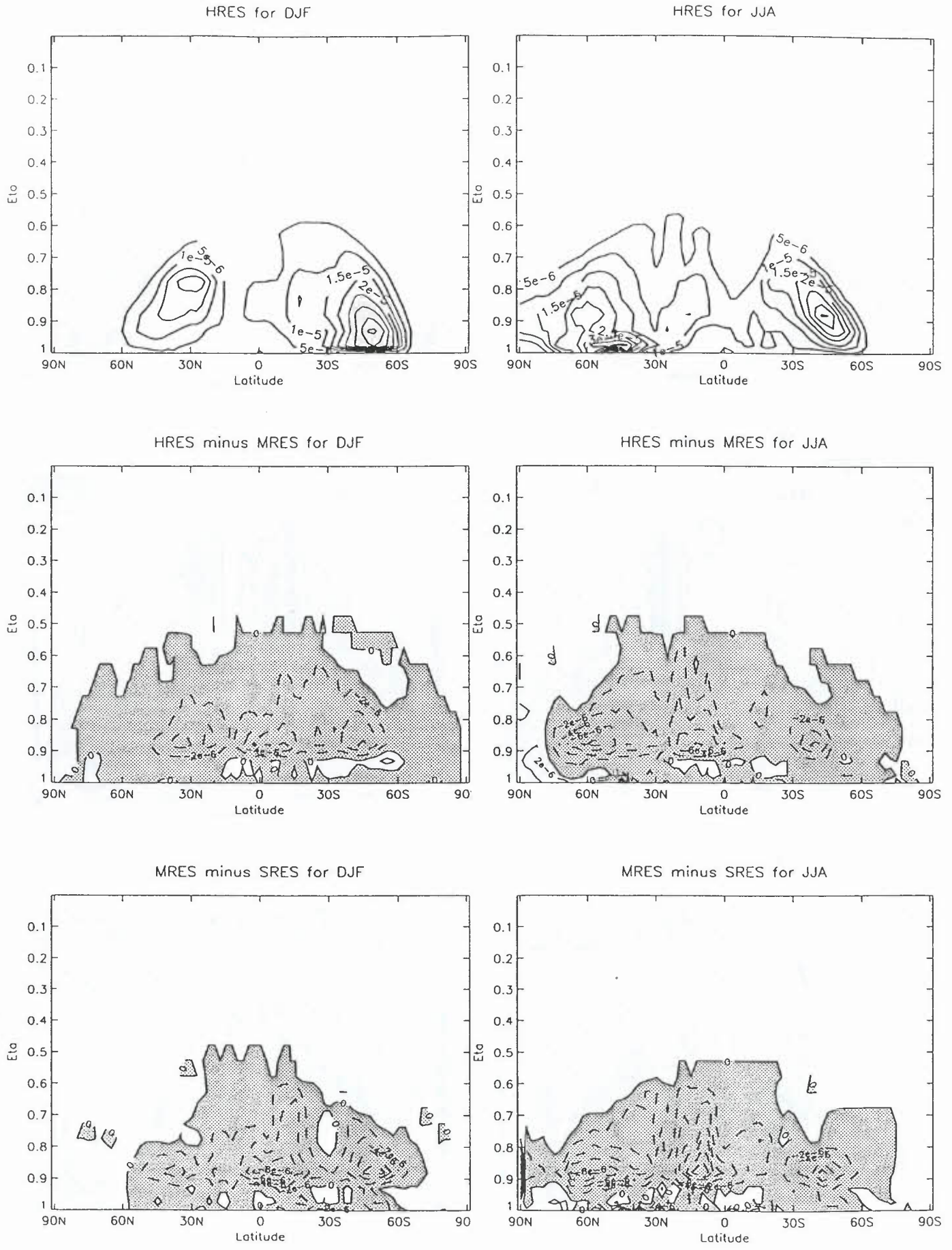

Fig 31 Cloud ice water

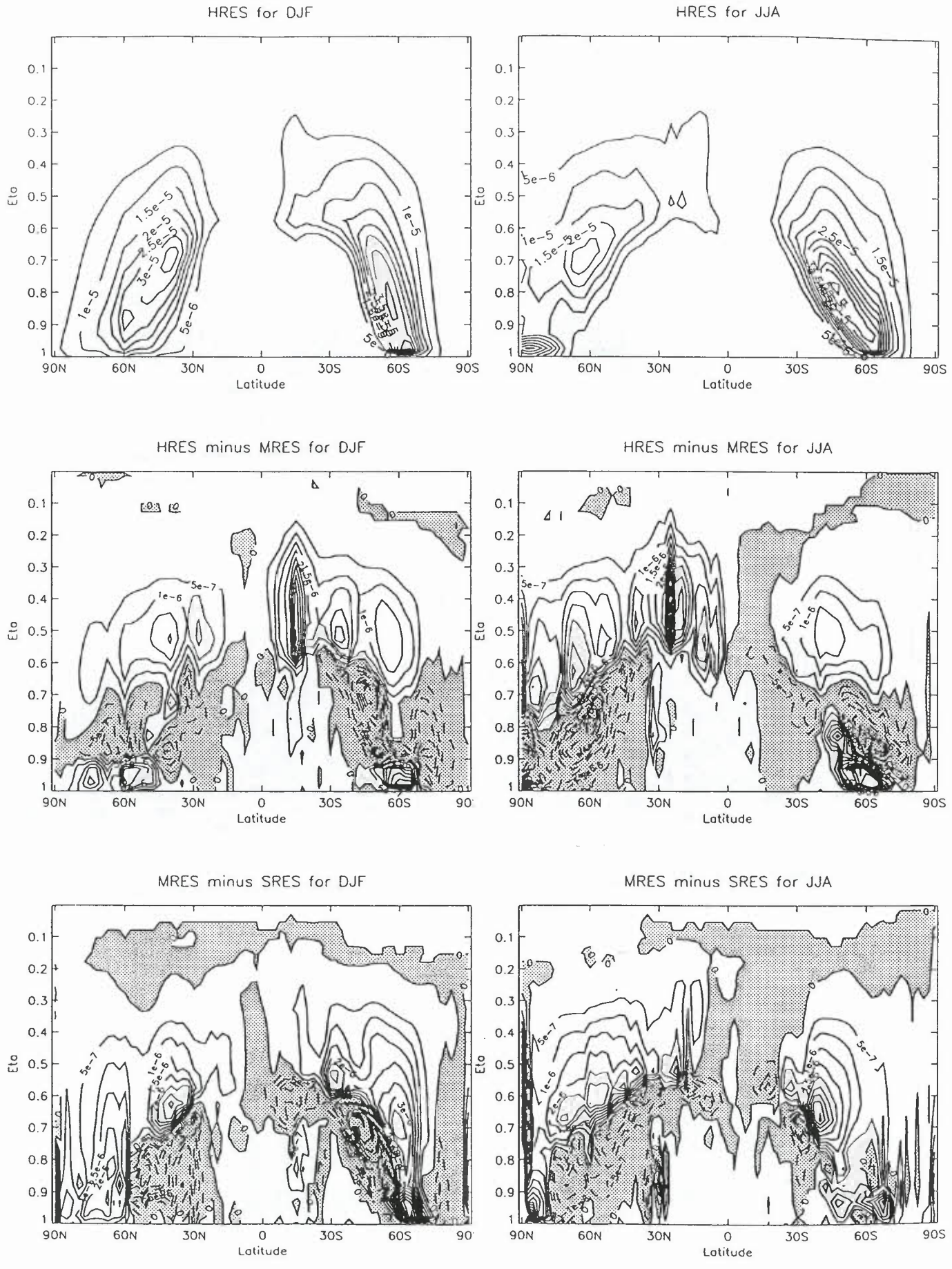

Fig 32 Net downward radiation at the top of the atmosphere model minus ERBE

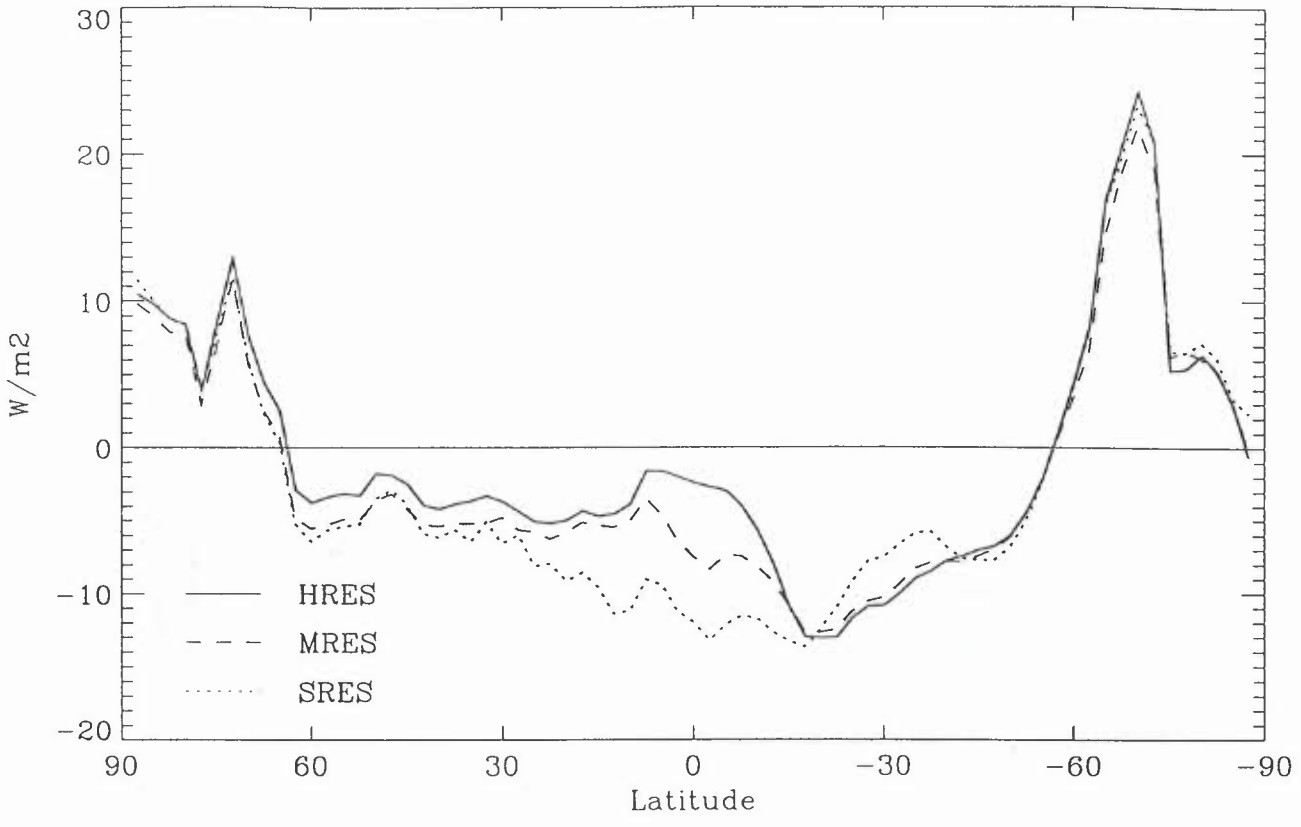

Fig 33 Albedo at the top of the atmosphere for

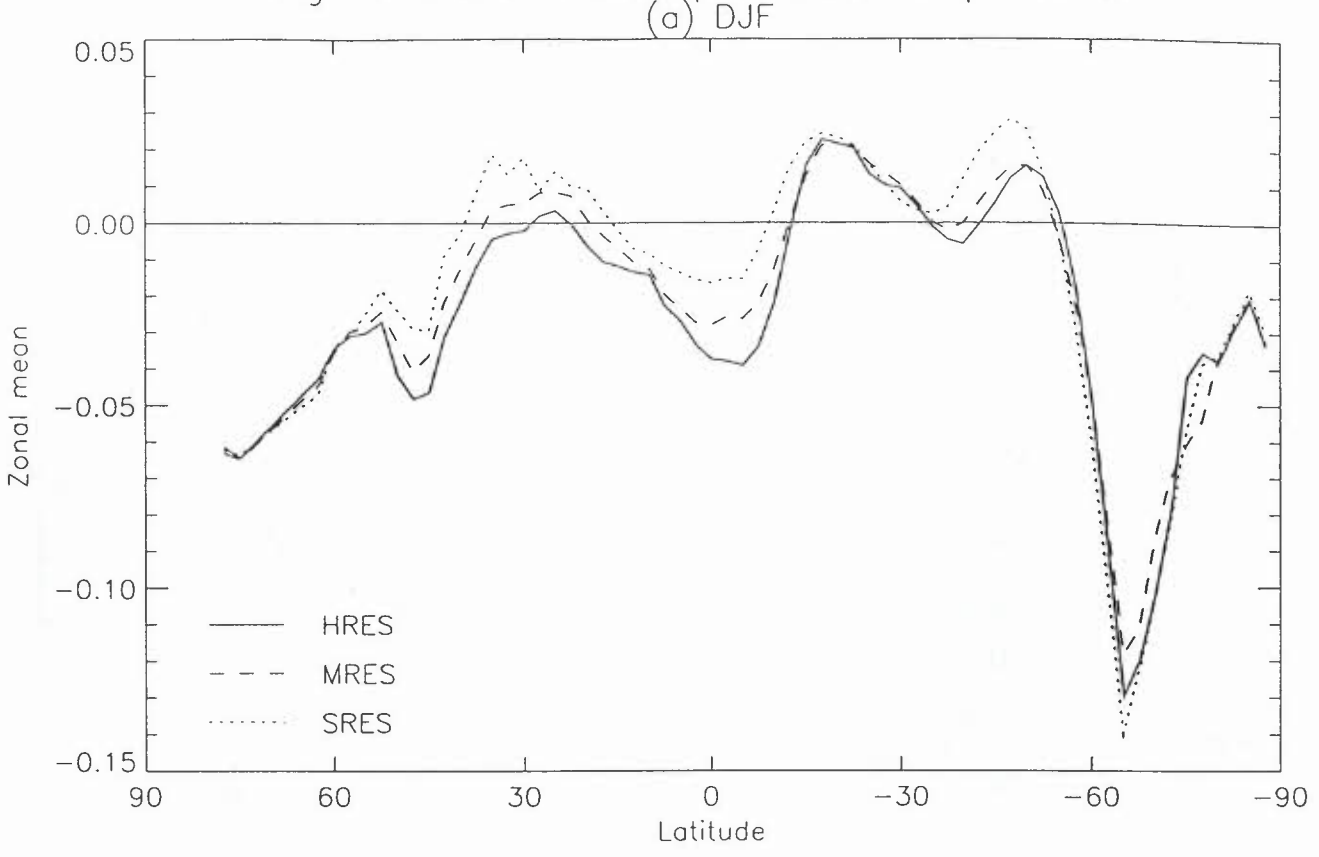

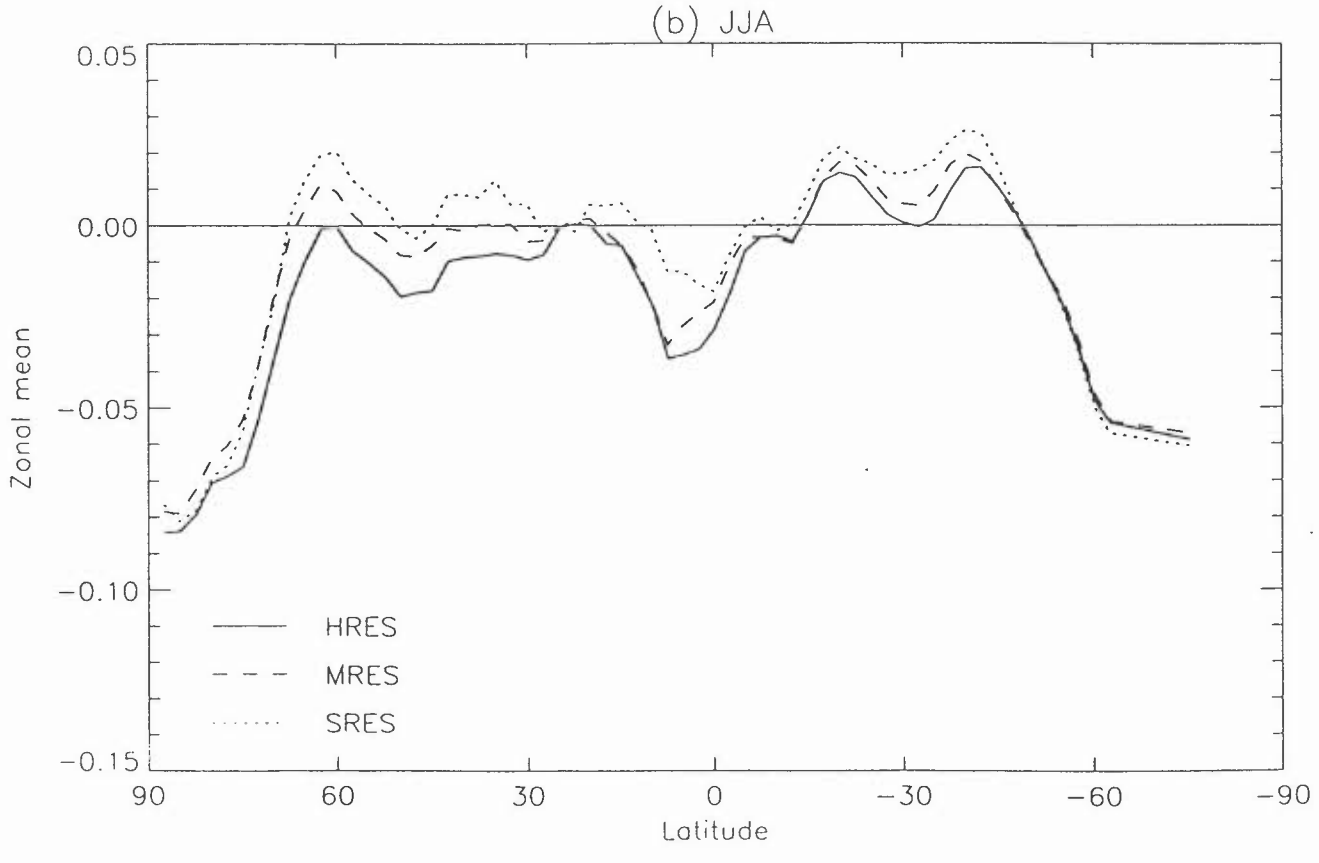

Fig 34 Outgoing longwave for
(a) DJF

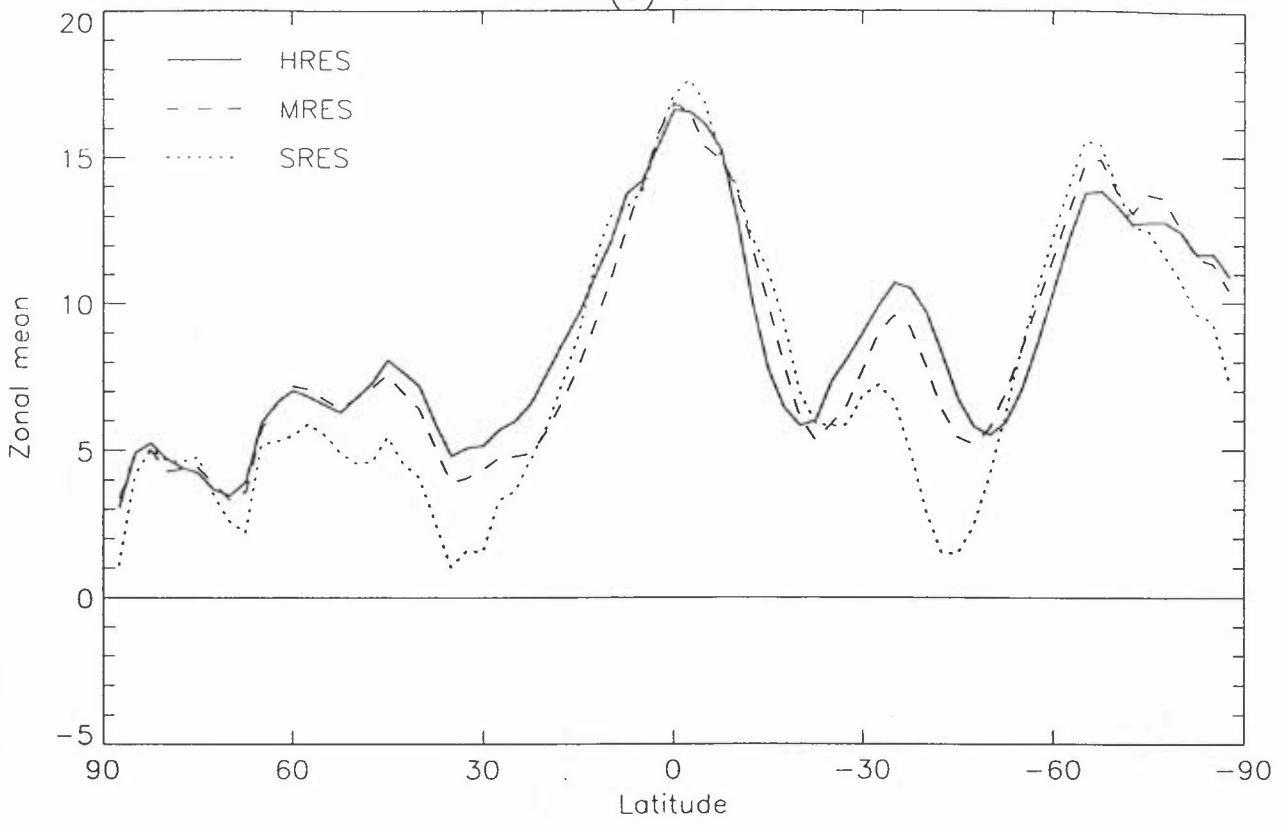

(b) JJA

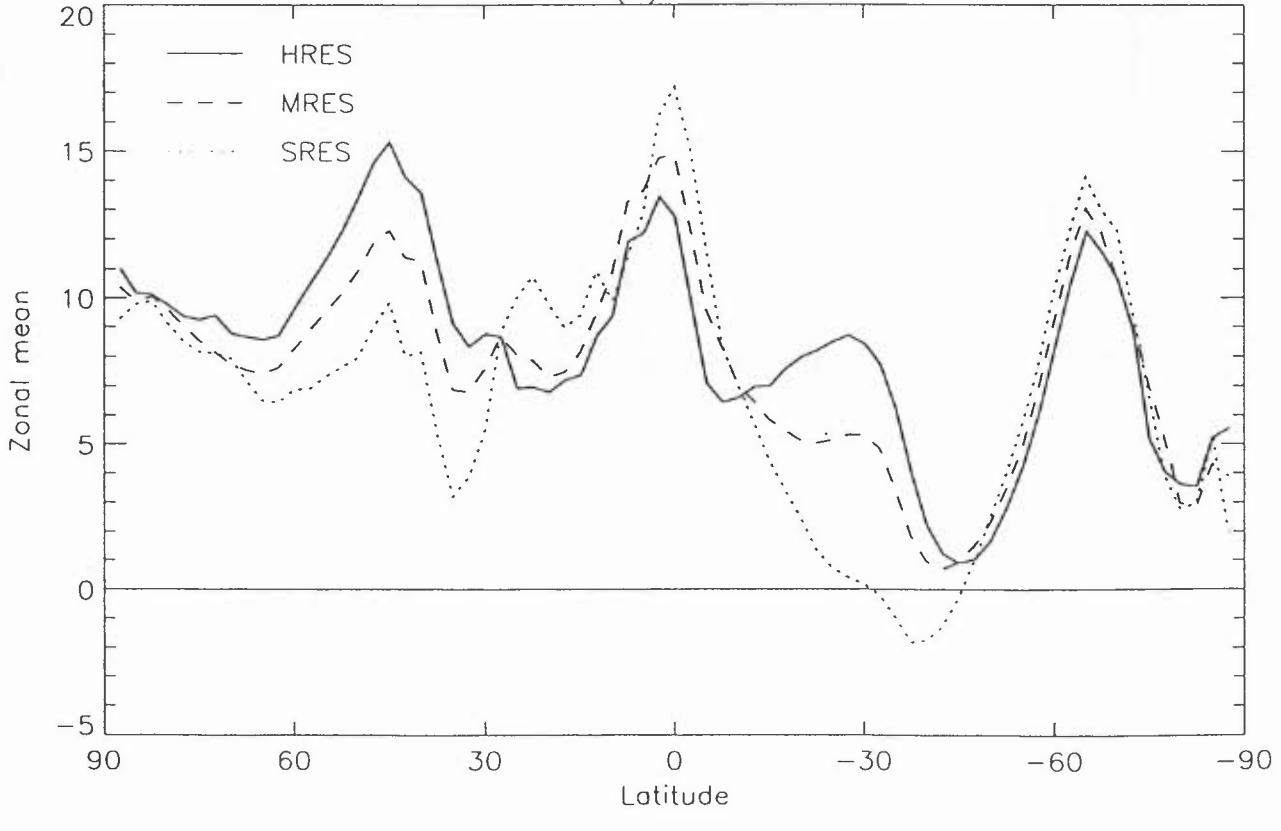

Fig 35 Shortwave cloud forcing for
(a) DJF

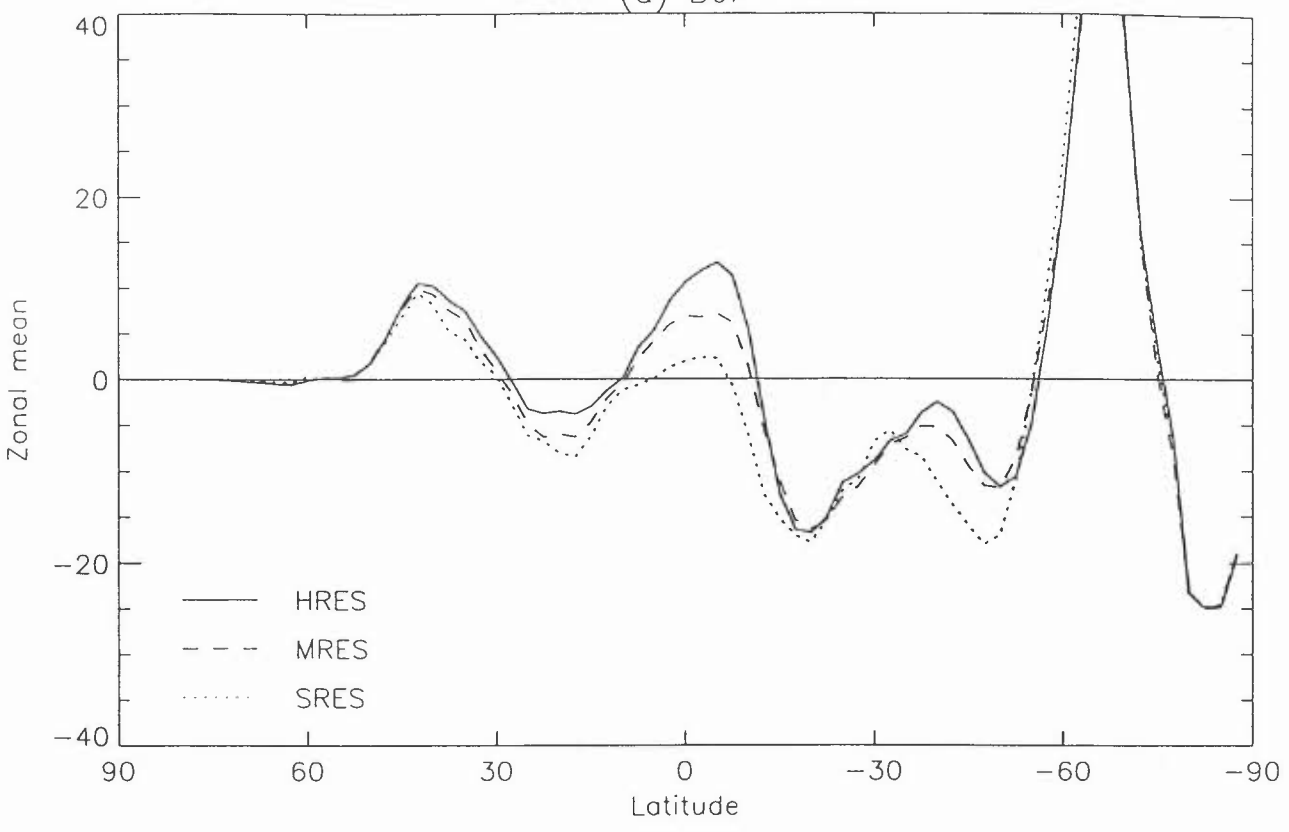

(b) JJA

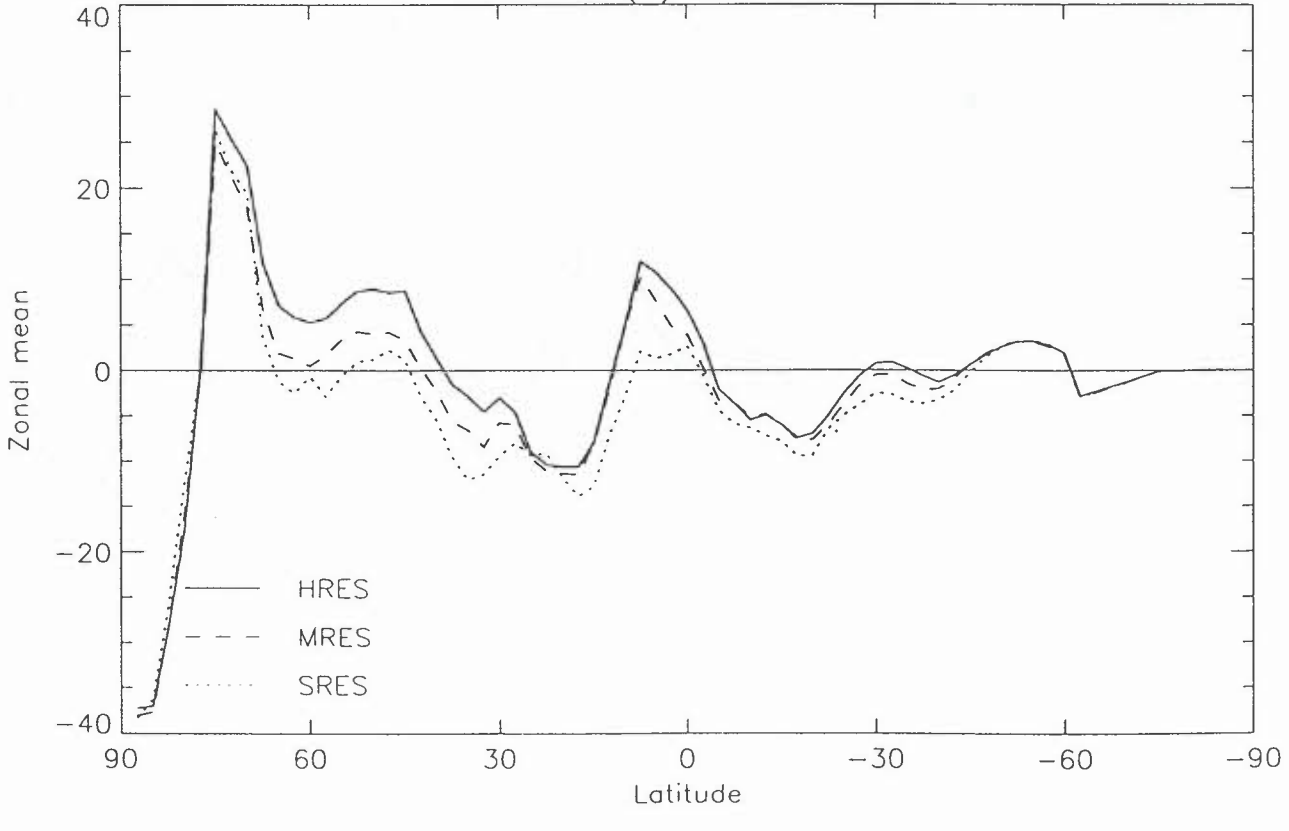

Fig 36 longwave cloud forcing for
(a) DJF

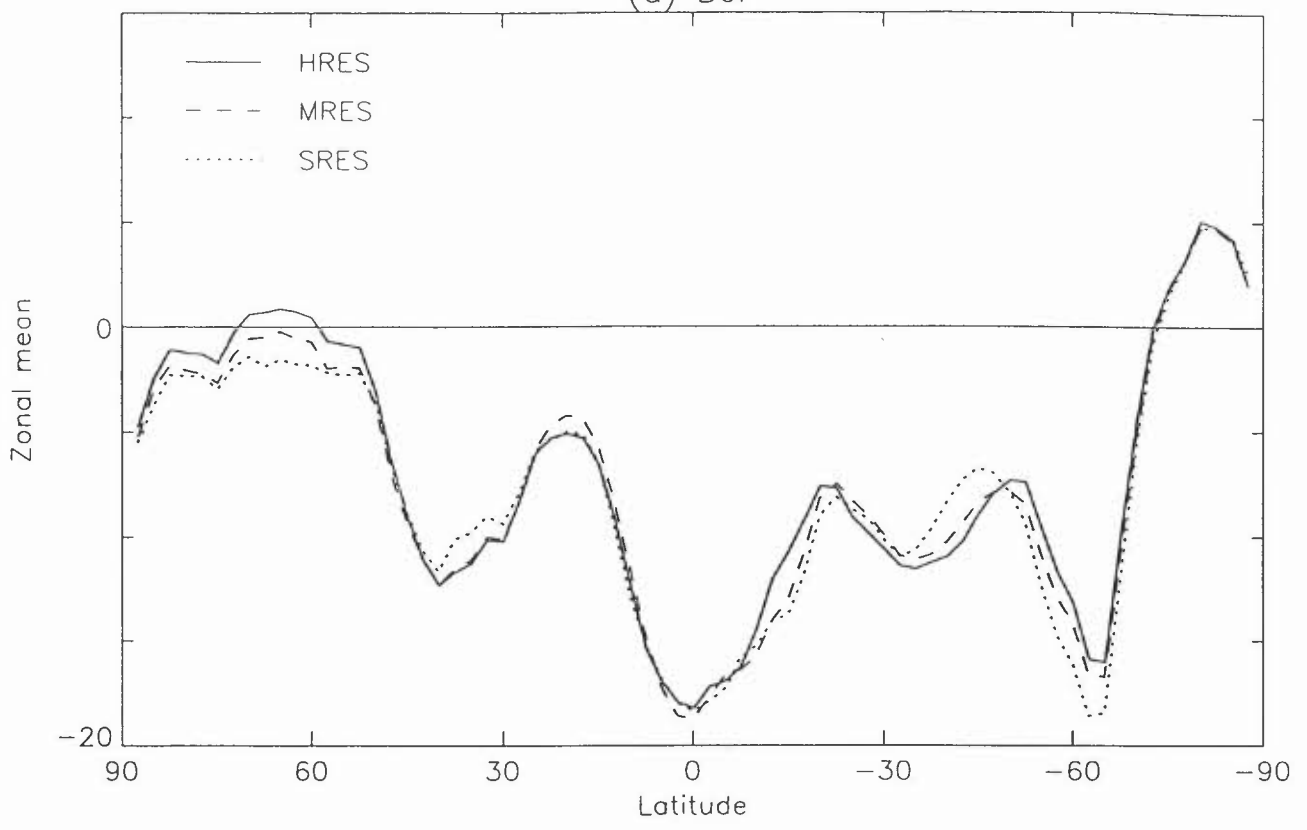

(b) JJA

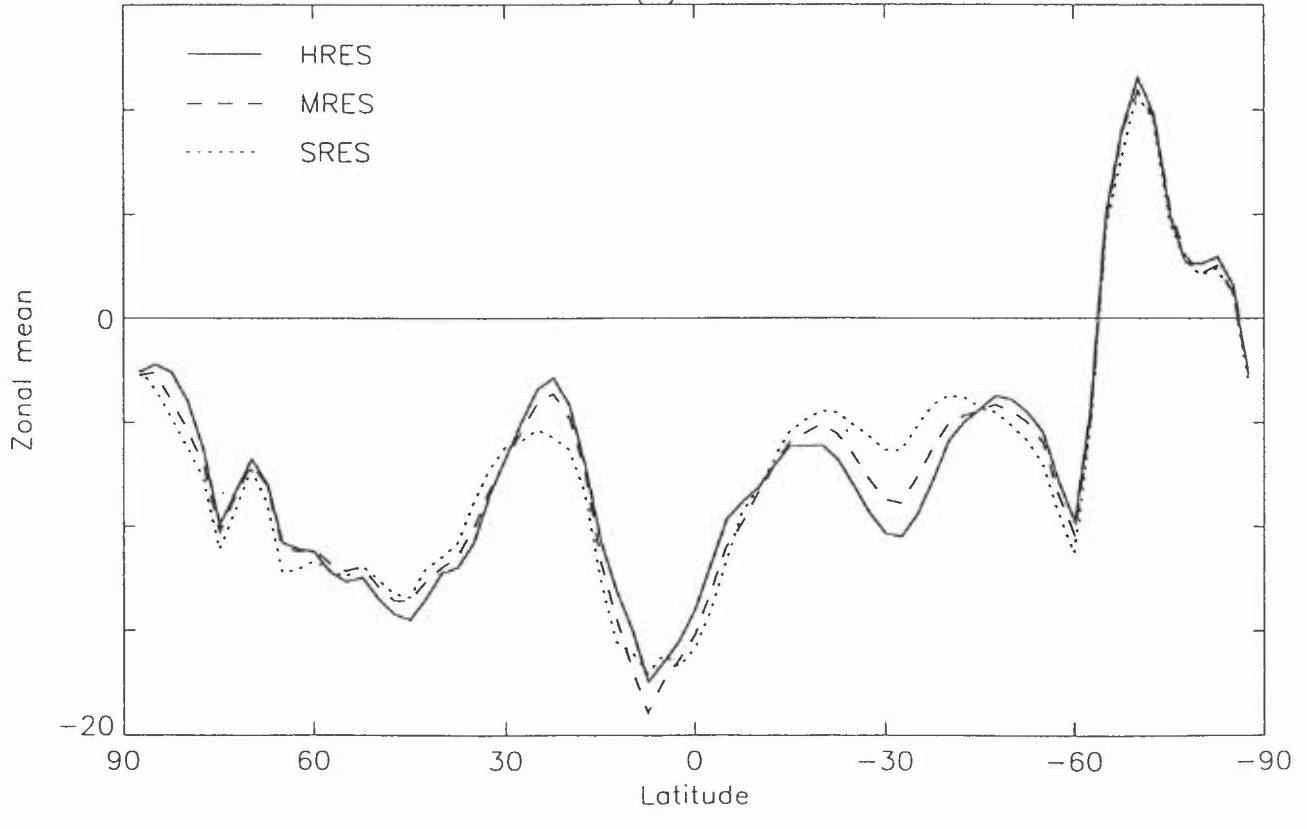

Fig 37 1.5m temperature for djf

(a) HRES

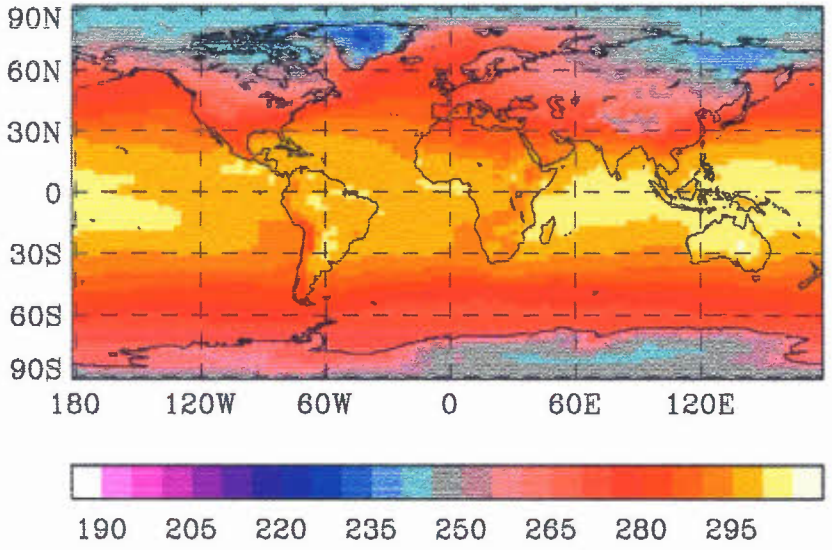

(b) HRES minus MRES

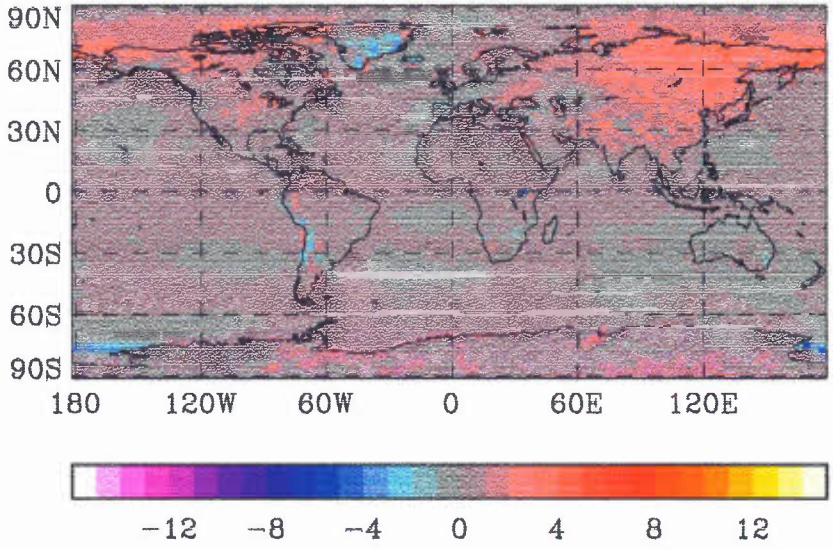

(c) MRES minus SRES

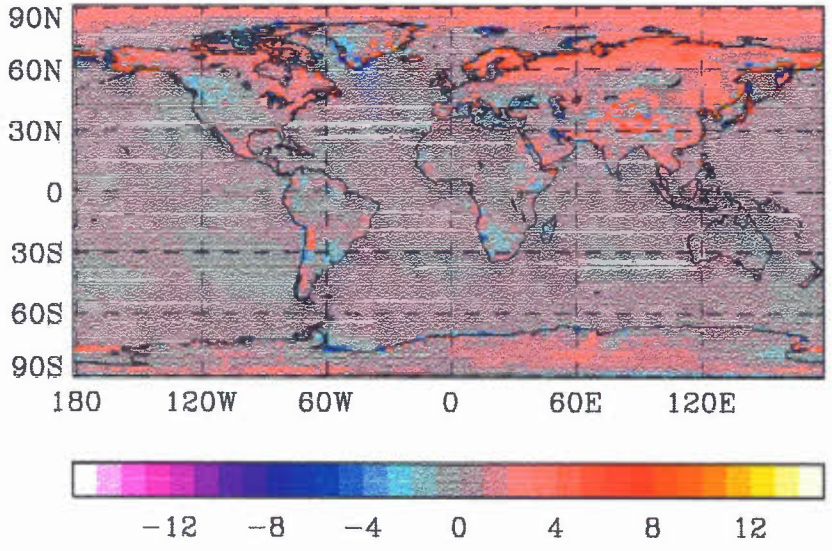

(d) HRES minus Legates & Willmott climatology

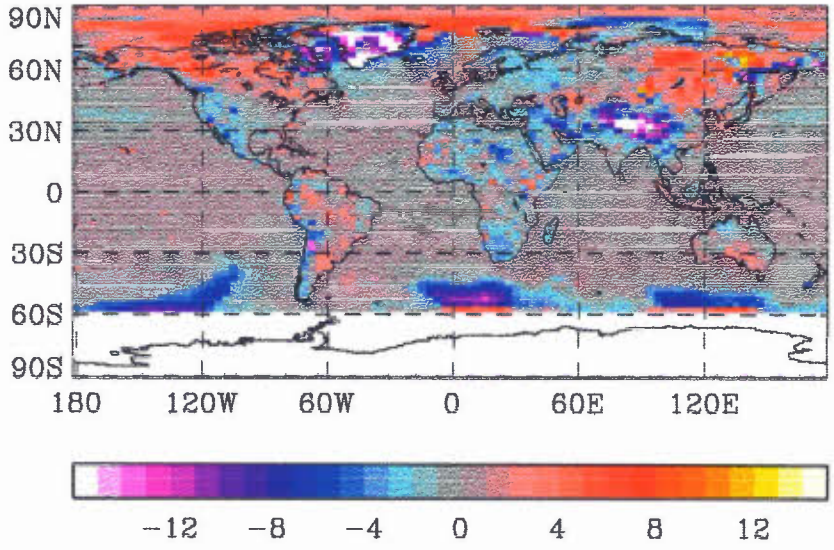

Fig 38 1.5m temperature for jja

(a) HRES

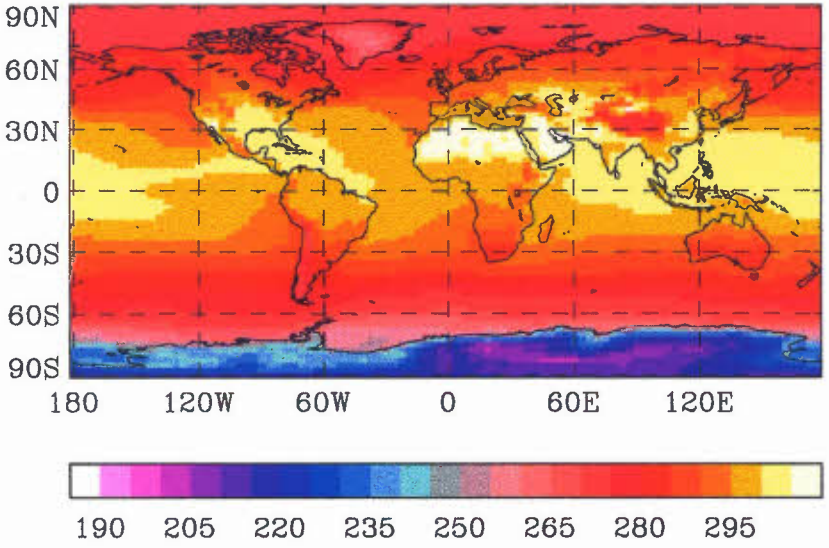

(b) HRES minus MRES

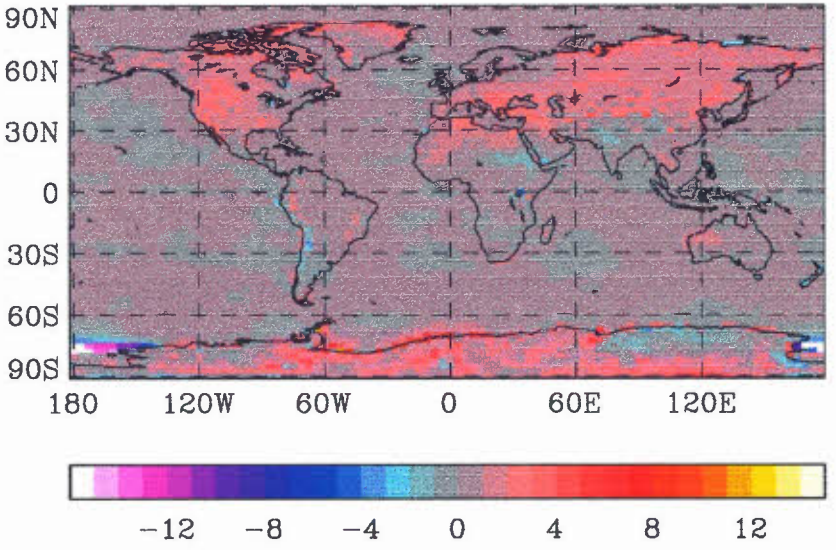

(c) MRES minus SRES

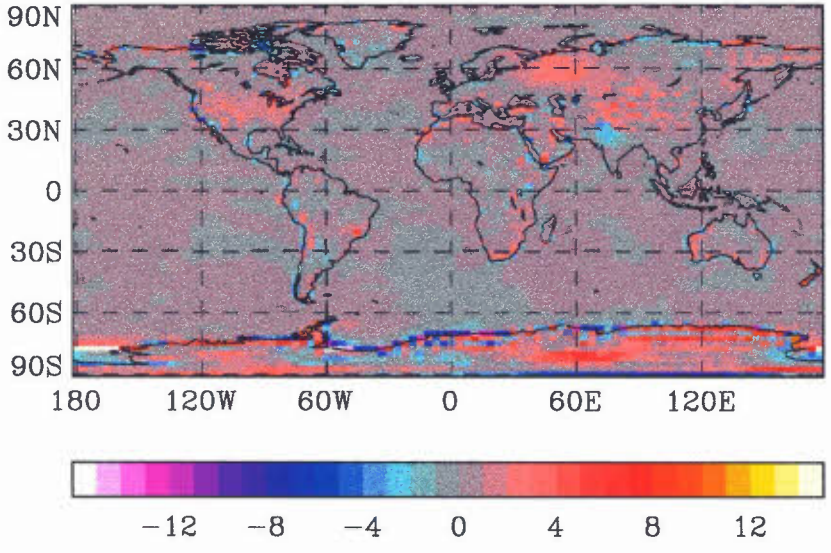

(d) HRES minus Legates & Willmott climatology

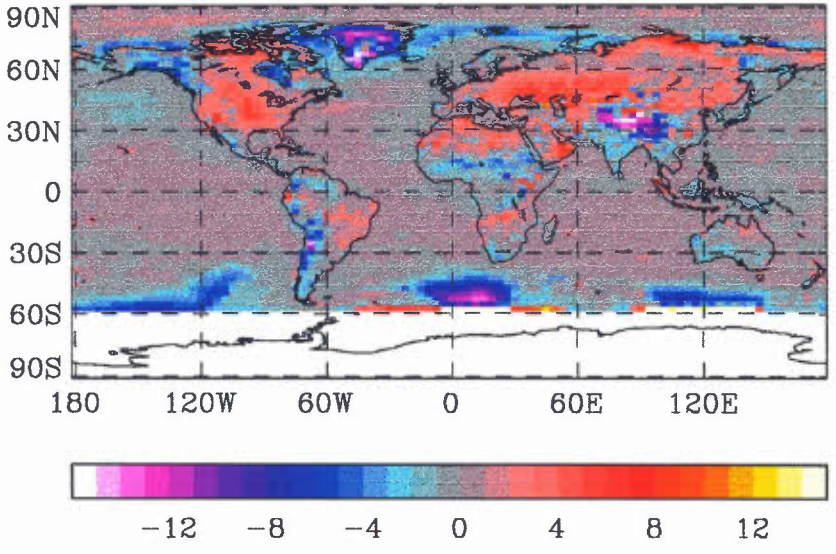

Fig 39

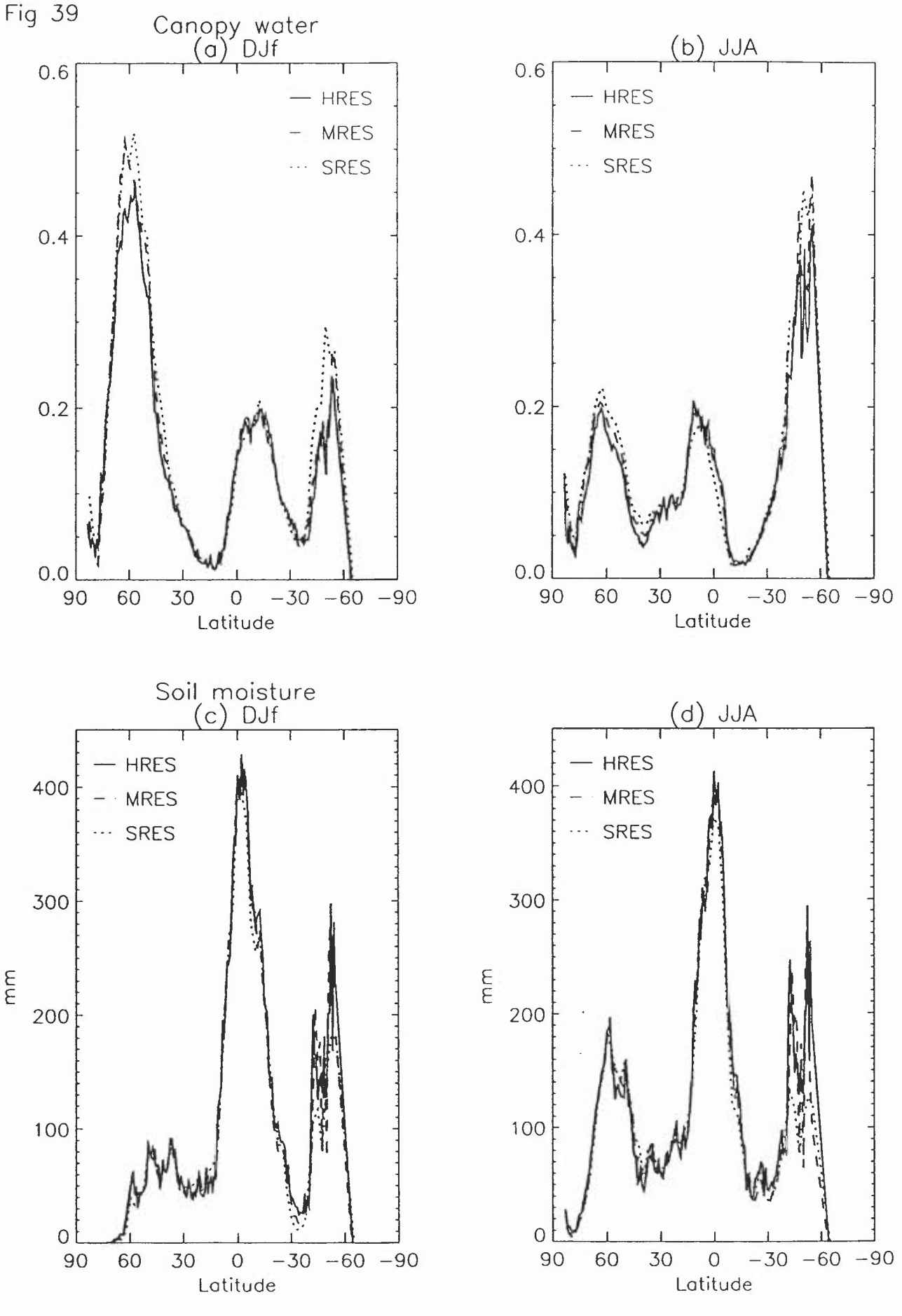
Canopy water
(a) DJf
(b) JJA
Soil moisture
(c) DJf
(d) JJA
HRES
MRES
SRES
0.0
0.2
0.4
0.6
0
100
200
300
400
mm
90
60
30
0
−30
−60
−90
Latitude

Fig 40

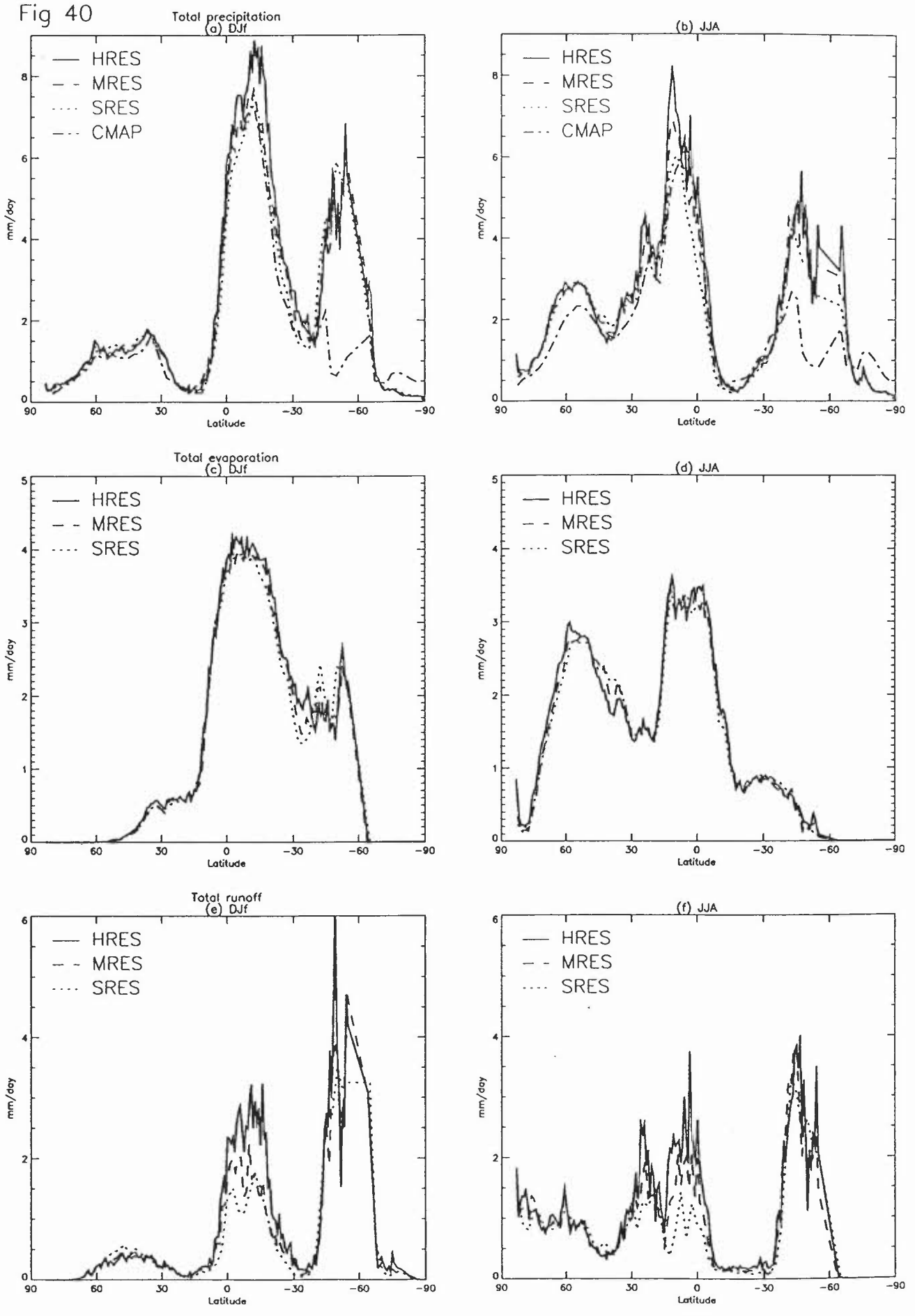
Total precipitation
(a) DJf
(b) JJA
Total evaporation
(c) DJf
(d) JJA
Total runoff
(e) DJf
(f) JJA
HRES
MRES
SRES
CMAP
mm/day
Latitude
90
60
30
0
-30
-60
-90

Fig 41 Zonal mean wind stress over the ocean

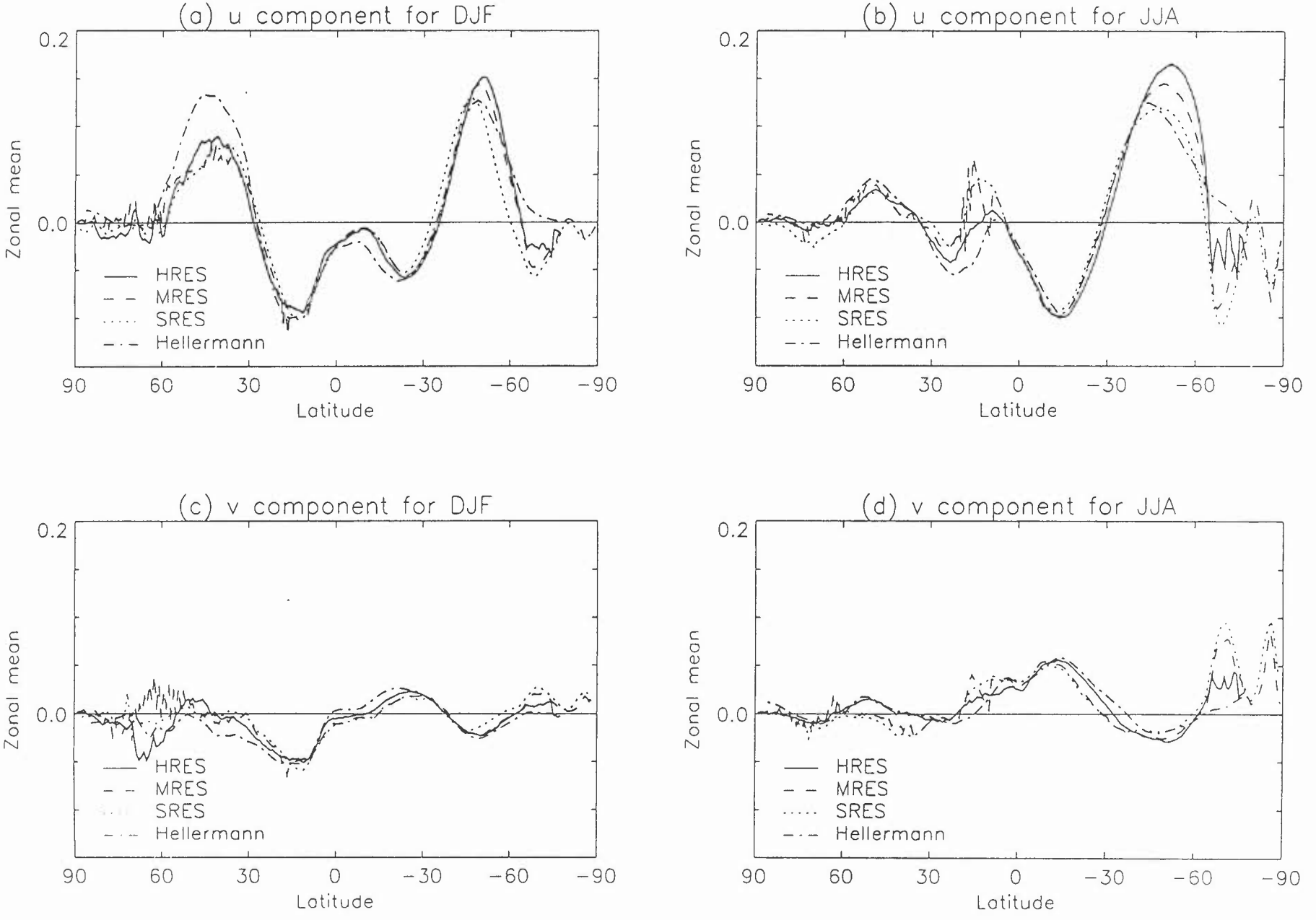

Fig 42 Net downward surface heating over the ocean model minus da Silva
(a) annual mean

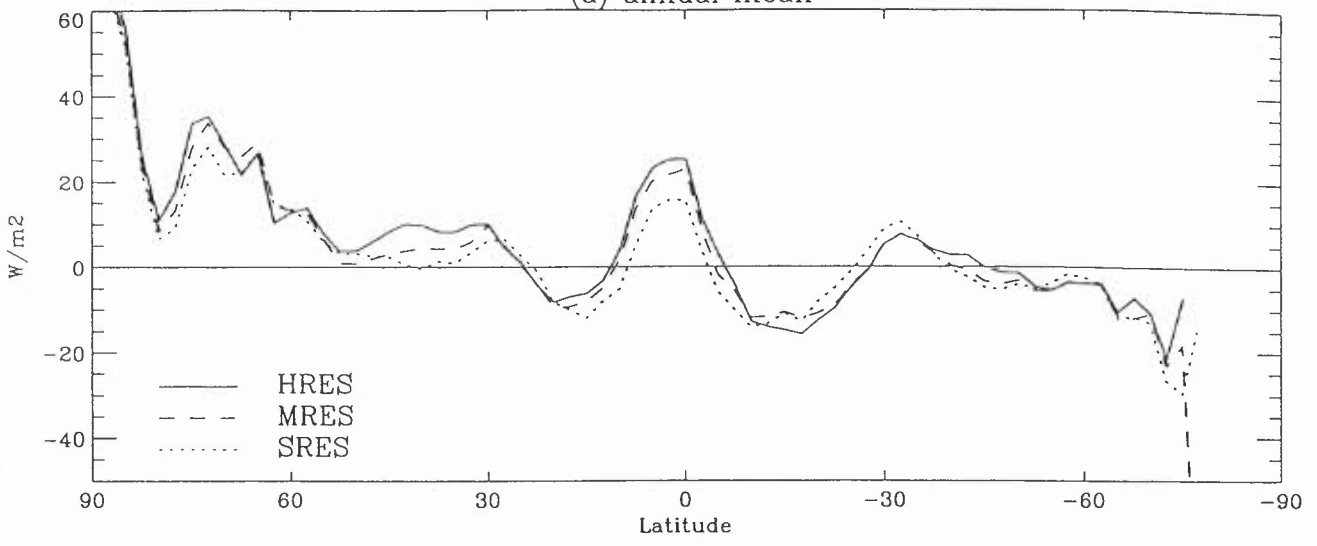

(b) DJF

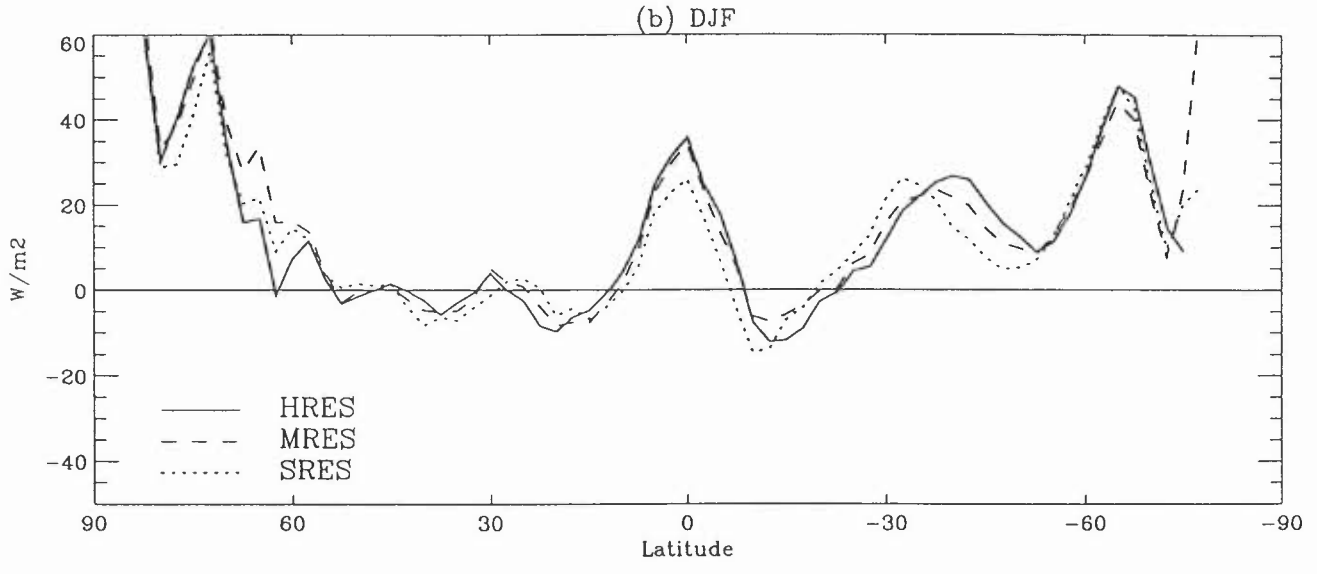

(c) JJA

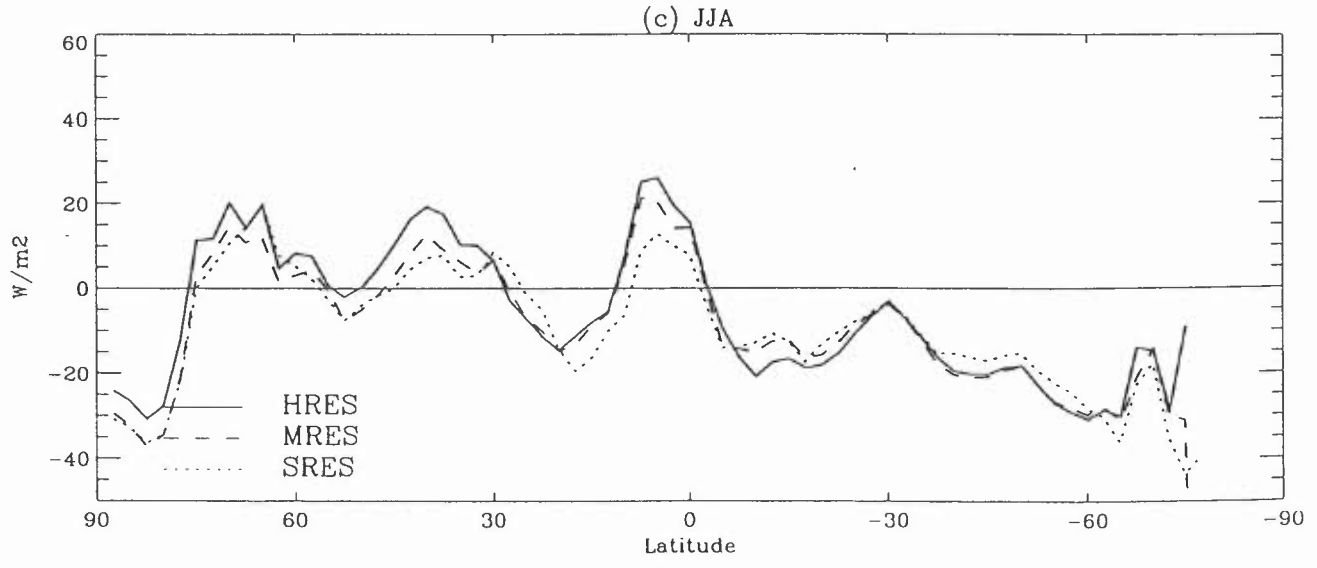

Fig 43 Annual mean model minus da Silva over the ocean

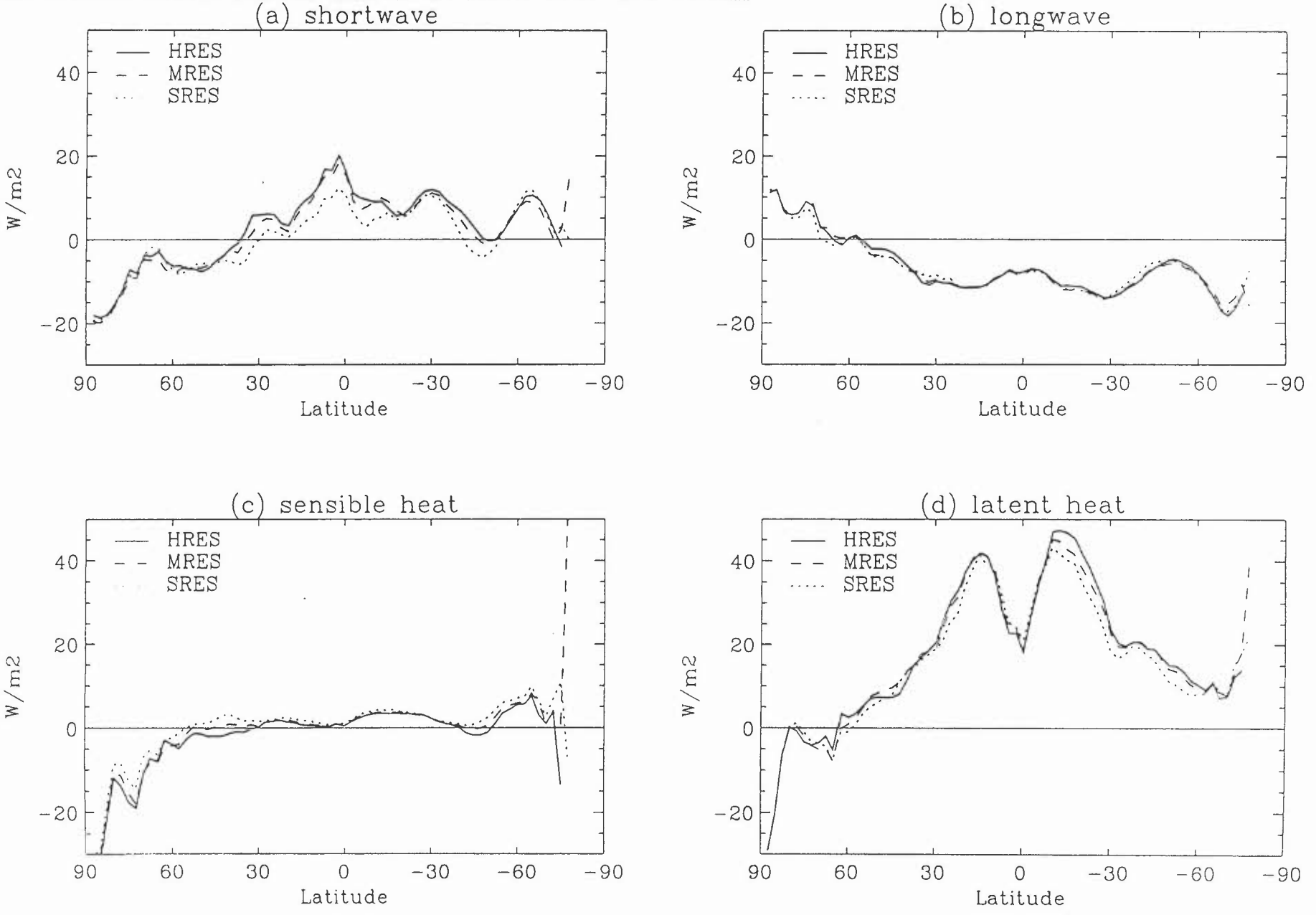

Fig 44 Blocking index northern hemisphere

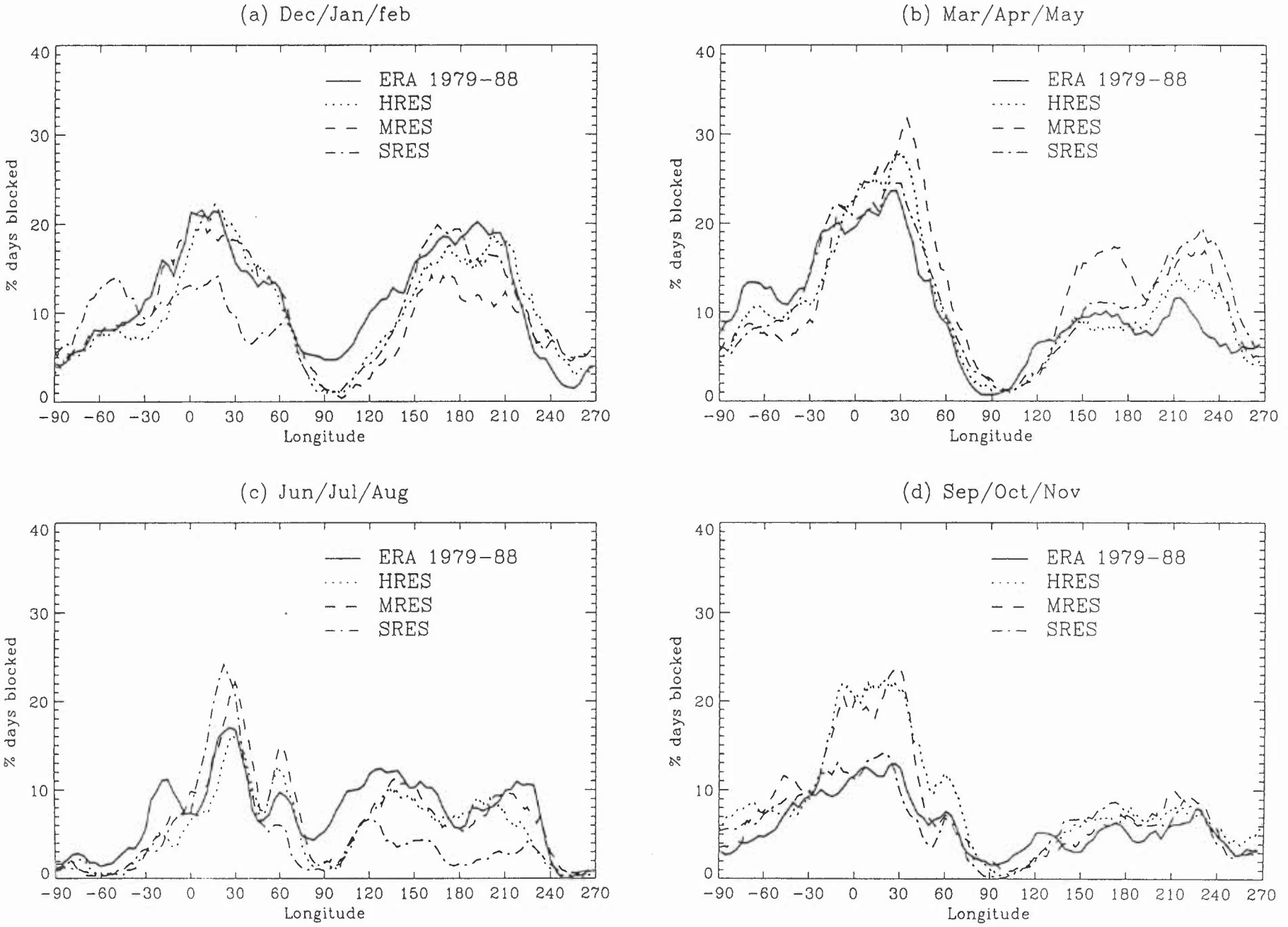

Fig 45 Blocking index southern hemisphere

(a) Dec/Jan/feb

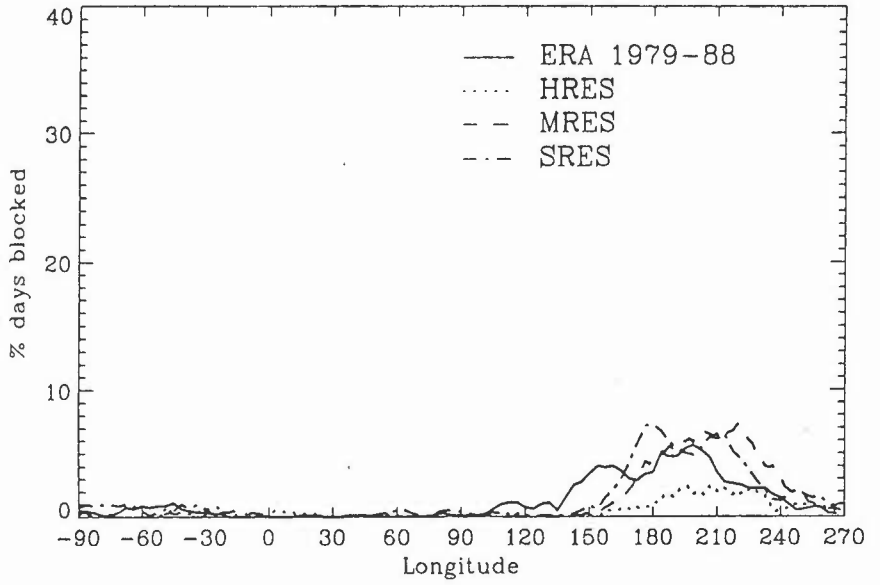

(b) Mar/Apr/May

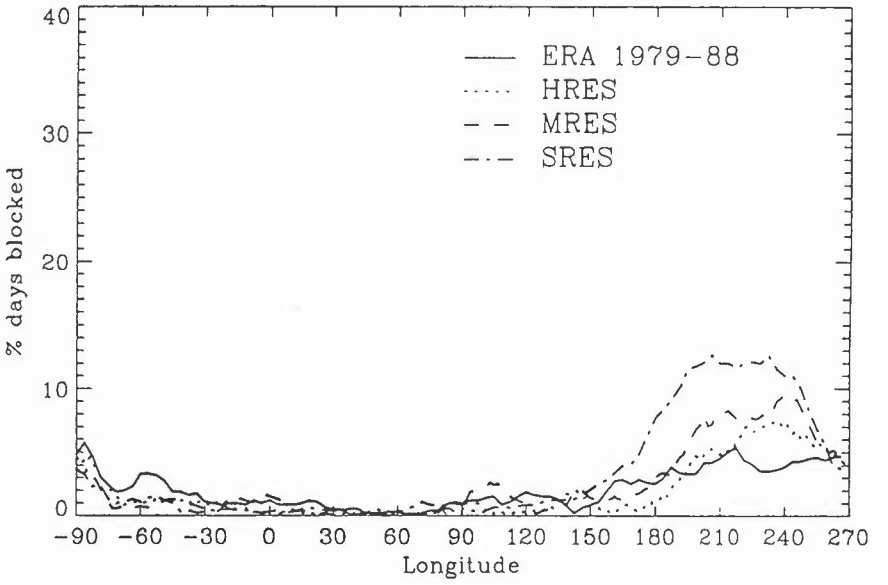

(c) Jun/Jul/Aug

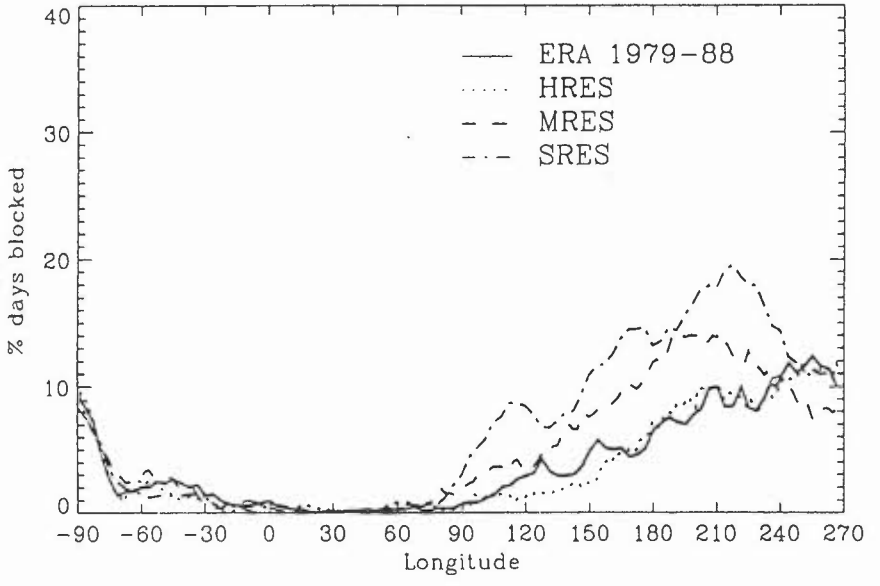

(d) Sep/Oct/Nov

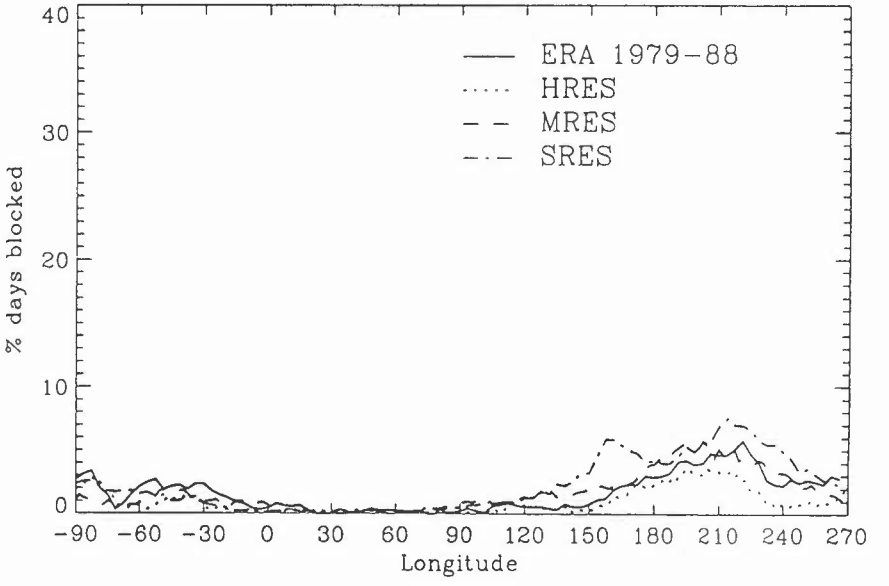

(a) ERA 1979–88

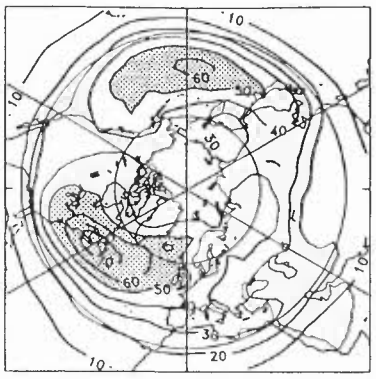

Contours every 10.m

(b) ERA 1979–88

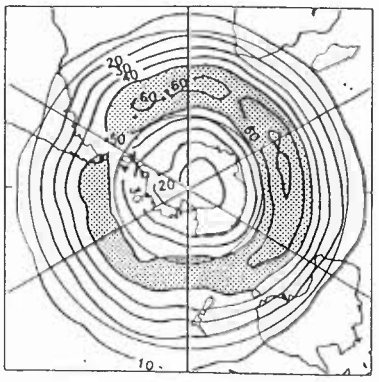

Contours every 10.m

(c) HRES

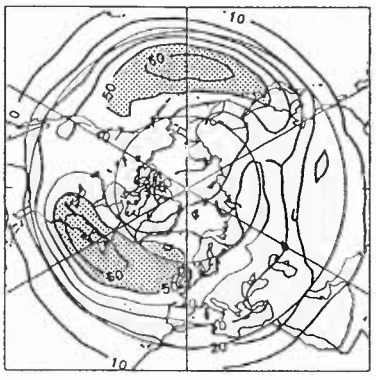

Contours every 10.m

(d) HRES

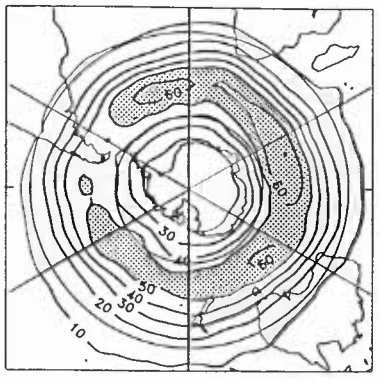

Contours every 10.m

(e) MRES

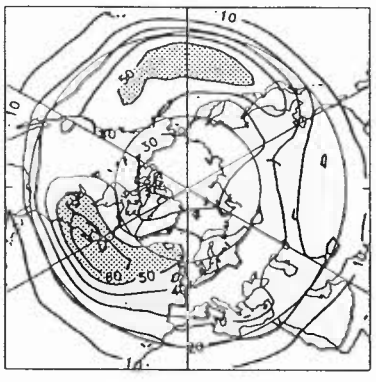

Contours every 10.m

(f) MRES

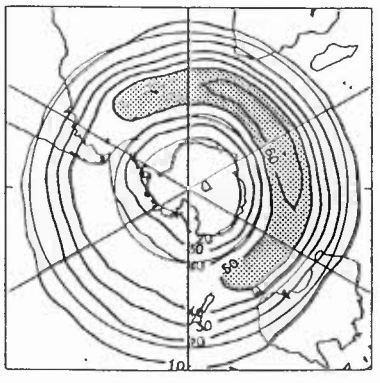

Contours every 10.m

(g) SRES

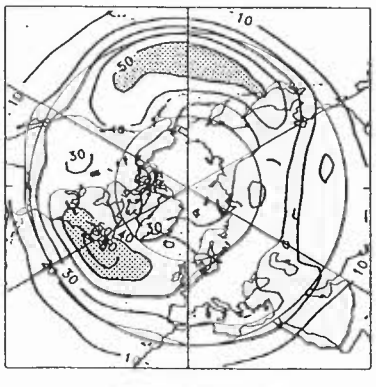

Contours every 10.m

(h) SRES

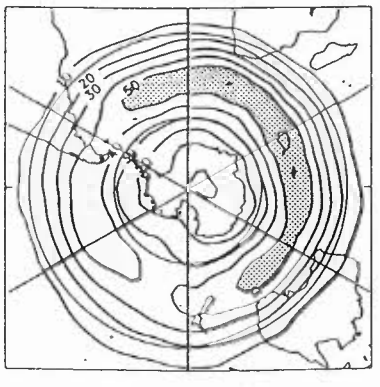

Contours every 10.m

Fig 46 s.d. of band pass filtered 500hPa height. Dec/Jan/Feb

(a) ERA 1979–88

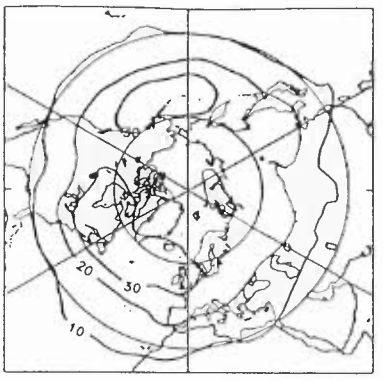

Contours every 10.m

(b) ERA 1979–88

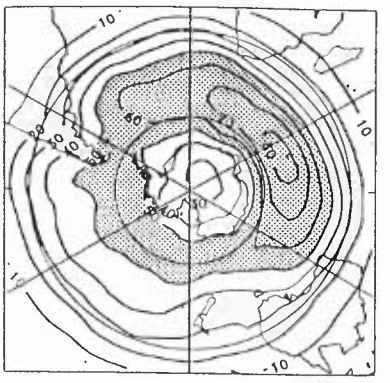

Contours every 10.m

(c) HRES

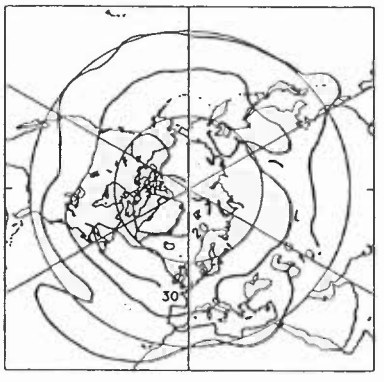

Contours every 10.m

(d) HRES

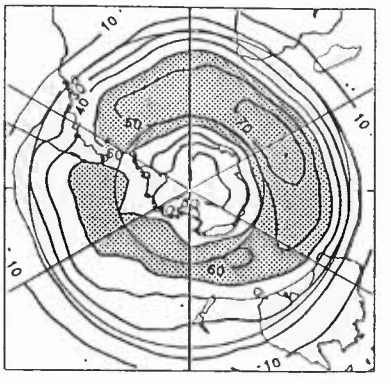

Contours every 10.m

(e) MRES

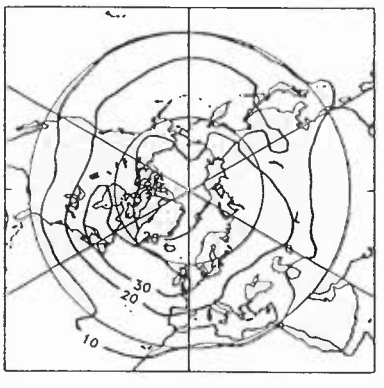

Contours every 10.m

(f) MRES

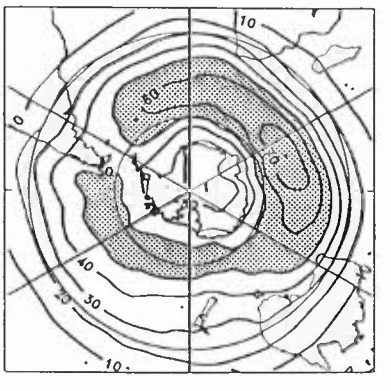

Contours every 10.m

(g) SRES

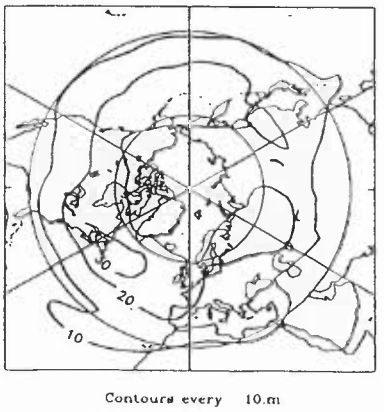

Contours every 10.m

(h) SRES

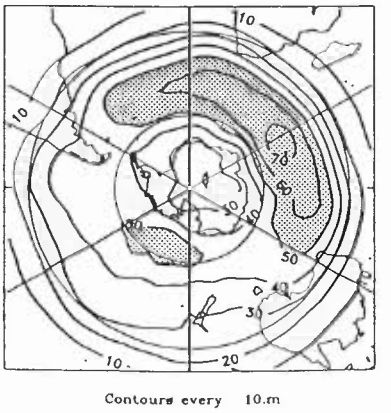

Contours every 10.m

Fig 47 s.d. of band pass filtered 500hPa height. Jun/Jul/Aug

(a) ERA 1979-88

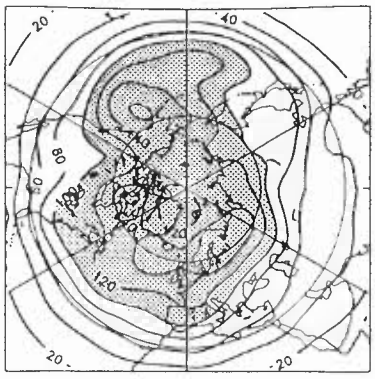

Contours every 20.m

(b) ERA 1979-88

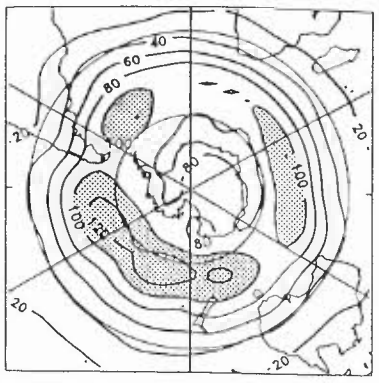

Contours every 20.m

(c) HRES

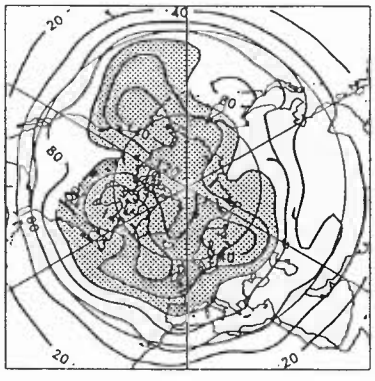

Contours every 20.m

(d) HRES

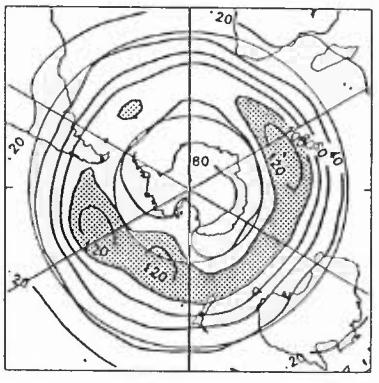

Contours every 20.m

(e) MRES

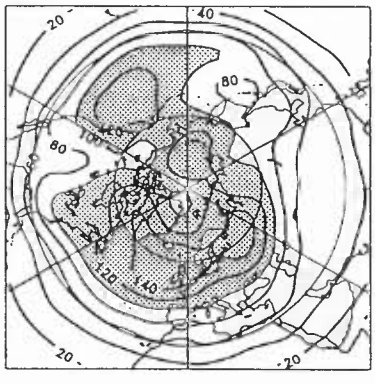

Contours every 20.m

(f) MRES

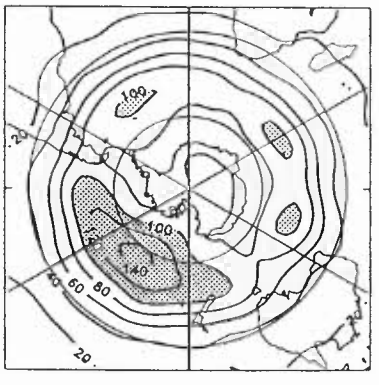

Contours every 20.m

(g) SRES

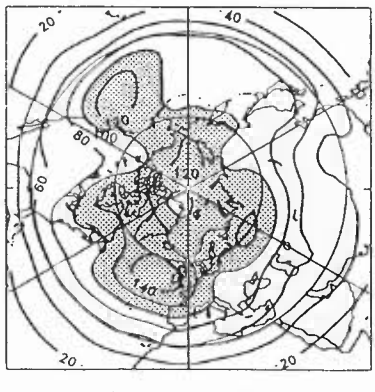

Contours every 20.m

(h) SRES

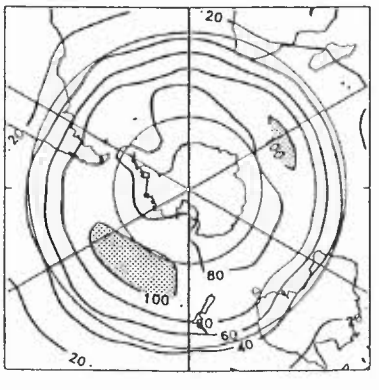

Contours every 20.m

Fig 48 s.d. of low pass filtered 500hPa height. Dec/Jan/Feb

(a) ERA 1979–88

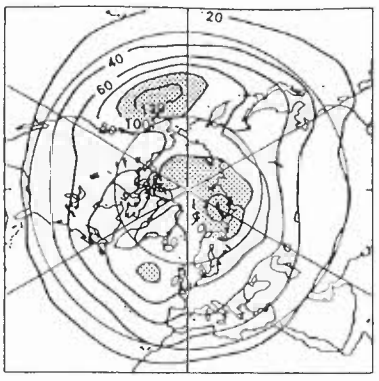

Contours every 20.m

(b) ERA 1979–88

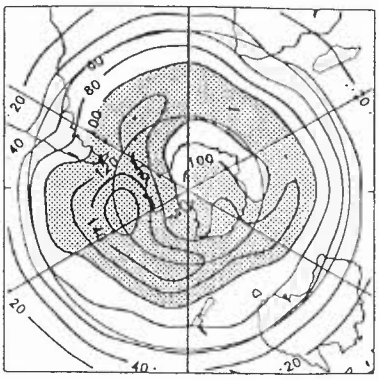

Contours every 20.m

(c) HRES

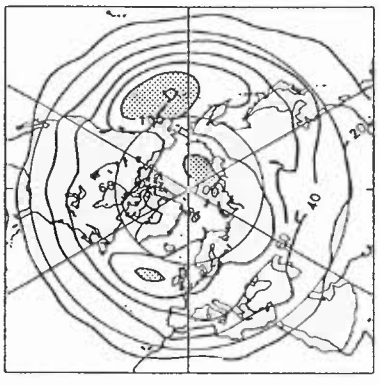

Contours every 20.m

(d) HRES

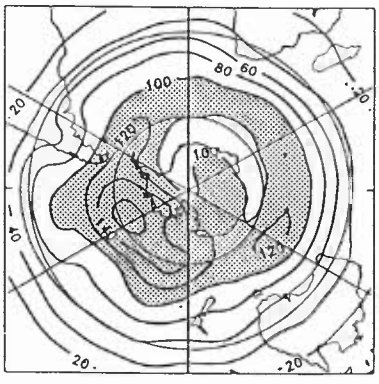

Contours every 20.m

(e) MRES

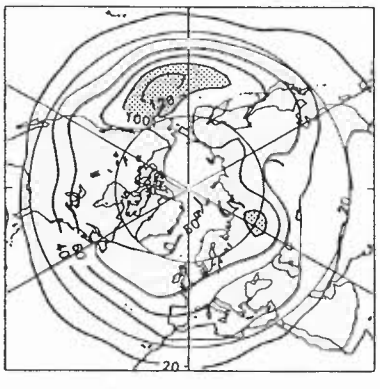

Contours every 20.m

(f) MRES

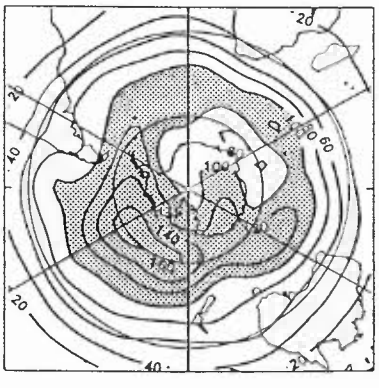

Contours every 20.m

(g) SRES

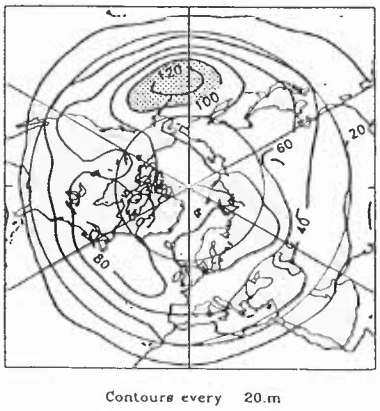

Contours every 20.m

(h) SRES

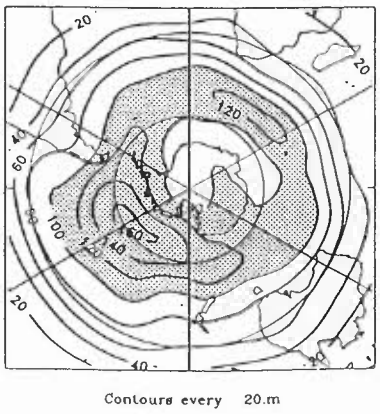

Contours every 20.m

Fig 49 s.d. of low pass filtered 500hPa height. Jun/Jul/Aug

Figure 50 Mean wave number 1 power spectrum for 1979 to 1988 200 hPa Velocity potential

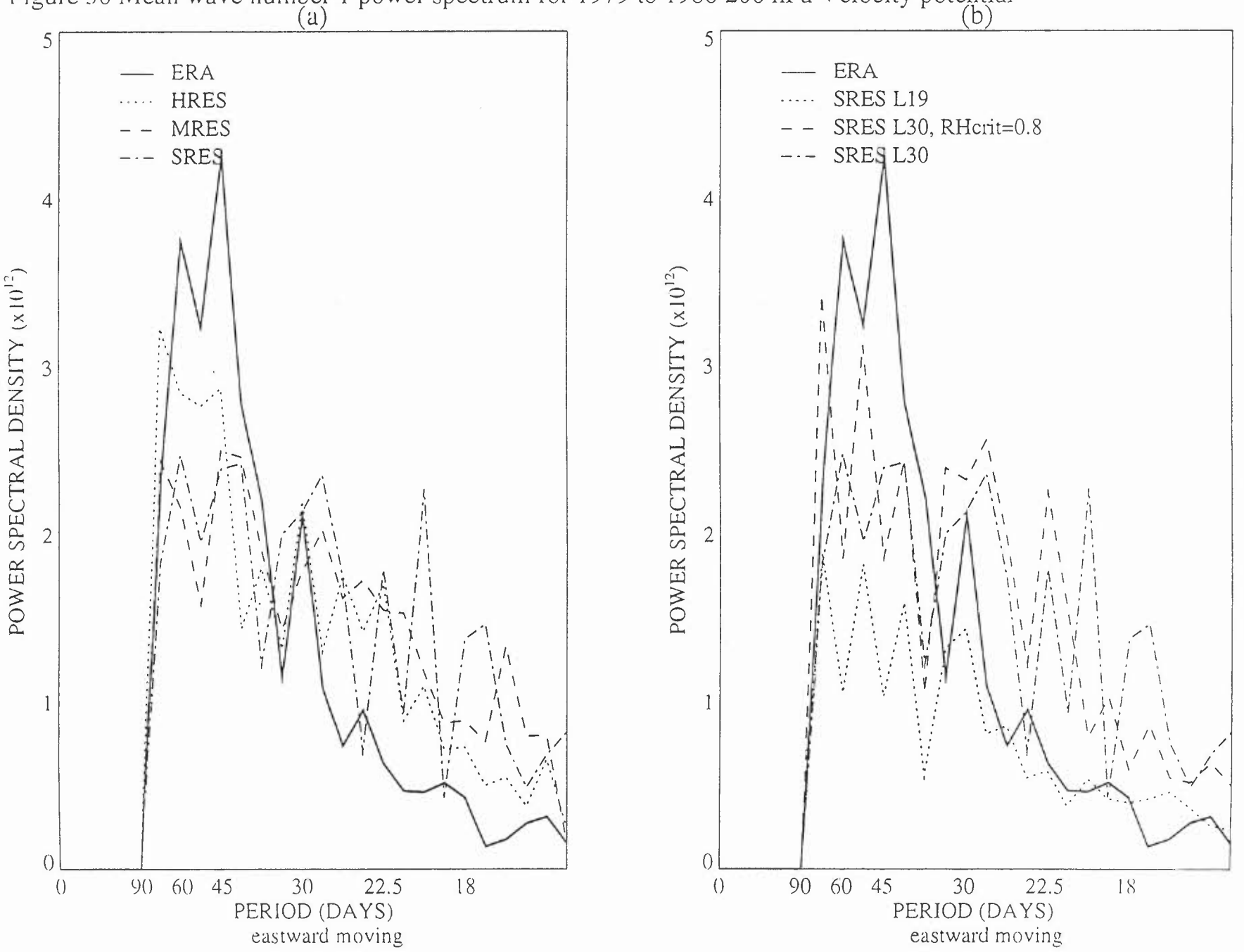

Figure 51 12 month running mean anomalies for NINO3 5N–5S 90–150W

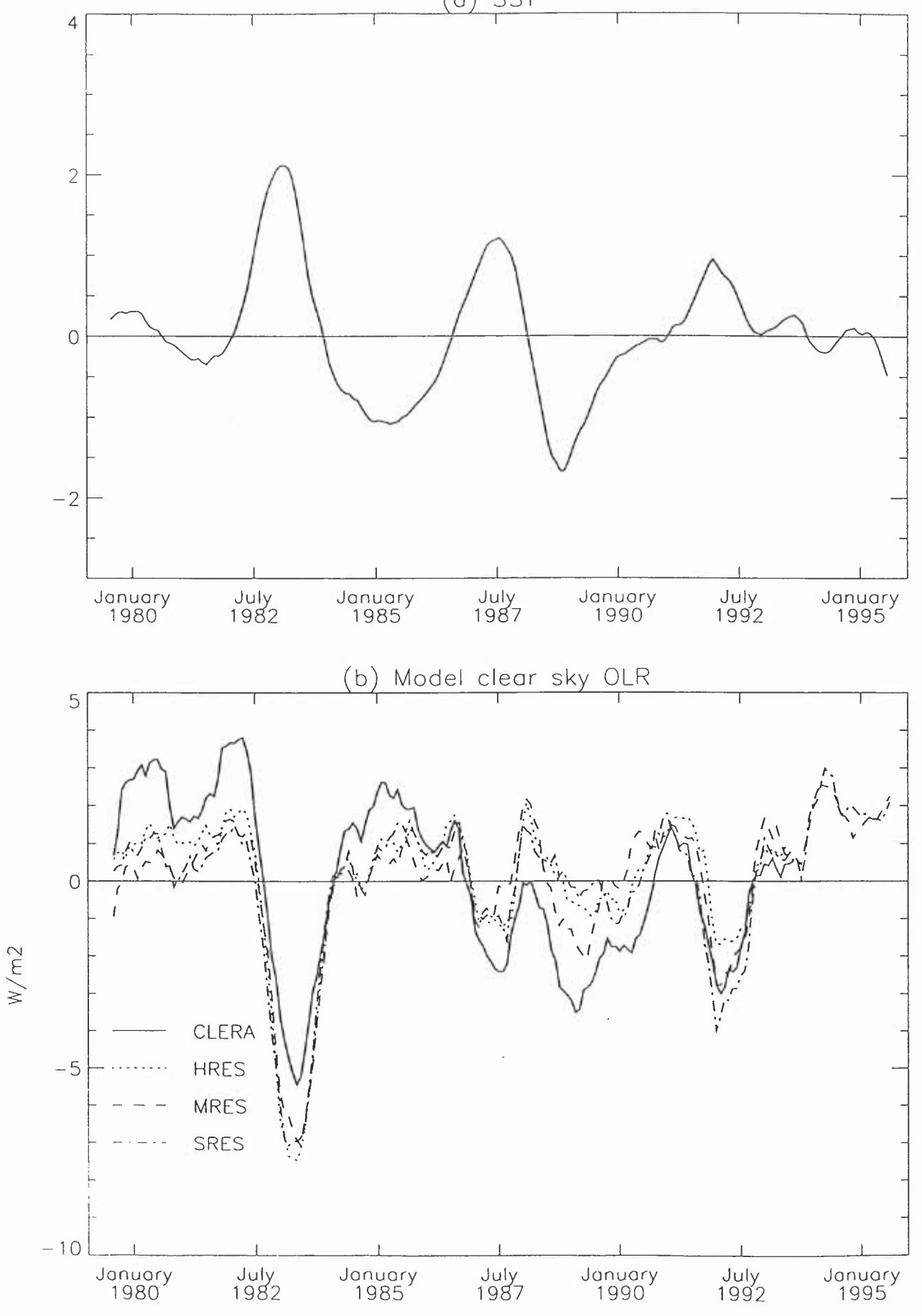

Figure 52 12 month running mean anomalies for 40–55N 10–50W

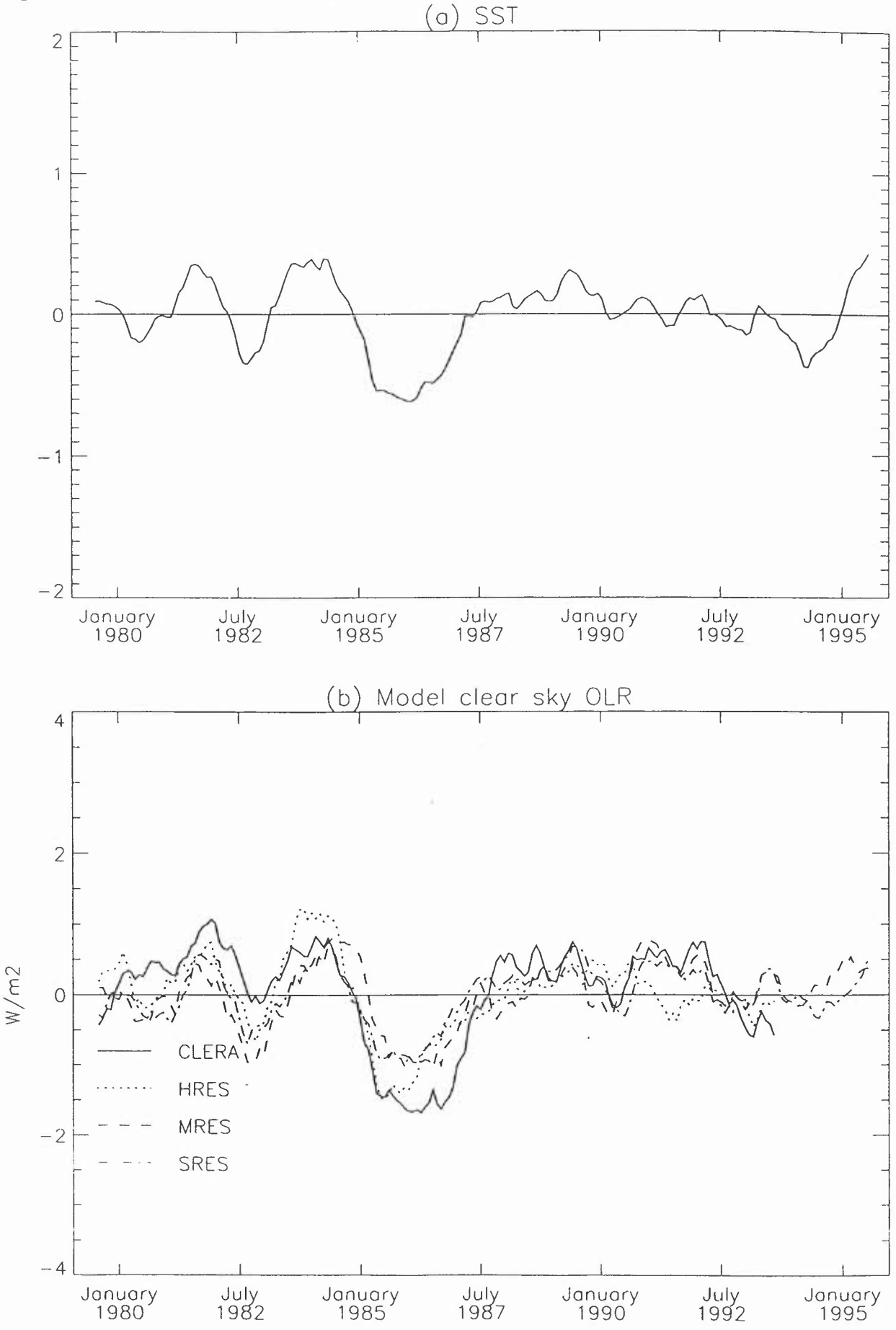

Figure 53 12 month running mean anomalies for 40–50N 180–210E

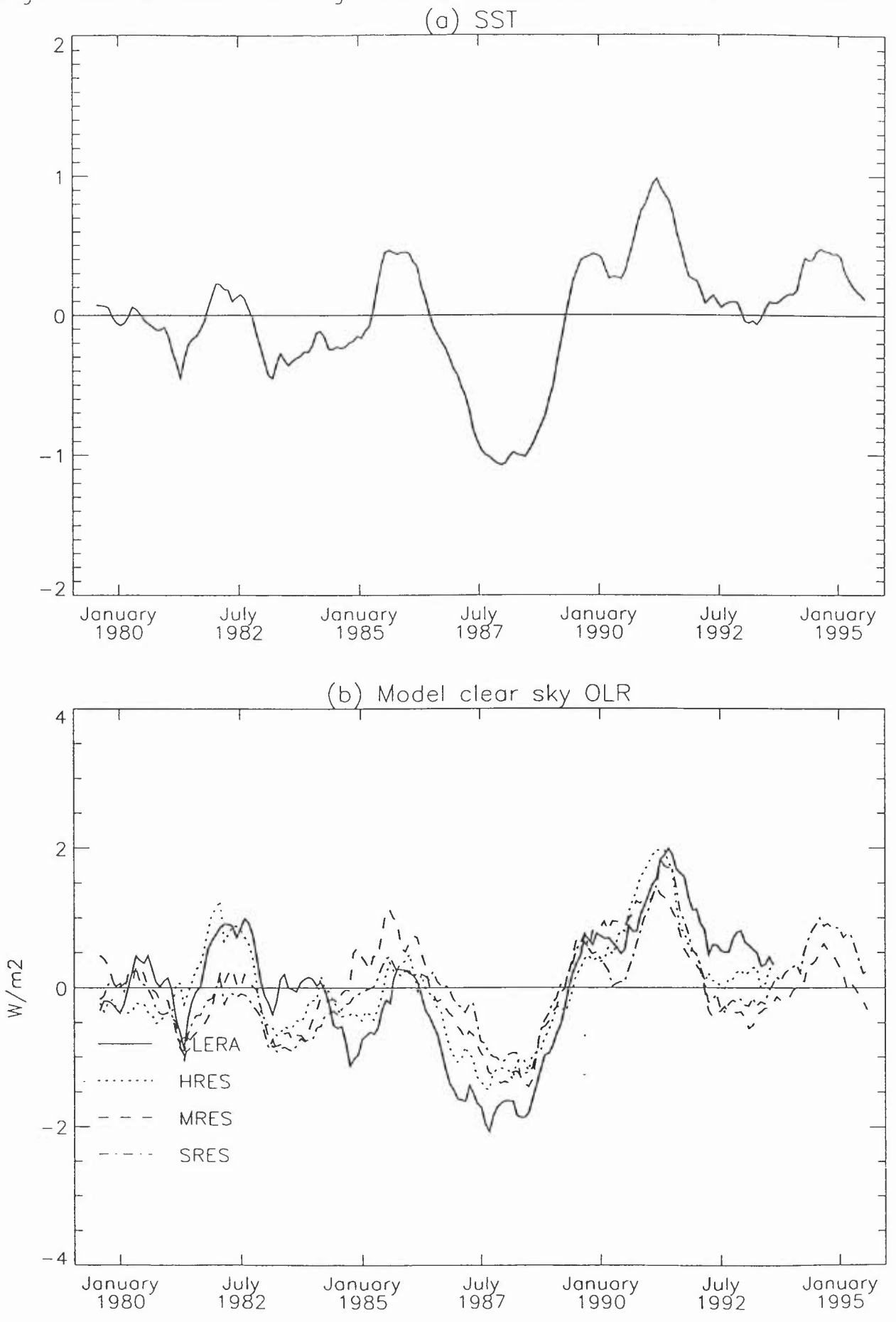

Fig 54 Standard deviation of mean sea level pressure for djf for 1979-88

(a) HRES

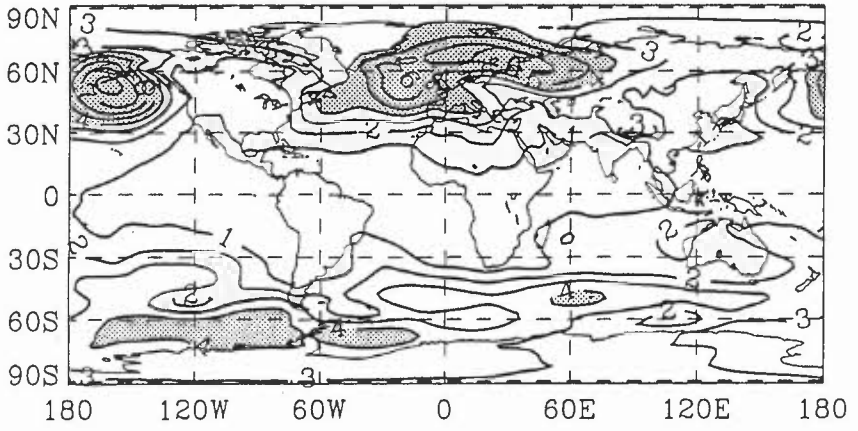

mean = 2.00 Contours every 1. hPa

(b) MRES

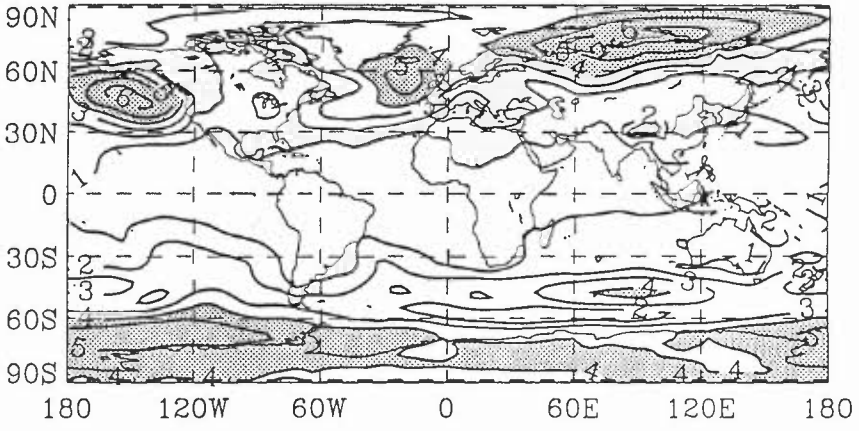

mean = 1.83 Contours every 1. hPa

(c) SRES

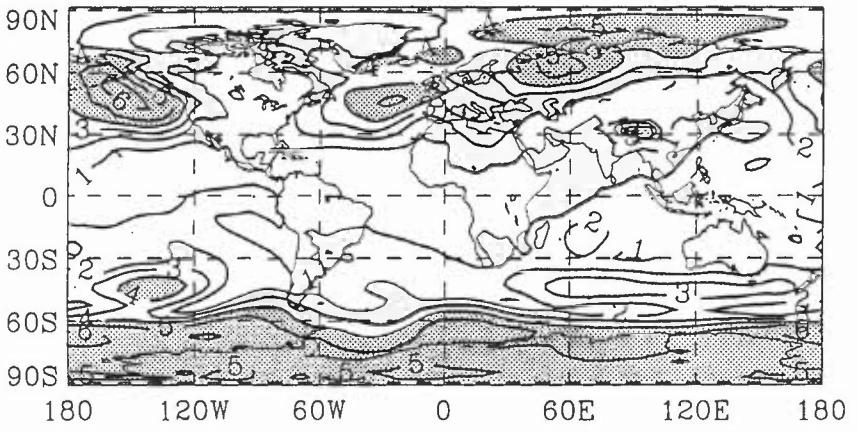

mean = 2.01 Contours every 1. hPa

(d) ERA 1979-88

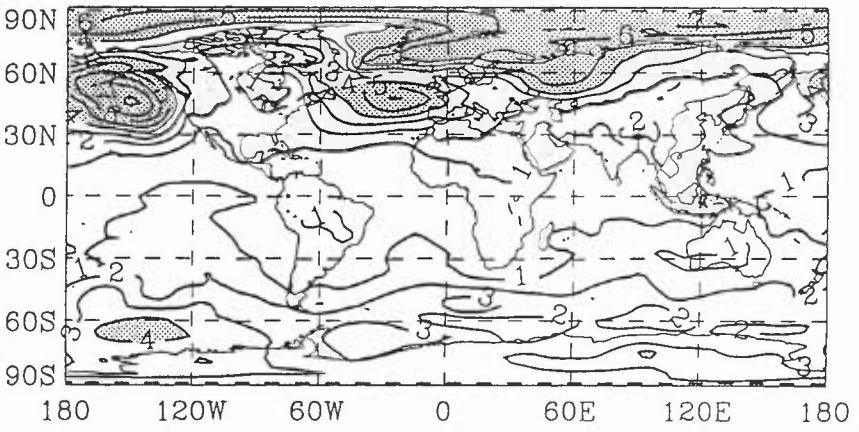

mean = 1.78 Contours every 1. hPa

Fig 55 Standard deviation of mean sea level pressure for jja for 1979–88

(a) HRES

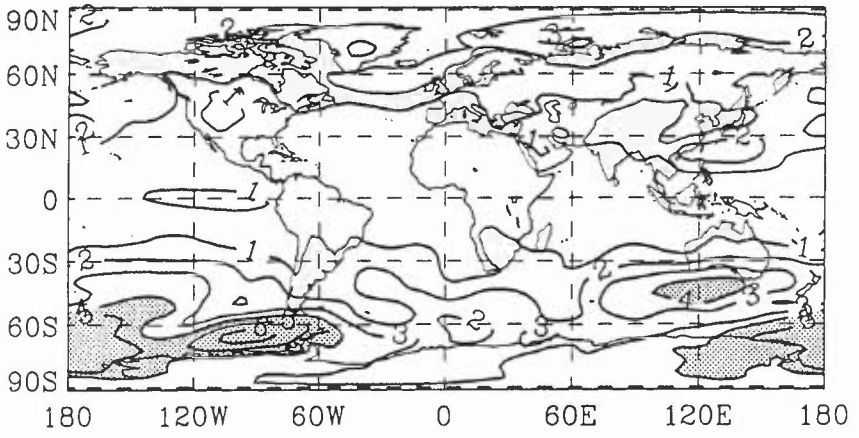

mean = 1.45 Contours every 1. hPa

(b) MRES

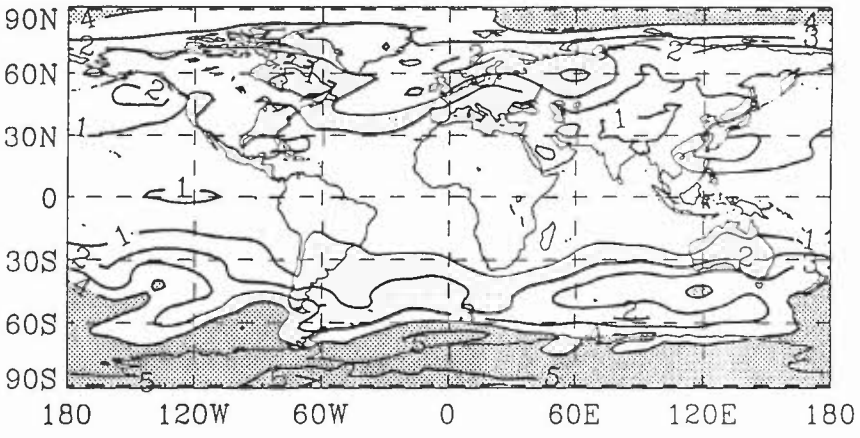

mean = 1.55 Contours every 1. hPa

(c) SRES

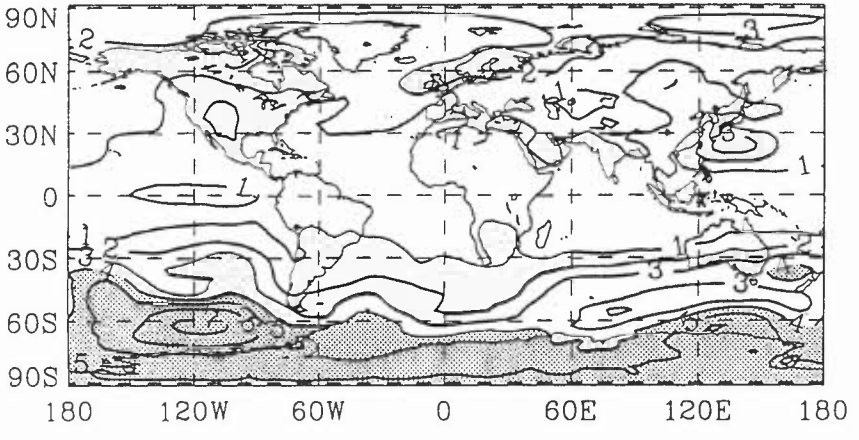

mean = 1.64 Contours every 1. hPa

(d) ERA 1979–88

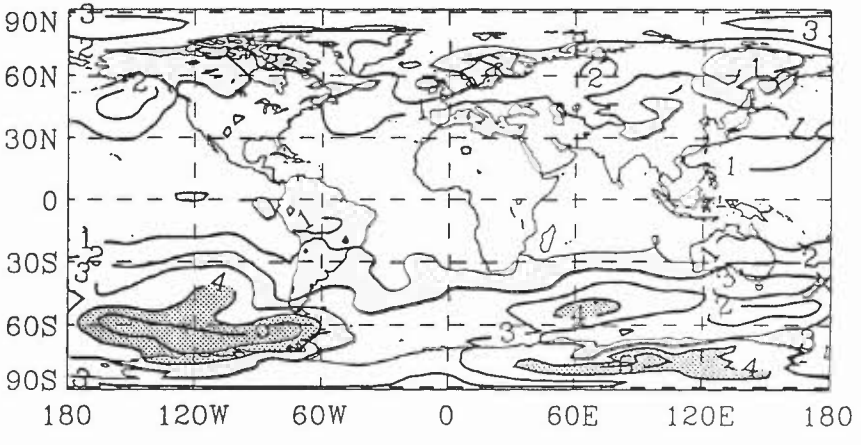

mean = 1.37 Contours every 1. hPa

Fig 56 T test for mean sea level pressure abbch minus abbci

(a) DJF

Fraction of the globe with 95% sig = 0.06

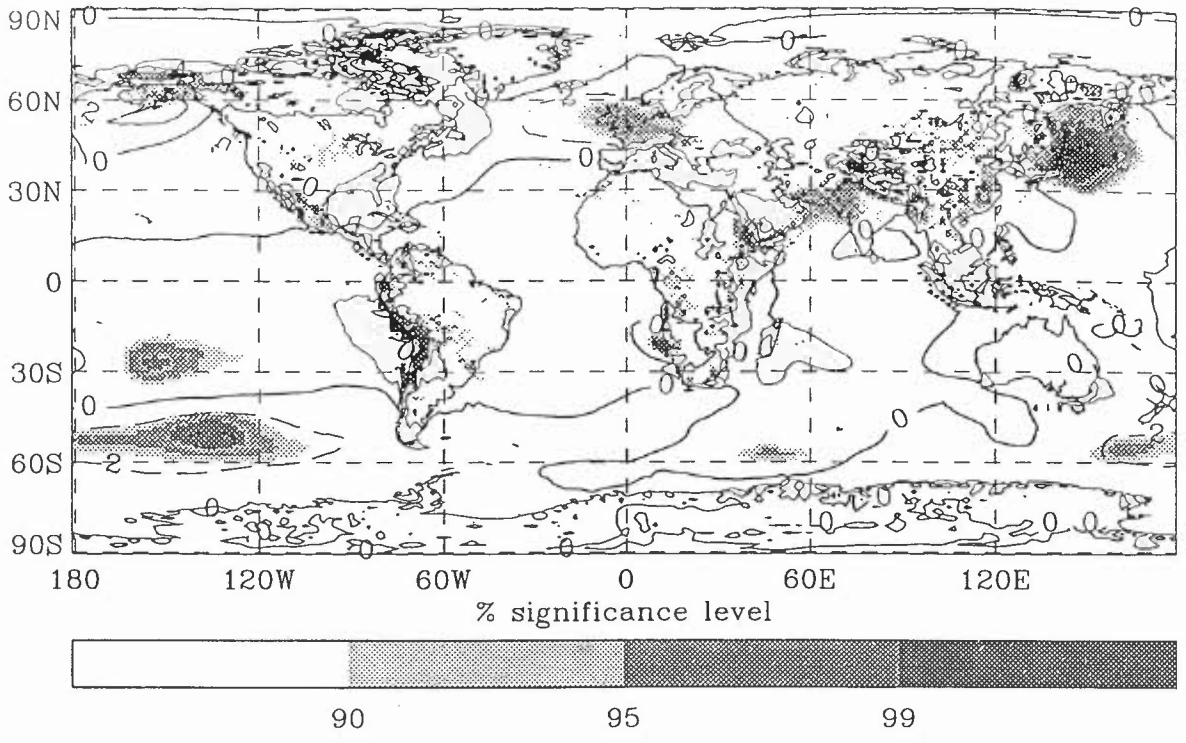

(b) JJA

Fraction of the globe with 95% sig = 0.09

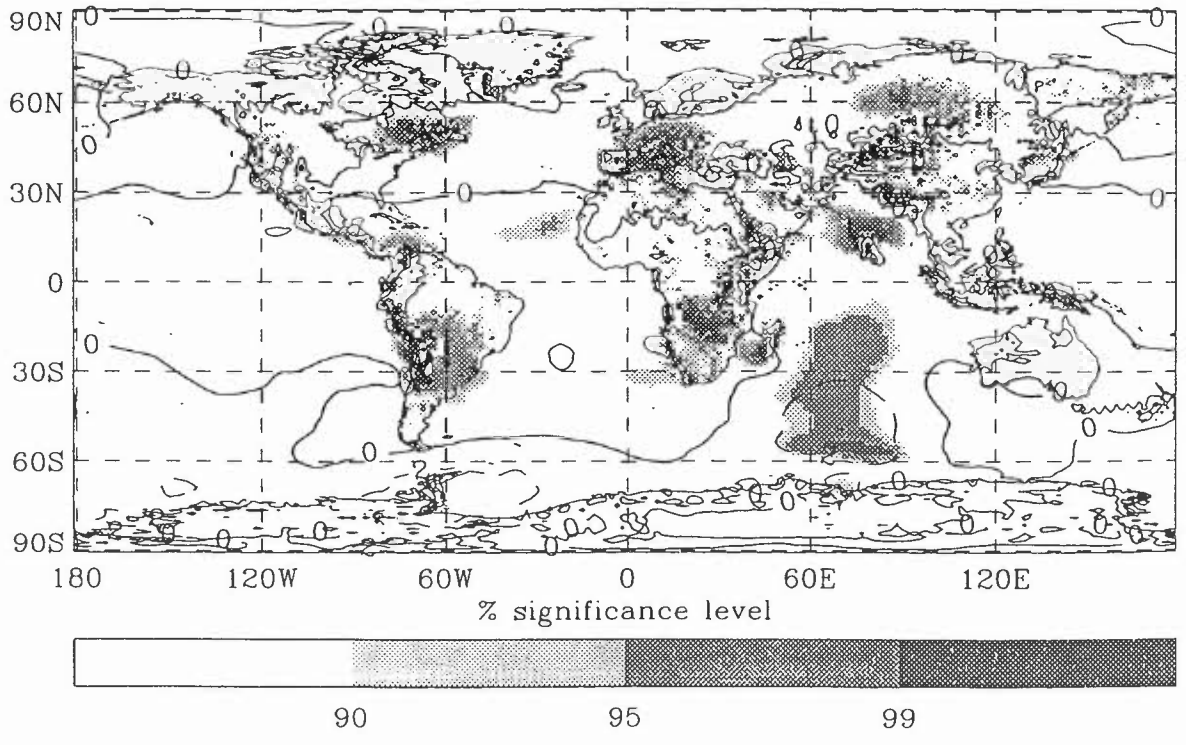

Fig 57 Orography for North America

(a) HRES

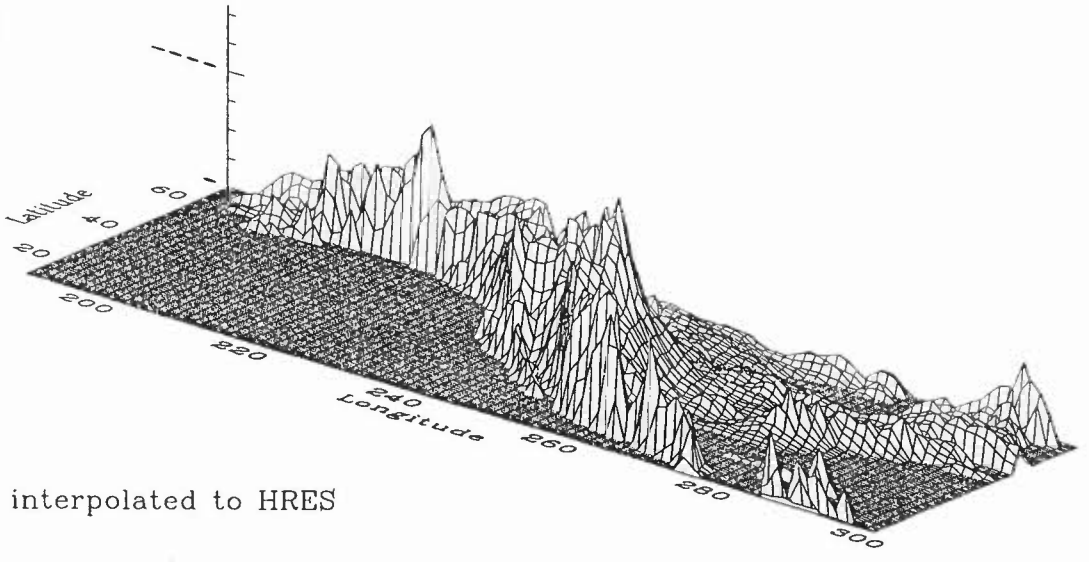

(b) SRES interpolated to HRES

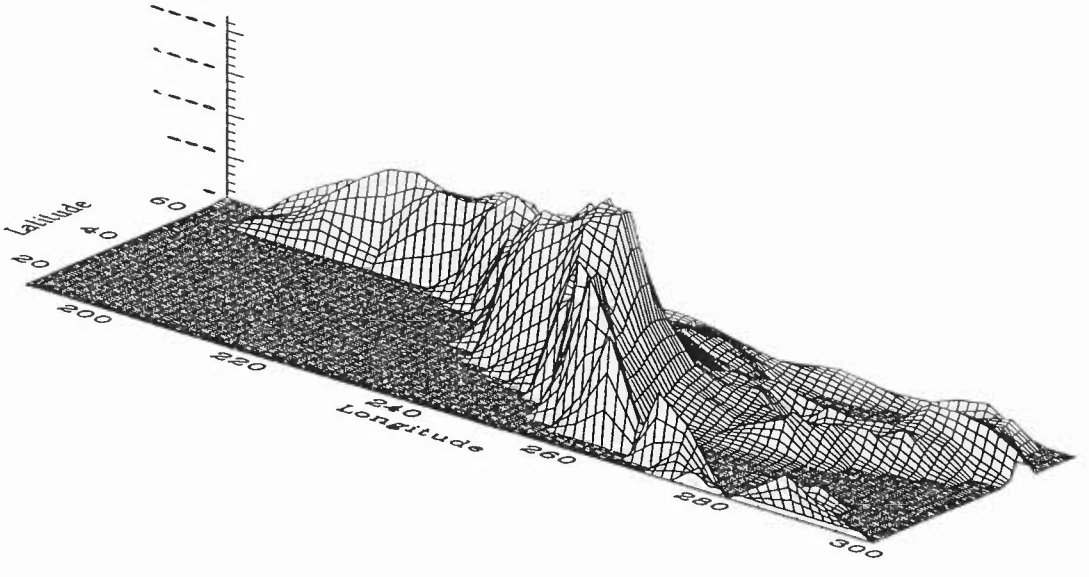

(c) SRES

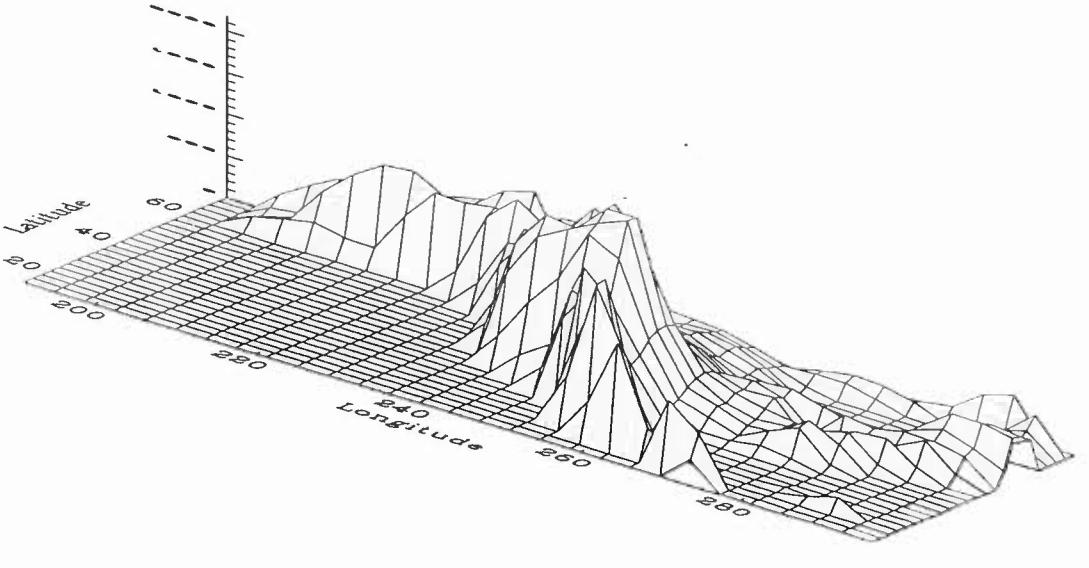

Fig 58 T test for mean sea level pressure abbcp minus abbcq

(a) DJF

Fraction of the globe with 95% sig = 0.06

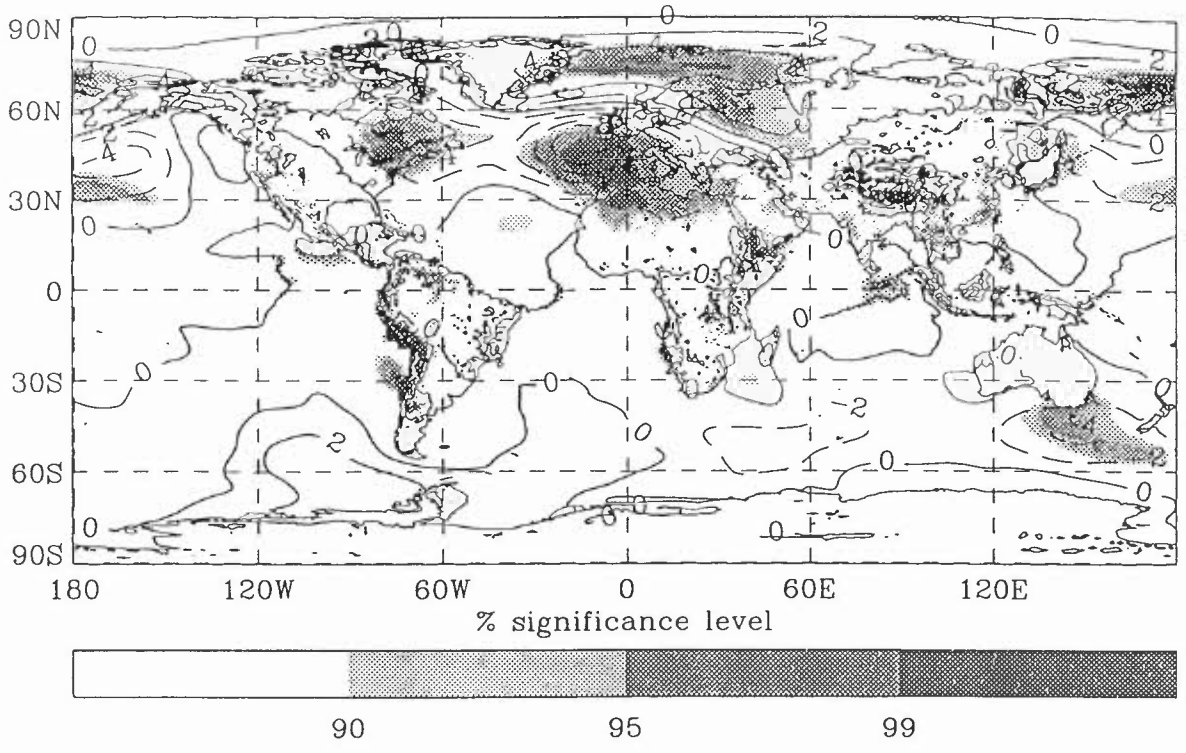

(b) JJA

Fraction of the globe with 95% sig = 0.11

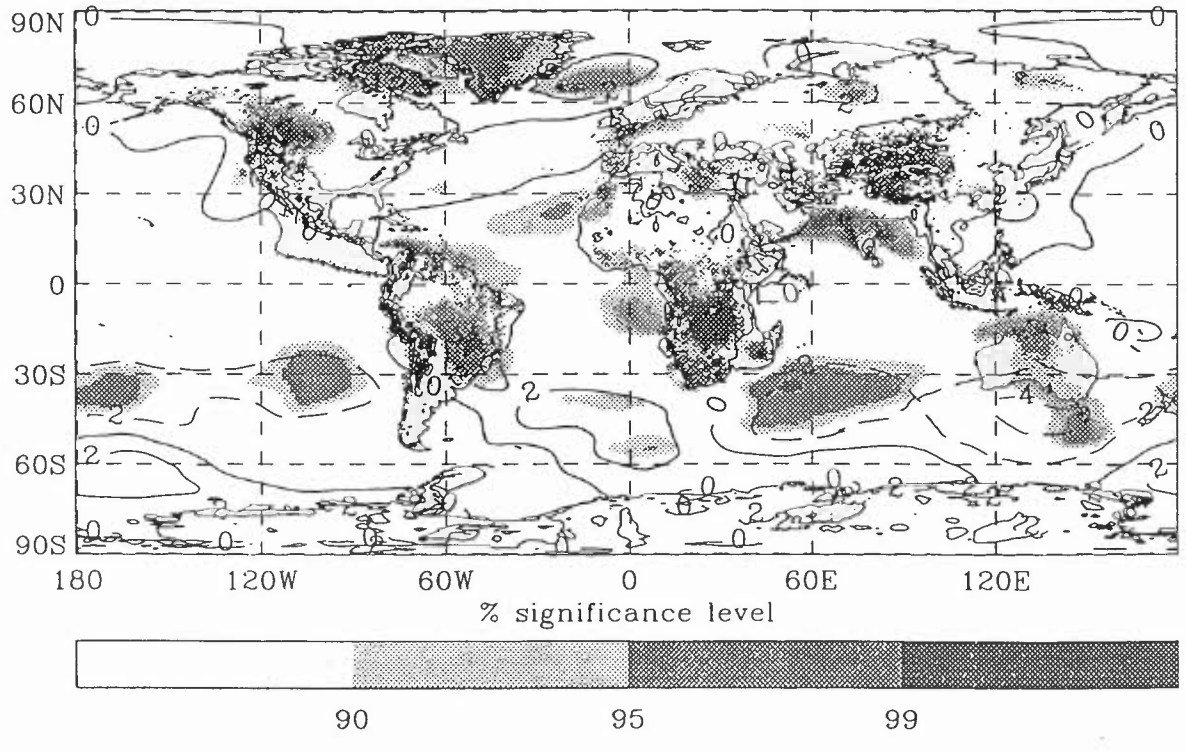

Fig 59 Amplitude of wave number 1 in geopotential height for djf

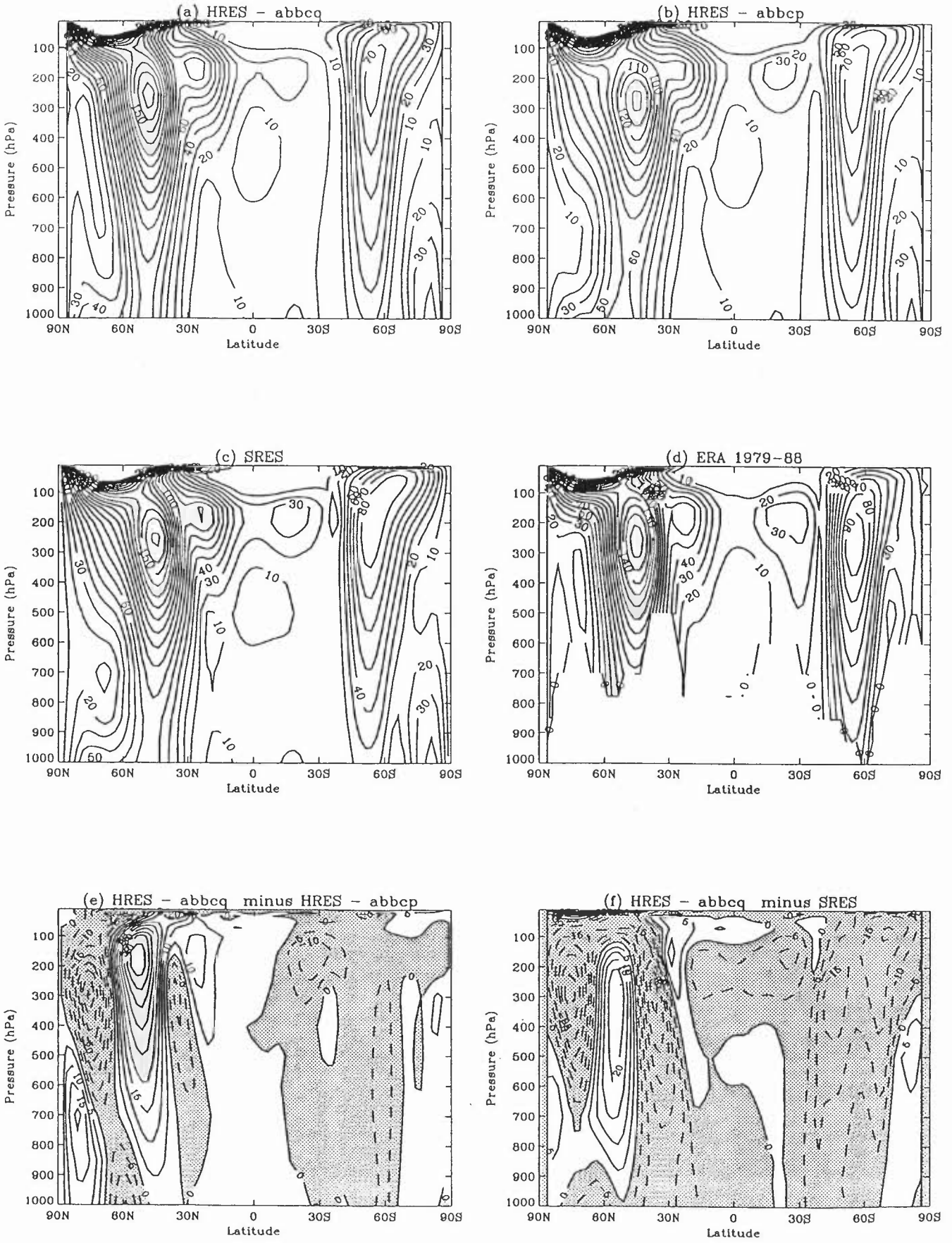

(a) Band pass DJF

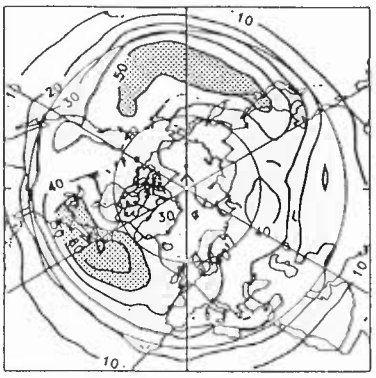

Contours every 10.m

(b) Band pass DJF

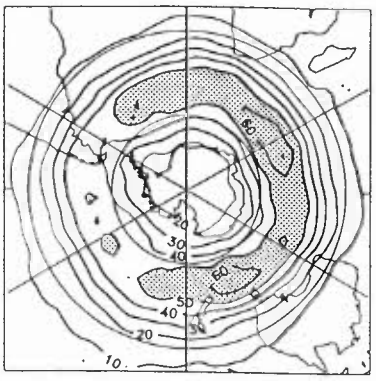

Contours every 10.m

(c) Band pass JJA

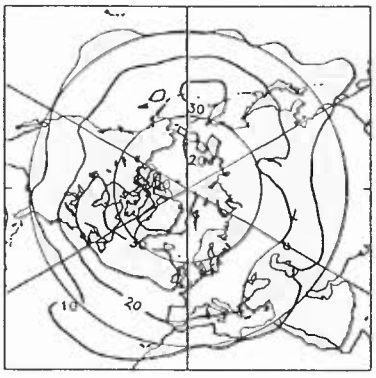

Contours every 10.m

(d) Band pass JJA

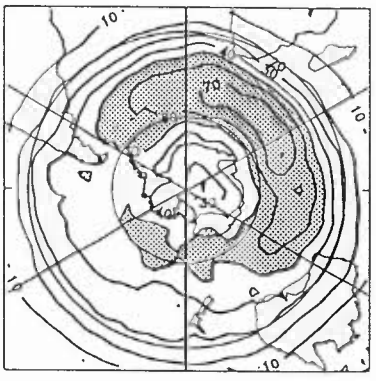

Contours every 10.m

(e) low pass DJF

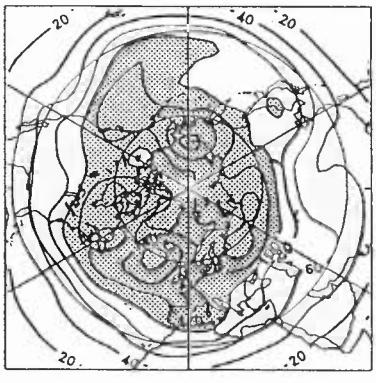

Contours every 20.m

(f) low pass DJF

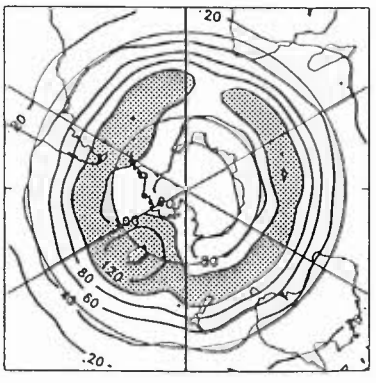

Contours every 20.m

(g) low pass JJA

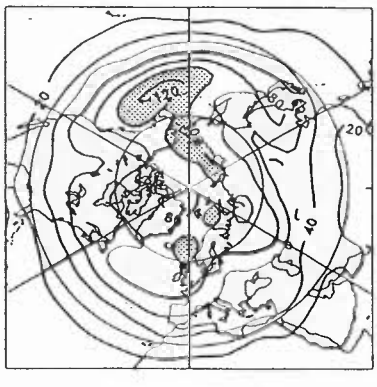

Contours every 20.m

(h) low pass JJA

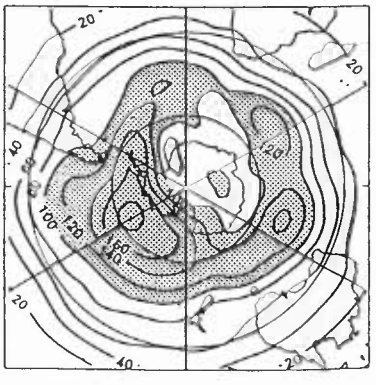

Contours every 20.m

Fig 60 Filtered 500 hPa heights for HRES abbcp